

# Two-body lepton-flavour-violating decays in a 2HDM with soft family-lepton-number breaking

Darius Jurčiukonis<sup>(1)‡</sup> and Luís Lavoura<sup>(2)§</sup>

<sup>(1)</sup> University of Vilnius, Institute of Theoretical Physics and Astronomy,  
Saulėtekio av. 3, LT-10222 Vilnius, Lithuania

<sup>(2)</sup> Universidade de Lisboa, Instituto Superior Técnico, CFTP,  
Av. Rovisco Pais 1, 1049-001 Lisboa, Portugal

July 30, 2021

## Abstract

We evaluate the decays  $\ell_1^\pm \rightarrow \ell_2^\pm \gamma$ ,  $Z \rightarrow \ell_1^+ \ell_2^-$ , and  $h \rightarrow \ell_1^+ \ell_2^-$ , where  $\ell_1$  and  $\ell_2$  are charged leptons with different flavours and  $h$  is the scalar particle with mass 125 GeV, in a two-Higgs-doublet model where all the Yukawa-coupling matrices conserve the lepton flavours but the Majorana mass terms of the right-handed neutrinos break the flavour lepton numbers. We find that (1) the decays  $\ell_1^\pm \rightarrow \ell_2^\pm \gamma$  require large Yukawa couplings and very light right-handed neutrinos in order to be visible, (2) the decays  $Z \rightarrow \ell_1^+ \ell_2^-$  will be invisible in all the planned experiments, but (3) the decays  $h \rightarrow \ell_1^+ \ell_2^-$  might be just around the corner.

---

<sup>‡</sup>darius.jurciukonis@tfai.vu.lt

<sup>§</sup>balio@cftp.tecnico.ulisboa.pt

# Contents

<b>1</b>	<b>Introduction</b>	<b>3</b>
<b>2</b>	<b>The model</b>	<b>5</b>
2.1	Scalar sector . . . . .	5
2.1.1	The matrices $\mathcal{U}$ and $\mathcal{V}$ . . . . .	5
2.1.2	Some interactions of the scalars . . . . .	6
2.2	Leptonic sector . . . . .	7
2.2.1	The matrices $U$ and $X$ . . . . .	7
2.2.2	The interactions of the leptons . . . . .	8
2.3	Restriction to a two-Higgs-doublet model . . . . .	9
2.4	Fit to the lepton-mixing data . . . . .	12
<b>3</b>	<b>Numerical results</b>	<b>13</b>
3.1	Details of the computation . . . . .	13
3.2	Evolution of BRs . . . . .	14
3.3	Fitting the BRs . . . . .	18
3.4	Benchmark points . . . . .	22
3.5	Amplitudes . . . . .	25
<b>4</b>	<b>Summary and conclusions</b>	<b>27</b>
<b>A</b>	<b>Passarino–Veltman functions</b>	<b>28</b>
<b>B</b>	$\ell_1^\pm \rightarrow \ell_2^\pm \gamma$	<b>32</b>
B.1	$H_a^\pm$ . . . . .	32
B.2	$W^\pm$ . . . . .	35
<b>C</b>	$Z \rightarrow \ell_1^+ \ell_2^-$	<b>38</b>
C.1	$H_a^\pm$ . . . . .	38
C.2	$W^\pm$ . . . . .	39
C.3	Diagrams with two neutrino internal lines . . . . .	40
<b>D</b>	$S_b^0 \rightarrow \ell_1^+ \ell_2^-$	<b>43</b>
D.1	Diagrams in which $S_b^0$ attaches to charged leptons . . . . .	43
D.2	Diagrams in which $S_b^0$ attaches to charged scalars . . . . .	44
D.3	Diagrams in which $S_b^0$ attaches to $W$ bosons . . . . .	45
D.4	Diagrams where $S_b^0$ attaches to neutrino lines . . . . .	46
<b>E</b>	<b>The <math>Z</math> invisible decay width</b>	<b>48</b>
<b>F</b>	<b>Constraints on the mass of the charged scalar</b>	<b>50</b>

# 1 Introduction

The well-established phenomenon of neutrino oscillations [1, 2] implies that the family lepton numbers are not unbroken symmetries of Nature. Therefore, other processes that violate those symmetries, like the two-body decays  $\ell_1^\pm \rightarrow \ell_2^\pm \gamma$ ,  $Z \rightarrow \ell_1^\pm \ell_2^\mp$ , and  $h \rightarrow \ell_1^\pm \ell_2^\mp$  may occur. (Here,  $h$  is the recently discovered scalar particle with mass  $m_h = 125 \text{ GeV}$ , and  $\ell_1$  and  $\ell_2$  are charged leptons with different flavours.) In the Standard Model (SM) those decays only appear at the one-loop level and they are suppressed by a GIM-like mechanism [3], due to the light-neutrino masses being very small and almost identical when compared to the Fermi scale. As a consequence, in the SM those lepton-flavour-violating (LFV) decays have very small rates and are, in practice, invisible. This fact renders them all the more inviting to explore both experimentally, as windows to New Physics, and theoretically, in extensions of the SM.

In table 1 we display the nine LFV two-body decays, the present upper bounds on their branching ratios, and the expected sensitivity of some future experiments. Note that, according

Decay	Present	Experiment	Future	Experiment
$\tau^\pm \rightarrow \mu^\pm \gamma$	$4.4 \times 10^{-8}$	BABAR (2010) [4]	$1 \times 10^{-9}$ $2 \times 10^{-9}$	BELLE-II [5] FCC-ee [6, 7]
$\tau^\pm \rightarrow e^\pm \gamma$	$3.3 \times 10^{-8}$	BABAR (2010) [4]	$3 \times 10^{-9}$	BELLE-II [5, 8]
$\mu^\pm \rightarrow e^\pm \gamma$	$4.2 \times 10^{-13}$	MEG (2016) [9]	$6 \times 10^{-14}$	MEG-II [10]
$Z \rightarrow \tau^\pm \mu^\mp$	$1.2 \times 10^{-5}$	DELPHI (1997) [11]	$\sim 10^{-6}$ $\sim 10^{-9}$	HL-LHC [6] FCC-ee [6, 7]
$Z \rightarrow \tau^\pm e^\mp$	$9.8 \times 10^{-6}$	OPAL (1995) [12]	$\sim 10^{-6}$ $\sim 10^{-9}$	HL-LHC [6] FCC-ee [6, 7]
$Z \rightarrow \mu^\pm e^\mp$	$7.5 \times 10^{-7}$	ATLAS (2014) [13]	$\sim 7 \times 10^{-8}$ $\sim 10^{-10}$	HL-LHC [6] FCC-ee [6, 7]
$h \rightarrow \tau^\pm \mu^\mp$	$2.5 \times 10^{-3}$	CMS (2018) [14]	$1.4 \times 10^{-4}$	FCC-ee [15]
$h \rightarrow \tau^\pm e^\mp$	$4.7 \times 10^{-3}$	ATLAS (2019) [16]	$1.6 \times 10^{-4}$	FCC-ee [15]
$h \rightarrow \mu^\pm e^\mp$	$6.1 \times 10^{-5}$	ATLAS (2019) [17]	$1.2 \times 10^{-5}$	FCC-ee [15]

Table 1: Present upper bounds and future sensitivities for the branching ratios of LFV decays.

to Ref. [6], the HL-LHC experiment for  $Z$  decays will lead to improvements of about one order of magnitude on the branching ratios from the full LHC samples; we have indicated those general indications through signs  $\sim$  in table 1.

In this paper we numerically compute the above-mentioned decays in a simple extension of the SM. That extension is a particular case of the scheme proposed in Ref. [18]: a multi-Higgs-doublet model where all the Yukawa-coupling matrices are diagonal in lepton-flavour space, because of the invariance of the dimension-four terms in the Lagrangian under the lepton-flavour symmetries, and the violation of the family lepton numbers arises only *softly* through the dimension-three Majorana mass terms of three right-handed neutrinos. In Ref. [18] the above-mentioned decays have been computed analytically within that general scheme. Here we check that analytical computation, but express the amplitudes through Passarino–Veltman (PV) functions. That allows us to use the resulting formulas in high-precision numerical computations and to establish the impact of the separate amplitudes on the branching ratios (BRs) of the LFV

decays. Although our analytical results allow one to study the LFV decays in a model with an arbitrary number of scalar doublets, in this paper we only perform the numerical computation in the context of a simple version of the two-Higgs-doublet model (2HDM).

The branching ratios of the LFV decays predicted by seesaw models like ours are usually small due to the strong suppression from the very large right-handed-neutrino masses [19, 20]. A recent paper [21] about the LFV Higgs decays in the framework of a general type-I seesaw model with mass-insertion approximation concludes that the maximal decay rates are far from the current experimental bounds. The inverse seesaw model, a specific realization of low-scale seesaw models, might yield larger decay rates [22–25].

There is a large number of theoretical papers on the LFV decays, therefore we refer only to some of them, grouping them according to the decays under consideration, since most of the research has been conducted on individual types of decays:

- LFV decays of charged leptons were analyzed in the context of the inverse seesaw model [22], of effective field theory [26–28], of 2HDMs [27, 29, 30], and of the flipped 3–3–1 model [31]. The current experimental and theoretical situation for these decays is reviewed in Ref. [32].
- The LFV  $Z$  decay rates have been computed in frameworks with massive Majorana neutrinos [33, 34], in the inverse seesaw model [24, 25], effective field theory [35–37], a general 2HDM [38], and the minimal 3–3–1 model [39].
- LFV Higgs decays were analyzed in the framework of the inverse seesaw model [22, 23, 40], 2HDM [41–48], effective field theory [49], 3–3–1 models [31, 50], and models with  $L_\mu - L_\tau$  symmetry [51, 52]. We also refer to the recent mini-review by Vicente [53].

As mentioned above, the LFV decays have been analyzed mainly for the separate sectors, but there are also studies that endeavour to combine the charged-lepton decays, the  $Z$  decays, and the Higgs decays together in the context of the 2HDM [54, 55]. Correlations among separate decay rates may exist, and some LFV decays may be constrained by other LFV decays. Some constraints could appear in several models, while other constraints operate only in specific models. For example, Ref. [24] shows that  $Z \rightarrow \tau^\pm \mu^\mp$  is constrained by  $\tau^\pm \rightarrow \mu^\pm \gamma$  in the inverse seesaw model; constraints on the  $Z$  decays from the LFV decays of charged leptons also emerge in the 2HDM [38] and in the minimal 3–3–1 model [39]. The authors of Ref. [43] claim that the decay  $h \rightarrow \tau^\pm \mu^\mp$  is constrained by  $\tau^\pm \rightarrow \mu^\pm \gamma$  in their specific 2HDM, but in Ref. [41] no such constraints have been found in the type-III 2HDM.

Thus, the simultaneous computation of all decays could provide new insights on the LFV decays. In this paper we perform the numerical study of all nine LFV two-body decays ( $\tau^\pm \rightarrow \mu^\pm \gamma$ ,  $\tau^\pm \rightarrow e^\pm \gamma$ ,  $\mu^\pm \rightarrow e^\pm \gamma$ ,  $Z/h \rightarrow \tau^\pm \mu^\mp$ ,  $Z/h \rightarrow \tau^\pm e^\mp$ , and  $Z/h \rightarrow \mu^\pm e^\mp$ ) in the context of the 2HDM with seesaw mechanism and flavour-conserving Yukawa couplings. Our purpose is to see under which circumstances the decay rates might be close to their present experimental upper bounds—namely, whether one has to resort to very large Yukawa couplings, to very low masses of the new scalar particles of the 2HDM, or to a very low seesaw scale. We want to elucidate which are the very relevant and the less relevant parameters of that model for the LFV decays.

In section 2 we review both the scalar and the leptonic sectors of our model. Section 3 describes our main results. Our findings are summarized in section 4. The Passarino–Veltman

functions relevant for the analytic computation are expounded in appendix A. The full one-loop analytical formulas for the LFV decays in terms of PV functions are collected in appendices B, C, and D. Appendix E is a dissertation on the invisible  $Z$  decay width and appendix F reviews some literature on lower bounds on the charged-Higgs mass.

## 2 The model

### 2.1 Scalar sector

#### 2.1.1 The matrices $\mathcal{U}$ and $\mathcal{V}$

In general,<sup>1</sup> we assume the existence of  $2n_d$  scalar  $SU(2)$  doublets

$$\Phi_k = \begin{pmatrix} \varphi_k^+ \\ \varphi_k^0 \end{pmatrix}, \quad \tilde{\Phi}_k = \begin{pmatrix} \varphi_k^{0*} \\ -\varphi_k^{+*} \end{pmatrix} \quad (k = 1, \dots, n_d). \quad (1)$$

We assume that no other scalar fields exist, except possibly  $SU(2)$  singlets of charge either 0 or  $\pm 1$ . The neutral fields  $\varphi_k^0$  have vacuum expectation values (VEVs)  $v_k/\sqrt{2}$  that may be complex. We use the formalism of Ref. [56], that was further developed in Refs. [18] and [57]. The scalar eigenstates of mass are  $n$  charged scalars  $H_a^+$  ( $a = 1, \dots, n$ ) and  $m$  real neutral scalars  $S_b^0$  ( $b = 1, \dots, m$ ), with  $n \geq n_d$  and  $m \geq 2n_d$ . The fields  $\varphi_k^+$  and  $\varphi_k^0$  are superpositions of the eigenstates of mass according to

$$\varphi_k^+ = \sum_{a=1}^n \mathcal{U}_{ka} H_a^+, \quad \varphi_k^0 = \frac{1}{\sqrt{2}} \left( v_k + \sum_{b=1}^m \mathcal{V}_{kb} S_b^0 \right). \quad (2)$$

The matrix  $\mathcal{U}$  is  $n_d \times n$  and the matrix  $\mathcal{V}$  is  $n_d \times m$ . In general, they are not unitary; however, there are matrices

$$\tilde{\mathcal{U}} = \begin{pmatrix} \mathcal{U} \\ \mathcal{T} \end{pmatrix}, \quad \tilde{\mathcal{V}} = \begin{pmatrix} \text{Re } \mathcal{V} \\ \text{Im } \mathcal{V} \\ \mathcal{R} \end{pmatrix} \quad (3)$$

that are  $n \times n$  unitary and  $m \times m$  real orthogonal, respectively. The matrices  $\mathcal{T}$  and  $\mathcal{R}$  account for the possible presence in the model of charged-scalar  $SU(2)$  singlets and of scalar gauge invariants, respectively. The unitarity of  $\tilde{\mathcal{U}}$  and the orthogonality of  $\tilde{\mathcal{V}}$  imply

$$\mathcal{U}\mathcal{U}^\dagger = \text{Re } \mathcal{V} \text{Re } \mathcal{V}^T = \text{Im } \mathcal{V} \text{Im } \mathcal{V}^T = 1_{n_d \times n_d}, \quad \text{Re } \mathcal{V} \text{Im } \mathcal{V}^T = 0_{n_d \times n_d}. \quad (4)$$

By definition,  $H_1^+ := G^+$  and  $S_1^0 := G^0$  are the ‘would-be Goldstone bosons’. Hence [57],

$$\mathcal{U}_{k1} = \frac{v_k}{v}, \quad \mathcal{V}_{k1} = i \frac{v_k}{v}, \quad (5)$$

where

$$v := \sqrt{\sum_{k=1}^{n_d} |v_k|^2} = \frac{2s_w m_W}{e} = \frac{2c_w s_w m_Z}{e}. \quad (6)$$

---

<sup>1</sup>Soon we shall restrict the model to  $n_d = 2$ .

In Eq. (6),  $s_w$  and  $c_w$  are the sine and the cosine, respectively, of the weak mixing angle. Clearly, because of Eqs. (5) and (6),

$$\sum_{k=1}^{n_d} |\mathcal{U}_{k1}|^2 = \sum_{k=1}^{n_d} |\mathcal{V}_{k1}|^2 = 1. \quad (7)$$

Thus,  $(\mathcal{V}^\dagger \mathcal{V})_{11} = 1$ .

In Eq. (3),  $\tilde{\mathcal{U}}$  is unitary and  $\tilde{\mathcal{V}}$  is orthogonal. Hence, because of Eq. (7), the first columns of  $\mathcal{T}$  and  $\mathcal{R}$  are identically zero. Therefore the orthogonality of  $\tilde{\mathcal{V}}$  implies that, for  $b \neq 1$ ,

$$\begin{aligned} 0 &= \sum_{k=1}^{n_d} (\text{Re } \mathcal{V}_{k1} \text{Re } \mathcal{V}_{kb} + \text{Im } \mathcal{V}_{k1} \text{Im } \mathcal{V}_{kb}) \\ &= \sum_{k=1}^{n_d} \text{Re} (\mathcal{V}_{k1}^* \mathcal{V}_{kb}) \\ &= \sum_{k=1}^{n_d} \text{Re} \left( -i \frac{v_k^*}{v} \mathcal{V}_{kb} \right) \\ &= \sum_{k=1}^{n_d} \text{Im} \left( \frac{v_k^*}{v} \mathcal{V}_{kb} \right). \end{aligned} \quad (8)$$

Thus,

$$x_b := \frac{1}{v} \sum_{k=1}^{n_d} v_k^* \mathcal{V}_{kb} \quad (b \neq 1) \quad (9)$$

is real. So,  $(\mathcal{V}^\dagger \mathcal{V})_{1b} = -ix_b$  is imaginary for all  $b \neq 1$ .

### 2.1.2 Some interactions of the scalars

The parameters  $x_b$  in Eq. (9) are important because they appear in the interaction of the neutral scalars  $S_b^0$  with two  $W$  gauge bosons [57]:

$$\mathcal{L} = \dots + \frac{em_W}{s_w} W_\mu^- W^{\mu+} \sum_{b=2}^m x_b S_b^0. \quad (10)$$

Another important interaction is the one of a  $W$  gauge boson with one neutral scalar and one charged scalar. It is given by [18]

$$\mathcal{L} = \dots + i \frac{e}{2s_w} \sum_{a=1}^n \sum_{b=1}^m [(\mathcal{U}^\dagger \mathcal{V})_{ab} W_\mu^+ (H_a^- \partial^\mu S_b^0 - S_b^0 \partial^\mu H_a^-) \quad (11a)$$

$$+ (\mathcal{V}^\dagger \mathcal{U})_{ba} W_\mu^- (S_b^0 \partial^\mu H_a^+ - H_a^+ \partial^\mu S_b^0)]. \quad (11b)$$

Also relevant in this paper is the interaction of a neutral scalar with two charged scalars. We parameterize it as

$$\mathcal{L} = \dots + \sum_{a,a'=1}^n \sum_{b=1}^m \lambda_{aa'b} H_a^- H_{a'}^+ S_b^0, \quad (12)$$

where the coefficients obey  $\lambda_{aa'b} = \lambda_{a'ab}^*$  because of the Hermiticity of  $\mathcal{L}$ . Equation (12) corresponds, when either  $a = 1$  or  $a' = 1$ , to an interaction of the charged would-be Goldstone bosons. The coefficients for those interactions may be shown—either by gauge invariance or indeed through an analysis of the scalar potential [18]—to be

$$\lambda_{1ab} = \frac{e(m_a^2 - m_b^2)}{2s_w m_W} (\mathcal{V}^\dagger \mathcal{U})_{ba}, \quad (13a)$$

$$\lambda_{a1b} = \frac{e(m_a^2 - m_b^2)}{2s_w m_W} (\mathcal{U}^\dagger \mathcal{V})_{ab}, \quad (13b)$$

$$\lambda_{11b} = \frac{-em_b^2}{2s_w m_W} x_b, \quad (13c)$$

where  $m_a$  is the mass of the charged scalar  $H_a^+$  and  $m_b$  is the mass of the neutral scalar  $S_b^0$ .

## 2.2 Leptonic sector

### 2.2.1 The matrices $U$ and $X$

We assume the existence of three right-handed neutrinos  $\nu_{\ell R}$ , where  $\ell = e, \mu, \tau$ . We assume that *the flavour lepton numbers are conserved in the Yukawa Lagrangian of the leptons*:

$$\mathcal{L}_Y = - \sum_{k=1}^{n_d} \sum_{\ell=e,\mu,\tau} \left[ \Phi_k^\dagger \bar{\ell}_R (\Gamma_k)_{\ell\ell} + \tilde{\Phi}_k^\dagger \bar{\nu}_{\ell R} (\Delta_k)_{\ell\ell} \right] \begin{pmatrix} \nu_{\ell L} \\ \ell_L \end{pmatrix} + \text{H.c.} \quad (14)$$

All the  $2n_d$  matrices  $\Gamma_k$  and  $\Delta_k$  are diagonal by assumption. The charged-lepton mass matrix  $M_\ell$  and the neutrino Dirac mass matrix  $M_D$  are

$$M_\ell = \sum_{k=1}^{n_d} \frac{v_k^*}{\sqrt{2}} \Gamma_k, \quad M_D = \sum_{k=1}^{n_d} \frac{v_k}{\sqrt{2}} \Delta_k, \quad (15)$$

respectively. The matrices  $M_\ell$  and  $M_D$  are diagonal just as the matrices  $\Gamma_k$  and  $\Delta_k$ , respectively. Without loss of generality, we choose the phases of the fields  $\ell_R$  in such a way that the diagonal matrix elements of  $M_\ell$  are real and positive, *viz.* they are the charged-lepton masses; thus,

$$\sum_{k=1}^{n_d} v_k^* (\Gamma_k)_{\ell\ell} = \sqrt{2} m_\ell \quad (\ell = e, \mu, \tau). \quad (16)$$

The neutrino mass terms are

$$\begin{aligned} \mathcal{L}_{\nu \text{ mass}} = & - \begin{pmatrix} \bar{\nu}_{eR}, & \bar{\nu}_{\mu R}, & \bar{\nu}_{\tau R} \end{pmatrix} M_D \begin{pmatrix} \nu_{eL} \\ \nu_{\mu L} \\ \nu_{\tau L} \end{pmatrix} \\ & - \frac{1}{2} \begin{pmatrix} \bar{\nu}_{eR}, & \bar{\nu}_{\mu R}, & \bar{\nu}_{\tau R} \end{pmatrix} M_R \begin{pmatrix} C \bar{\nu}_{eR}^T \\ C \bar{\nu}_{\mu R}^T \\ C \bar{\nu}_{\tau R}^T \end{pmatrix} + \text{H.c.}, \end{aligned} \quad (17)$$

where  $C$  is the charge-conjugation matrix in Dirac space. The flavour-space matrix  $M_R$  is *non-diagonal* and symmetric; it is the sole origin of lepton mixing in this model.

There are six physical Majorana neutrino fields  $\nu_i = C\bar{\nu}_i^T$  ( $i = 1, \dots, 6$ ). The three  $\nu_{\ell L}$  and the three  $\nu_{\ell R}$  are superpositions thereof [18]:

$$\nu_{\ell L} = \sum_{i=1}^6 U_{\ell i} P_L \nu_i, \quad \nu_{\ell R} = \sum_{i=1}^6 X_{\ell i} P_R \nu_i, \quad (18)$$

where  $P_L := (1 - \gamma_5)/2$  and  $P_R := (1 + \gamma_5)/2$  are the projectors of chirality. The matrices  $U$  and  $X$  are  $3 \times 6$ . The matrix

$$U_6 := \begin{pmatrix} U \\ X^* \end{pmatrix} \quad (19)$$

is  $6 \times 6$  and unitary, hence

$$UU^\dagger = 1_{3 \times 3}, \quad U^\dagger U + X^T X^* = 1_{6 \times 6}. \quad (20)$$

The matrix  $U_6$  diagonalizes the full  $6 \times 6$  neutrino mass matrix as

$$U_6^T \begin{pmatrix} 0_{3 \times 3} & M_D^T \\ M_D & M_R \end{pmatrix} U_6 = \hat{m} := \text{diag}(m_1, \dots, m_6). \quad (21)$$

In Eq. (21), the  $m_i$  ( $i = 1, \dots, 6$ ) are non-negative real;  $m_i$  is the mass of the neutrino  $\nu_i$ . From Eq. (21),

$$U \hat{m} U^T = 0_{3 \times 3}, \quad X \hat{m} U^\dagger = M_D. \quad (22)$$

The matrix  $M_D$  is diagonal. Therefore,  $M_D^\dagger M_D = U \hat{m} (1_{6 \times 6} - U^T U^*) \hat{m} U^\dagger = U \hat{m}^2 U^\dagger$  is diagonal. It follows from Eqs. (20) and (22) that

$$X^\dagger M_D U = \hat{m} U^\dagger U. \quad (23)$$

Equation (21) implies  $M_D^T X^* = U^* \hat{m}$ . Therefore,

$$X_{\ell i} = U_{\ell i} \frac{m_i}{(M_D^*)_{\ell \ell}}. \quad (24)$$

### 2.2.2 The interactions of the leptons

The charged-current Lagrangian is

$$\mathcal{L}_{\text{cc}} = \frac{e}{\sqrt{2}s_w} \sum_{\ell=e,\mu,\tau} \sum_{i=1}^6 (W_\sigma^- U_{\ell i} \bar{\ell} \gamma^\sigma P_L \nu_i + W_\sigma^+ U_{\ell i}^* \bar{\nu}_i \gamma^\sigma P_L \ell). \quad (25)$$

The neutral-current Lagrangian is

$$\mathcal{L}_{\text{nc}} = \frac{eZ_\sigma}{2c_w s_w} \sum_{\ell=e,\mu,\tau} \bar{\ell} \gamma^\sigma [(s_w^2 - c_w^2) P_L + 2s_w^2 P_R] \ell \quad (26a)$$

$$+ \frac{eZ_\sigma}{4c_w s_w} \sum_{i,j=1}^6 \bar{\nu}_i \gamma^\sigma (q_{ij} P_L - q_{ji} P_R) \nu_j, \quad (26b)$$



where

$$q_{ij} := (U^\dagger U)_{ij}. \quad (27)$$

When extracting the Feynman rule for the vertex from line (26b), one must multiply by a factor 2 because the  $\nu_i$  are Majorana fields.

The charged scalars interact with the charged leptons and the neutrinos through

$$\mathcal{L}_Y \supset \sum_{a=1}^n \sum_{\ell=e,\mu,\tau} \sum_{i=1}^6 [H_a^- \bar{\ell} (R_{ali} P_R - L_{ali} P_L) \nu_i + H_a^+ \bar{\nu}_i (R_{ali}^* P_L - L_{ali}^* P_R) \ell]. \quad (28)$$

The coefficients in Eq. (28) are given by

$$R_{ali} = \sum_{k=1}^{n_d} \mathcal{U}_{ka}^* (\Delta_k^\dagger X)_{\ell i}, \quad L_{ali} = \sum_{k=1}^{n_d} \mathcal{U}_{ka}^* (\Gamma_k U)_{\ell i}. \quad (29)$$

The neutral scalars interact with the charged leptons and with the neutrinos through

$$\mathcal{L}_Y \supset - \sum_{b=1}^m \sum_{\ell=e,\mu,\tau} \frac{S_b^0}{\sqrt{2}} \bar{\ell} (\gamma_{b\ell} P_L + \gamma_{b\ell}^* P_R) \ell \quad (30a)$$

$$- \sum_{b=1}^m \sum_{i,j=1}^6 \frac{S_b^0}{2\sqrt{2}} \bar{\nu}_i (f_{bij} P_L + f_{bij}^* P_R) \nu_j. \quad (30b)$$

When extracting the Feynman rule for the vertex from line (30b), one must multiply by a factor 2 because the  $\nu_i$  are Majorana fields. The coefficients in Eq. (30) are given by

$$\gamma_{b\ell} = \sum_{k=1}^{n_d} \mathcal{V}_{kb}^* (\Gamma_k)_{\ell\ell}, \quad f_{bij} = \sum_{k=1}^{n_d} \mathcal{V}_{kb} (X^\dagger \Delta_k U + U^T \Delta_k X^*)_{ij}. \quad (31)$$

Notice that  $f_{bij} = f_{bji}$ .

The reader may now appreciate the practical computation of the amplitudes for  $\ell_1^\pm \rightarrow \ell_2^\pm \gamma$  (appendix B),  $Z \rightarrow \ell_1^+ \ell_2^-$  (appendix C), and  $S_b^0 \rightarrow \ell_1^+ \ell_2^-$  (appendix D). Those amplitudes are expressed in terms of the Passarino–Veltman functions expounded in appendix A.

## 2.3 Restriction to a two-Higgs-doublet model

In the numerical computations in this paper, we work in the context of a two-Higgs-doublet model without any scalar  $SU(2)$  singlets. We use, without loss of generality, the ‘Higgs basis’, wherein only the first scalar doublet has a VEV, and moreover that VEV is real and positive:

$$\Phi_1 = \begin{pmatrix} G^+ \\ (v + \rho_1 + iG^0)/\sqrt{2} \end{pmatrix}, \quad \Phi_2 = \begin{pmatrix} H^+ \\ (\rho_2 + i\eta)/\sqrt{2} \end{pmatrix}. \quad (32)$$

In this basis,  $G^+ = H_1^+$  is the charged would-be Goldstone boson and  $H^+ = H_2^+$  is a physical charged scalar. Thus, the matrix  $\mathcal{U}$  defined through Eq. (2) is the  $2 \times 2$  unit matrix. Moreover,  $G^0 = S_1^0$  is the neutral would-be Goldstone boson, and [58]

$$\begin{pmatrix} S_2^0 \\ S_3^0 \\ S_4^0 \end{pmatrix} = T \begin{pmatrix} \rho_1 \\ \rho_2 \\ \eta \end{pmatrix}, \quad (33)$$

where  $T$  is a real orthogonal  $3 \times 3$  matrix. Without loss of generality, we restrict  $T_{11}$ ,  $T_{21}$ , and  $T_{31}$  to be non-negative—this corresponds to a choice for the signs of  $S_2^0$ ,  $S_3^0$ , and  $S_4^0$ , respectively. Without loss of generality, we choose the phase of the doublet  $\Phi_2$  in such a way that  $T_{12} + iT_{13}$  is real and non-negative; thus,  $T_{12} + iT_{13} = \sqrt{1 - T_{11}^2}$ . The matrix  $\mathcal{V}$  defined through Eq. (2) is given by

$$\mathcal{V} = \begin{pmatrix} i & T_{11} & T_{21} & T_{31} \\ 0 & \sqrt{1 - T_{11}^2} & T_{22} + iT_{23} & T_{32} + iT_{33} \end{pmatrix}. \quad (34)$$

Then,

$$\mathcal{V}^\dagger \mathcal{V} = \begin{pmatrix} 1 & -iT_{11} & -iT_{21} & -iT_{31} \\ iT_{11} & 1 & \pm iT_{31} & \mp iT_{21} \\ iT_{21} & \mp iT_{31} & 1 & \pm iT_{11} \\ iT_{31} & \pm iT_{21} & \mp iT_{11} & 1 \end{pmatrix} \quad \text{for } \det T = \pm 1. \quad (35)$$

We are interested only in  $S_2^0$ , *viz.* in the index  $b = 2$ . Through the definition (9),

$$x_2 = T_{11}. \quad (36)$$

We use the notation  $m_h$  for the mass of  $S_2^0$ ; since  $S_2^0$  is supposed to be the scalar discovered at the LHC,  $m_h = 125 \text{ GeV}$ . We use the notation  $m_{H^+}$  for the mass of the charged scalar  $H^+$ . The masses of  $S_3^0$  and  $S_4^0$  are unimportant in this paper.

We use the following notation [59] for the matrix elements of  $\Gamma_{1,2}$  and  $\Delta_{1,2}$ :

$$(\Gamma_2)_{\ell\ell} = \gamma_\ell, \quad (\Delta_1)_{\ell\ell} = d_\ell, \quad (\Delta_2)_{\ell\ell} = \delta_\ell, \quad (37)$$

while  $(\Gamma_1)_{\ell\ell} = \sqrt{2}m_\ell/v$ . Clearly,

$$M_D = \frac{v}{\sqrt{2}} \text{diag} (d_e, d_\mu, d_\tau). \quad (38)$$

From Eq. (24),

$$X_{\ell i} = \frac{\sqrt{2}}{d_\ell^*} U_{\ell i} \frac{m_i}{v}. \quad (39)$$

We use both Eqs. (31) and the definition (27) to derive

$$\gamma_{2\ell} = x_2 \frac{\sqrt{2}m_\ell}{v} + \sqrt{1 - x_2^2} \gamma_\ell, \quad (40a)$$

$$f_{2ij} = x_2 \frac{\sqrt{2}(m_i q_{ij} + m_j q_{ji})}{v} + \sqrt{1 - x_2^2} (X^\dagger \Delta_2 U + U^T \Delta_2 X^*)_{ij}. \quad (40b)$$

The scalar  $S_2^0$  couples to pairs of gauge bosons according to the Lagrangian [57]

$$\mathcal{L} = \dots + \frac{e}{s_w} S_2^0 \left( m_W W_\mu^+ W^{\mu-} + \frac{m_Z}{2c_w} Z_\mu Z^\mu \right) x_2. \quad (41)$$

It couples to the  $\tau$  leptons through the Lagrangian—*cf.* Eq. (30a)—

$$\mathcal{L} = \dots - S_2^0 \bar{\tau} \left( \frac{x_2 e m_\tau}{2s_w m_W} + \frac{\sqrt{1 - x_2^2} \text{Re } \gamma_\tau}{\sqrt{2}} - \frac{\sqrt{1 - x_2^2} \text{Im } \gamma_\tau}{\sqrt{2}} \gamma_5 \right) \tau. \quad (42)$$

One knows from the LHC results that these couplings should be quite close to their SM values. This means that  $x_2$  should be close to 1 and that both  $\sqrt{1-x_2^2} \operatorname{Re} \gamma_\tau$  and  $\sqrt{1-x_2^2} \operatorname{Im} \gamma_\tau$  should be quite smaller than  $x_2 e m_\tau / (s_w m_W)$ . In practice, in our fits we enforce the conditions

$$|x_2| \geq 0.95, \quad (43a)$$

$$\left| x_2 + \frac{\sqrt{2} s_w m_W}{e m_\tau} \sqrt{1-x_2^2} \operatorname{Re} \gamma_\tau \right| \geq 0.95, \quad (43b)$$

$$\left| \frac{m_W}{m_\tau} \sqrt{1-x_2^2} \operatorname{Im} \gamma_\tau \right| \leq 0.3. \quad (43c)$$

These conditions are meant to ensure that the squared couplings agree with the SM ones to within, approximately, 10% level.<sup>2</sup>

We parameterize the vertex of  $S_2^0$  with two charged scalars through Eq. (12). We already know from Eqs. (13) that

$$\lambda_{212} = \lambda_{122} = \frac{e (m_{H^+}^2 - m_h^2)}{2 s_w m_W} \sqrt{1-x_2^2}, \quad (44a)$$

$$\lambda_{112} = -\frac{e m_h^2}{2 s_w m_W} x_2. \quad (44b)$$

The value of  $\lambda_{222}$ , *i.e.* of the coupling  $H^- H^+ S_2^0$ , depends on the scalar potential. If we write the quartic part of the scalar potential of the 2HDM in the standard notation [60]

$$\begin{aligned} V_4 = & \frac{\lambda_1}{2} (\Phi_1^\dagger \Phi_1)^2 + \frac{\lambda_2}{2} (\Phi_2^\dagger \Phi_2)^2 + \lambda_3 \Phi_1^\dagger \Phi_1 \Phi_2^\dagger \Phi_2 + \lambda_4 \Phi_1^\dagger \Phi_2 \Phi_2^\dagger \Phi_1 \\ & + \left[ \frac{\lambda_5}{2} (\Phi_1^\dagger \Phi_2)^2 + (\lambda_6 \Phi_1^\dagger \Phi_1 + \lambda_7 \Phi_2^\dagger \Phi_2) \Phi_1^\dagger \Phi_2 + \text{H.c.} \right], \end{aligned} \quad (45)$$

then [58]

$$\lambda_{222} = -\frac{2 s_w m_W}{e} \left( x_2 \lambda_3 + \sqrt{1-x_2^2} \operatorname{Re} \lambda_7 \right). \quad (46)$$

The coupling  $\lambda_{222}$  is important for  $S_2^0 \rightarrow \ell_1^+ \ell_2^-$ ; there is a diagram for that decay wherein  $S_2^0$  attaches to  $H^- H^+$ . However, in practice that diagram gives amplitudes (D5) that are always much smaller than the dominant amplitudes (D4) and (D11). We have found that, for  $-1 < \lambda_3 < 7$  and  $|\operatorname{Re} \lambda_7| < 1.5$  [61], the branching ratios  $\operatorname{BR}(S_2^0 \rightarrow \ell_1^+ \ell_2^-)$  are almost completely independent of  $\lambda_{222}$ .<sup>3</sup> Thereafter we have kept  $\lambda_3 = \operatorname{Re} \lambda_7 = 1$  fixed.

<sup>2</sup>The LHC results also suggest that the couplings of the Higgs particle to the top and bottom quarks should be quite close to the SM ones. However, since in our model we do not specify the Yukawa couplings of the quarks, we refrain from imposing any constraint arising from the quark sector.

<sup>3</sup>There is an exception to this behaviour when  $1 - T_{11} \lesssim 10^{-7}$ , *i.e.* when one is extremely close to the situation of alignment. In this case the amplitudes (D4) and (D11) are strongly suppressed and the exact value of  $\lambda_{222}$  becomes quite relevant. However, in that very contrived case the branching ratios of  $S_2^0 \rightarrow \ell_1^+ \ell_2^-$  all become very close to zero and, therefore, uninteresting to us, since in this paper we are looking for the possibility of largish lepton-flavour-changing branching ratios.

## 2.4 Fit to the lepton-mixing data

The lepton mixing matrix  $U$  is in the charged-current Lagrangian (25). It is a  $3 \times 6$  matrix. We must connect it to the standard PMNS  $3 \times 3$  unitary matrix. In order to make this connection we use the seesaw approximation [62–66], which is valid when the eigenvalues of  $M_R$  are very much larger than the (diagonal) matrix elements of  $M_D$ . The  $3 \times 3$  symmetric matrix

$$\mathcal{M}_\nu = -M_D^T M_R^{-1} M_D \quad (47)$$

is diagonalized by an unitary matrix  $V$  as

$$V^T \mathcal{M}_\nu V = \text{diag}(n_1, n_2, n_3) := \hat{n}, \quad (48)$$

where the  $n_p$  ( $p = 1, 2, 3$ ) are real and positive. It follows from Eqs. (47) and (48) that

$$M_R = -M_D V \hat{n}^{-1} V^T M_D^T. \quad (49)$$

In our fitting program we input the PMNS matrix  $V$ ,<sup>4</sup> the Yukawa couplings  $d_{e,\mu,\tau}$ , and the three  $n_p$ . We firstly write the matrix  $M_D$  given by Eq. (38). We then determine  $M_R$  through Eq. (49). We use  $M_R$  and  $M_D$  to construct the  $6 \times 6$  matrix

$$\begin{pmatrix} 0_{3 \times 3} & M_D^T \\ M_D & M_R \end{pmatrix}. \quad (50)$$

We diagonalize the matrix (50) through the unitary matrix  $U_6$  as in Eq. (21). We thus find both  $U$ , *viz.* the  $3 \times 6$  upper submatrix of  $U_6$ , and the neutrino masses  $m_i$  ( $i = 1, \dots, 6$ ). Because the seesaw approximation is very good, one obtains  $m_i \approx n_i$  for  $i = 1, 2, 3$  and moreover the  $3 \times 3$  left submatrix of  $U$  turns out approximately equal to  $V$ . We order the heavy-neutrino masses as  $m_4 \leq m_5 \leq m_6$ .

Since the  $n_p$  are many orders of magnitude below the Fermi scale, the matrix elements of  $M_R$  are much above the Fermi scale unless the Yukawa couplings  $d_\ell$  are extremely small. When we want to lower the seesaw scale, we lower the inputted  $d_\ell$ .

For the  $n_p$  we use the light-neutrino masses. The cosmological bound [67] is

$$\sum_{p=1}^3 n_p \approx \sum_{\text{light neutrinos}} m_\nu < 0.12 \text{ eV}, \quad (51)$$

together with the squared-mass differences  $\Delta_{\text{solar}} = n_2^2 - n_1^2$  and  $\Delta_{\text{atmospheric}} = |n_3^2 - n_1^2|$ , that are taken from phenomenology. The lightest-neutrino mass is kept free; we let it vary in between  $10^{-5} \text{ eV}$  and  $\sim 0.03 \text{ eV}$  for normal ordering ( $n_1 < n_3$ ), and in between  $10^{-5} \text{ eV}$  and  $\sim 0.015 \text{ eV}$  for inverted ordering ( $n_3 < n_1$ ); the upper bound on the lightest-neutrino mass is indirectly provided by the cosmological bound (51). The smallest  $n_p$  cannot be allowed to be zero because  $\hat{n}^{-1}$  appears in Eq. (49). For the matrix  $V$  we use the parameterization [68]

$$V = \begin{pmatrix} c_{12}c_{13} & s_{12}c_{13} & \epsilon^* \\ -s_{12}c_{23} - c_{12}s_{23}\epsilon & c_{12}c_{23} - s_{12}s_{23}\epsilon & s_{23}c_{13} \\ s_{12}s_{23} - c_{12}c_{23}\epsilon & -c_{12}s_{23} - s_{12}c_{23}\epsilon & c_{23}c_{13} \end{pmatrix} \times \text{diag}(1, e^{i\alpha_{21}/2}, e^{i\alpha_{31}/2}), \quad (52)$$

---

<sup>4</sup>Recall that in our model there is conservation of the flavour lepton numbers in the Yukawa couplings and therefore the charged-lepton mass matrix is diagonal from the start.

where  $\epsilon \equiv s_{13} \exp(i\delta)$ ,  $c_{pq} = \cos \theta_{pq}$ , and  $s_{pq} = \sin \theta_{pq}$  for  $(pq) = (12), (13), (23)$ .

Three different groups [69–71] have derived, from the data provided by various neutrino-oscillation experiments, values for the mixing angles  $\theta_{pq}$ , for the phase  $\delta$ , and for  $\Delta_{\text{solar}}$  and  $\Delta_{\text{atmospheric}}$ . The results of the three groups (especially the  $1\sigma$  bounds) are different, but in Ref. [69] the values of the observables are in between the bounds of Refs. [70] and [71]. In this paper we use the  $3\sigma$  data from Ref. [69] that are summarised in table 2. The Majorana phases

Quantity	Best fit	$1\sigma$ range	$3\sigma$ range
$\Delta_{\text{solar}} / (10^{-5} \text{eV}^2)$	7.55	7.39–7.75	7.05–8.14
$\Delta_{\text{atmospheric}} / (10^{-3} \text{eV}^2)$ (NO)	2.50	2.47–2.53	2.41–2.60
$\Delta_{\text{atmospheric}} / (10^{-3} \text{eV}^2)$ (IO)	2.42	2.34–2.47	2.31–2.51
$\sin^2 \theta_{12} / 10^{-1}$	3.20	3.04–3.40	2.73–3.79
$\sin^2 \theta_{23} / 10^{-1}$ (NO)	5.47	5.17–5.67	4.45–5.99
$\sin^2 \theta_{23} / 10^{-1}$ (IO)	5.51	5.21–5.69	4.53–5.98
$\sin^2 \theta_{13} / 10^{-2}$ (NO)	2.160	2.091–2.243	1.96–2.41
$\sin^2 \theta_{13} / 10^{-2}$ (IO)	2.220	2.144–2.146	1.99–2.44
$\delta / \text{rad}$ (NO)	3.80	3.33–4.46	2.73–6.09
$\delta / \text{rad}$ (IO)	4.90	4.43–5.31	3.52–6.09

Table 2: The neutrino-oscillation parameters used in our fits [69].

$\alpha_{21}$  and  $\alpha_{31}$  are kept free in our analysis.

## 3 Numerical results

### 3.1 Details of the computation

We have generated the complete set of diagrams for each process in Feynman gauge by using the package **FeynMaster** [72], with a modified version of the **FeynRules** Standard-Model file to account for the six neutrinos, for lepton flavour mixing, and for the additional Higgs doublet. The amplitudes generated automatically by **FeynMaster** were expressed through Passarino–Veltman (PV) functions by using the package **FeynCalc** and specific functions of **FeynMaster**. All the amplitudes were checked by performing the computations manually.

For numerical calculations we made two separate programs, one with **Mathematica** and another one with **Fortran**. Because of the very large differences among

the mass scale of the light neutrinos, between  $10^{-5} \text{eV}$  and  $0.1 \text{eV}$ ,

the mass scale of the charged leptons, between  $100 \text{keV}$  and  $1 \text{GeV}$ ,

and the mass scale of the heavy neutrinos, between  $100 \text{GeV}$  and  $10^{16} \text{GeV}$ ,

there are both numerical instabilities and delicate cancellations in the calculations. These numerical problems could be solved with the high-precision numbers that **Mathematica** allows. However, this strongly slows down the calculations. Fortunately, numerical inaccuracies occur

only for very small values (less than  $10^{-30}$ ) of the branching ratios (BRs), therefore we were able to use a program written with **Fortran** to implement the minimization procedure and to find BRs within ranges relevant to experiment. Some parts of the **Fortran** code (such as the module for matrix diagonalization) have used quadruple precision to avoid inaccuracies, but most of the code has used just double precision so that the computational speed was sufficient for minimization. The final results were checked with the high precision afforded by **Mathematica**.

The numerical computation of the PV functions was performed by using the **Fortran** library **Collier** [73], which is designed for the numerical evaluation of one-loop scalar and tensor integrals. A major advantage of this library over the **LoopTools** package [74] is that it avoids numerical instabilities when the neutrino masses are very large, even when one only uses double precision. The integrals were checked with **Mathematica**'s high-precision numbers and **Package-X** [75] analytic expressions of one-loop integrals.

In order to find adequate numerical values for the parameters we have constructed a  $\chi^2$  function to be minimized:

$$\chi^2 = \sum_{i=1}^n \left[ \Theta(O_i^b - O_i^v) \left( \frac{O_i^b}{O_i^v} \right)^2 + \Theta(O_i^v - O_i^b) \left( \frac{O_i^v - O_i^b}{k} \right)^2 \right], \quad (53)$$

where  $n$  is the total number of observables to be fitted; in this case this is usually nine, since we fit the BRs of the nine LFV decays in order to find them within the ranges accessible to experiment. In Eq. (53),  $\Theta$  is the Heaviside step function,  $O_i^v$  is the computed value of each observable,  $O_i^b$  is the experimental upper bound on the observable, which is given in table 1, and  $k$  is an appropriately small number that short-circuits the minimization algorithm when  $O_i^v$  turns out larger than  $O_i^b$ .<sup>5</sup> The  $\chi^2$  function (53) works well even when the calculated BRs and the experimental upper bounds differ by many orders of magnitude. We fit by minimizing  $\chi^2$  with respect to the model parameters—the Yukawa couplings  $d_\ell$ ,  $\delta_\ell$ , and  $\gamma_\ell$ , the PMNS-matrix parameters, and the parameter  $T_{11}$  of the 2HDM. The mass of the lightest neutrino is randomly generated before the minimization of the  $\chi^2$  function, in order to explore the full range of the neutrino masses.

The minimization of  $\chi^2$  is not an easy task because of the large number of model parameters that, moreover, may differ by several orders of magnitude, and because there is always a large number of local minima. However, we don't try to find absolute minima, *i.e.* BRs asymptotically close to the experimental upper bound; our purpose is rather to search under which circumstances the decay rates may be in experimentally accessible ranges.

The inputted values of the masses of the leptons and bosons were taken from Ref. [68]. We have used  $s_w^2 = 0.22337$  and  $e \equiv \sqrt{4\pi\alpha}$ , where  $\alpha$  is the fine-structure constant. The phenomenological neutrino-oscillation data have been taken from Ref. [69] and are in table 2.

### 3.2 Evolution of BRs

In this subsection we discuss the way the BRs change when some input parameters are varied. We introduce the shorthands  $\text{BR}(\ell)$ ,  $\text{BR}(Z)$ , and  $\text{BR}(h)$  for the branching ratios of the decays

---

<sup>5</sup>In practice, in each case we have tried various values of  $k$  before settling on the one that worked best, *i.e.* that maximized the efficiency of the minimization algorithm for each problem at hand. Since the observables *viz.* the branching ratios are very small,  $k \sim 10^{-20}$  was a typical order of magnitude.

$\ell_1^\pm \rightarrow \ell_2^\pm \gamma$ ,  $Z \rightarrow \ell_1^\pm \ell_2^\mp$ , and  $h \rightarrow \ell_1^\pm \ell_2^\mp$ , respectively. We also define the parameter  $\tilde{T}_{11} \equiv 1 - T_{11} = 1 - x_2$ , the lower bound  $Y_{\min} = 10^{-6}$ , and the upper bound  $Y_{\max} = \sqrt{4\pi} \approx 3.5$  on the moduli of the Yukawa coupling constants.

In order to estimate the impact of the Yukawa coupling constants on the BRs, we have fixed their ratios in the following way:  $d_\tau/d_\mu = d_\mu/d_e = 1.1$ ,  $\delta_\tau/\delta_\mu = \delta_\mu/\delta_e = 1.1$ , and  $\gamma_\tau/\gamma_\mu = \gamma_\mu/\gamma_e = 1.1$ ; then, only  $d_\tau$ ,  $\delta_\tau$ , and  $\gamma_\tau$  are varied, and the other Yukawa couplings vary together with them through the fixed ratios. In this way we are able to display the behaviour of all three processes, *viz.*  $(\ell_1, \ell_2) = (\tau, \mu)$ ,  $(\tau, e)$ , and  $(\mu, e)$  at once, while keeping the Yukawa couplings in narrow ranges but without finetuning them.<sup>6</sup>

In this subsection we assume the neutrino mass ordering to be normal. The mass of the lightest neutrino is kept fixed at  $m_1 = 0.01$  eV while the neutrino squared-mass differences and the oscillation parameters are kept fixed at their best-fit values in table 2; the Majorana phases are kept equal to zero. The mass of the charged scalar is fixed at  $m_{H^\pm} = 750$  GeV and the 2HDM parameters at  $\lambda_3 = \lambda_7 = 1$  and  $\tilde{T}_{11} = 10^{-5}$ .

In Fig. 1 we display the BRs against  $d_\tau$  when  $\delta_\tau$  and  $\gamma_\tau$  are kept equal to  $\sqrt{4\pi}$ . Notice, in the upper and lower horizontal scales of Fig. 1, that the mass  $m_4$  of the lightest heavy neutrino increases with increasing  $d_\tau$  approximately as  $m_4 \propto d_\tau^2$ . One observes, in the top-left panel of Fig. 1, that the BRs of the  $\tau^\pm$  decays achieve values comparable with the experimental upper bounds for a narrow range of the  $d_\ell$ , *viz.* for  $4 \times 10^{-7} < d_\ell < 2 \times 10^{-6}$ . The branching ratio  $\text{BR}(\mu^\pm \rightarrow e^\pm \gamma)$  remains above its experimental upper bound for  $d_\ell$  as large as  $10^{-5}$ . One sees that, for these values of the  $d_\ell$ , the heavy-neutrino masses are small ( $m_4 \lesssim 10^5$  GeV).

The behaviour of the  $\text{BR}(Z)$  is shown in the bottom-left panel of Fig. 1; it is similar to the behaviour of the  $\text{BR}(\ell)$ , as one might foresee from the similarities in the amplitudes. Unfortunately, because of a small factor in the decay width, *cf.* Eq. (C2), the computed  $\text{BR}(Z)$  are smaller by more than six orders of magnitude than the present experimental upper bounds.

We see a completely different behaviour of the  $\text{BR}(h)$  in the right side of Fig. 1. The branching ratios of the 125 GeV particle achieve values comparable to the experimental upper bounds for a wide range of  $d_\ell$  and even for very large heavy-neutrino masses.

The main message of Fig. 1 is that all nine BRs would be very small without the charged scalar  $H^\pm$ . The contributions to the amplitudes from the diagrams with  $H^\pm$  are able to increase some BRs in some circumstances by several orders of magnitude.

The branching ratios behave differently against the Yukawa couplings  $\delta_\ell$ , as shown in Fig. 2. We see that all the BRs increase with increasing  $\delta_\ell$ ;  $\text{BR}(\ell)$  and  $\text{BR}(h)$  reach the experimental upper bounds for  $\delta_\ell \gtrsim 0.1$ . Those BRs may therefore be obtained in experimentally observable ranges, but only if  $\delta_\ell$  is close to its upper perturbativity bound (and the  $d_\ell$  are very small, as they are in Fig. 2).

The dependence of  $\text{BR}(\ell)$  and  $\text{BR}(Z)$  from the couplings  $\gamma_\ell$  is weak, as shown in the left panel of Fig. 3. The reason for this is that in the dominant amplitudes, *viz.* the ones in Eq. (B14), the couplings  $d_\ell$  and  $\delta_\ell$  have much stronger impact than the couplings  $\gamma_\ell$ ; the impact of  $\gamma_\ell$  becomes visible only for very small  $\delta_\ell$ . The impact of the  $\gamma_\ell$  is much stronger on the  $\text{BR}(h)$ ; in the right panel of Fig. 3 one sees that the experimental upper bounds are reached when  $\gamma_\ell \gtrsim 1$  for appropriate values of the other parameters.

---

<sup>6</sup>One may check, for instance in Fig. 9 below, that the couplings  $d_\ell$  and  $\delta_\ell$  must be in narrow ranges if one wants to simultaneously obtain experimentally attainable  $\text{BR}(\ell)$  and  $\text{BR}(h)$ .

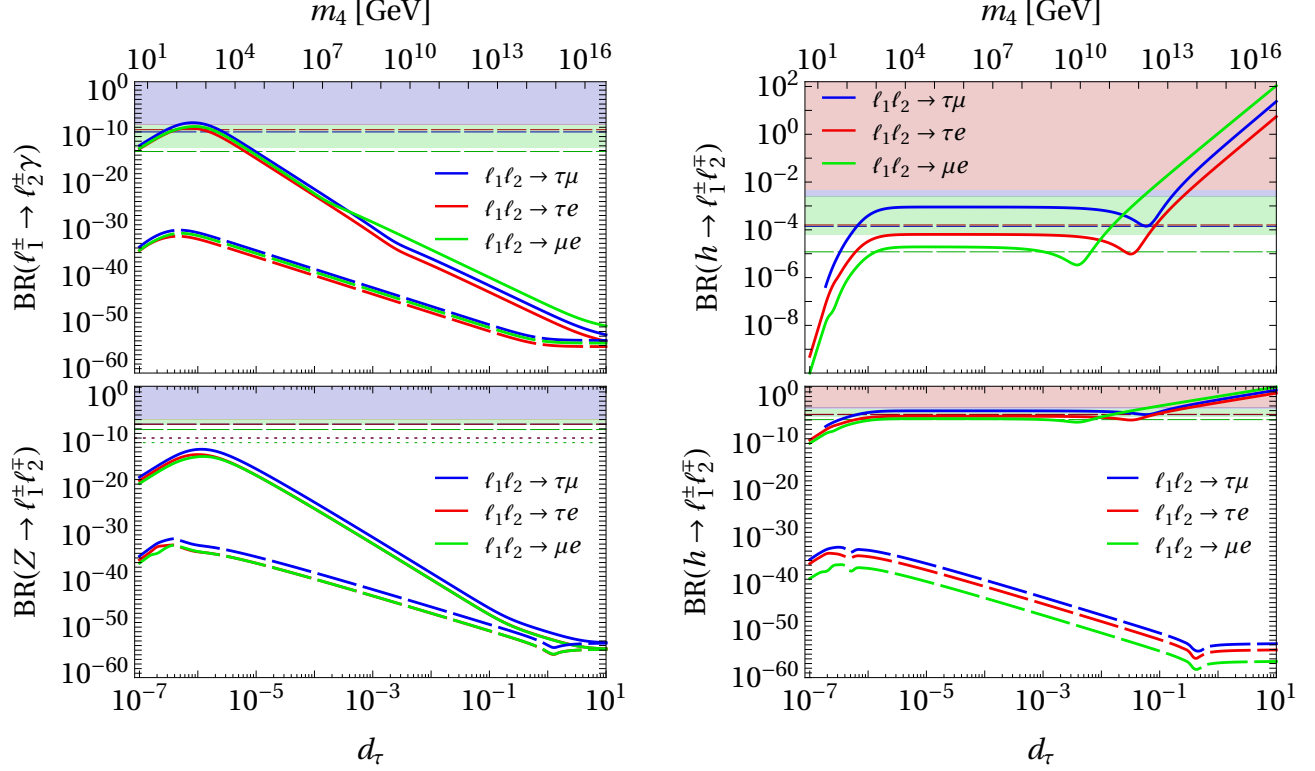


Figure 1: The branching ratios as functions of the Yukawa coupling  $d_\tau$ . The Yukawa couplings  $\delta_\tau = \gamma_\tau = Y_{\max}$ ; the other Yukawa couplings are fixed through the ratios described in the main text. Full lines represent the contribution of all amplitudes; dashed lines represent the contribution of amplitudes that do not involve the charged scalar  $H^\pm$ . The shadowed bands are excluded by the present experimental data; the dashed/dotted horizontal lines show the future experimental sensitivities described in table 1. The colours of shadowed bands coincide with the colours of the lines, *viz.* blue for  $(\ell_1, \ell_2) = (\tau, \mu)$ , red for  $(\ell_1, \ell_2) = (\tau, e)$ , and green for  $(\ell_1, \ell_2) = (\mu, e)$ . The upper-right panel is a zoom of the bottom-right one.

In Figs. 1 and 3 we have seen that the behaviour of  $\text{BR}(h)$  is different from the one of  $\text{BR}(Z)$  and  $\text{BR}(\ell)$ . This happens because of different amplitudes and also additional parameters, *viz.* both  $\tilde{T}_{11} = 1 - x_2$  and the triple-scalar couplings  $\lambda_3$  and  $\lambda_7$ , which arise in the diagram of Fig. 18 where  $h$  attaches to two charged scalars with couplings given by Eqs. (44) and (46). However, due to the small value of the factor  $\sqrt{1 - x_2^2}$  in the second term of Eq. (46), the impact of  $\lambda_7$  on  $\text{BR}(h)$  is almost imperceptible. The impact of  $\lambda_3$  becomes visible only for  $\tilde{T}_{11} \lesssim 10^{-7}$ , *i.e.* when one is extremely close to the ‘alignment’ situation  $\tilde{T}_{11} = 1$ , as shown in the left panel of Fig. 4. For the sake of simplicity, from now on we assume  $\lambda_3 = \lambda_7 = 1$  everywhere in our analysis.

The parameter  $\tilde{T}_{11}$  has a strong impact on the  $\text{BR}(h)$ , as shown in the right panel of Fig. 4, and is important when we try to make the  $\text{BR}(h)$  and  $\text{BR}(\ell)$  simultaneously close to the experimental bounds. In Fig. 5 we illustrate the behaviour of  $\tilde{T}_{11}$  *versus* the Yukawa couplings for fixed  $\text{BR}(h)$ . In the left panel of Fig. 5 we keep fixed either  $\text{BR}(h \rightarrow \tau^\pm \mu^\mp) = 2 \times 10^{-3}$ ,



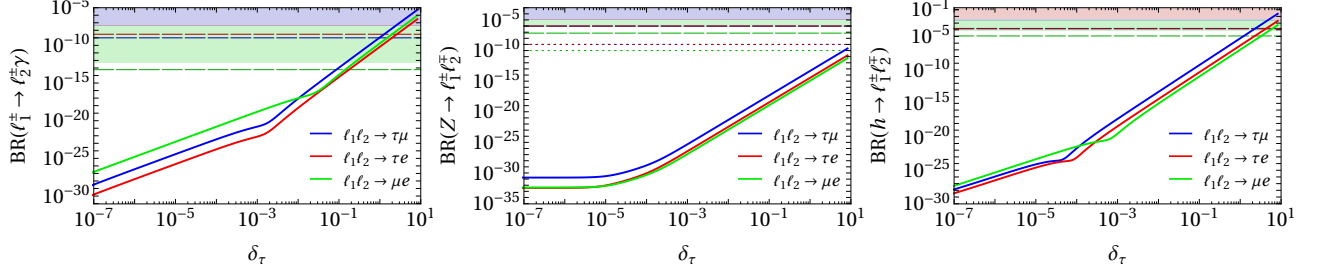


Figure 2: The branching ratios as functions of the Yukawa coupling  $\delta_\tau$ , while  $\delta_e$  and  $\delta_\mu$  are determined through their ratios to  $\delta_\tau$  as described in the main text. The couplings  $d_\tau = Y_{\min}$  and  $\gamma_\tau = Y_{\max}$  are kept fixed.

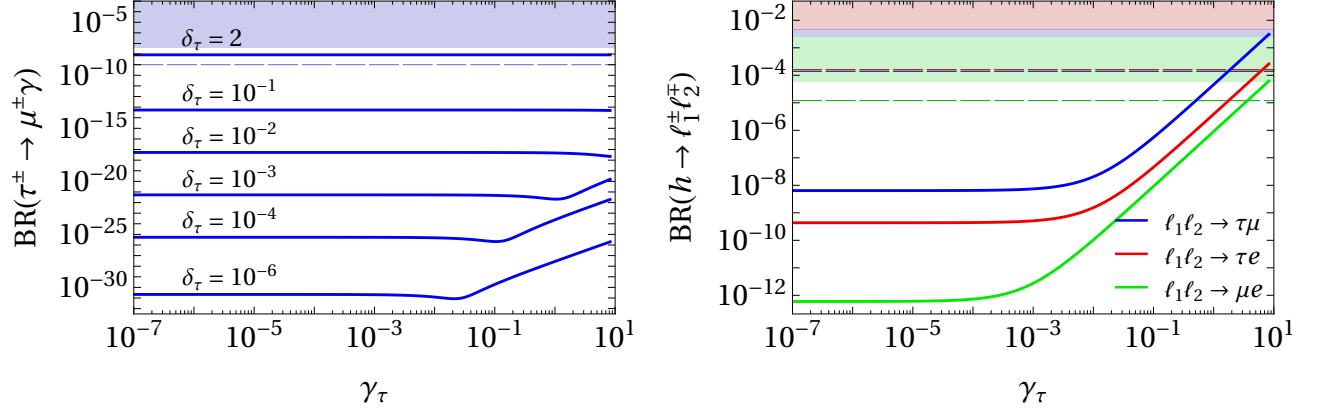


Figure 3: The branching ratios as functions of the Yukawa coupling  $\gamma_\tau$ . Left panel:  $\text{BR}(\tau^\pm \rightarrow \mu^\pm \gamma)$  versus  $\gamma_\tau$  for various values of  $\delta_\tau$ . Right panel: the three  $\text{BR}(h)$  versus  $\gamma_\tau$  for  $\delta_\tau = Y_{\max}$ . In both panels  $d_\tau = Y_{\min}$ ; the other couplings are determined through the ratios described in the main text.

or  $\text{BR}(h \rightarrow \tau^\pm e^\mp) = 2 \times 10^{-3}$ , or  $\text{BR}(h \rightarrow \mu^\pm e^\mp) = 4 \times 10^{-5}$  (these values are close to the experimental bounds) and we depict the dependence of  $\tilde{T}_{11}$  on  $d_\tau$ , while  $\delta_\tau = Y_{\max}$  and  $\gamma_\tau = Y_{\max}$  are kept invariant. The lines in this figure are the inverse of the lines in the top-right panel of Fig. 1. We see that the  $\text{BR}(h)$  may be fitted for a wide range of the Yukawa couplings  $d_\ell$  by varying just the parameter  $\tilde{T}_{11}$ . The right panel of Fig. 5 displays the relationship among  $\tilde{T}_{11}$ ,  $\gamma_\ell$ , and  $\delta_\ell$ , for fixed  $\text{BR}(h \rightarrow \tau^\pm \mu^\mp) = 2 \times 10^{-3}$  and  $d_\tau = Y_{\min}$ . We see that the parameter  $\tilde{T}_{11}$  is able to fit  $\text{BR}(h)$  only for quite large values of the Yukawa couplings  $\gamma_\ell$  and  $\delta_\ell$ . Still, the strong impact of  $\tilde{T}_{11}$  and of the  $\gamma_\ell$  on the  $\text{BR}(h)$  allow one to fit them together with the  $\text{BR}(\ell)$  close to experimental upper bounds, with quite restricted  $d_\ell$  and  $\delta_\ell$  of course. If one attempts to fit only the three  $\text{BR}(h)$ , then  $\tilde{T}_{11}$  and the Yukawa couplings may be more relaxed.

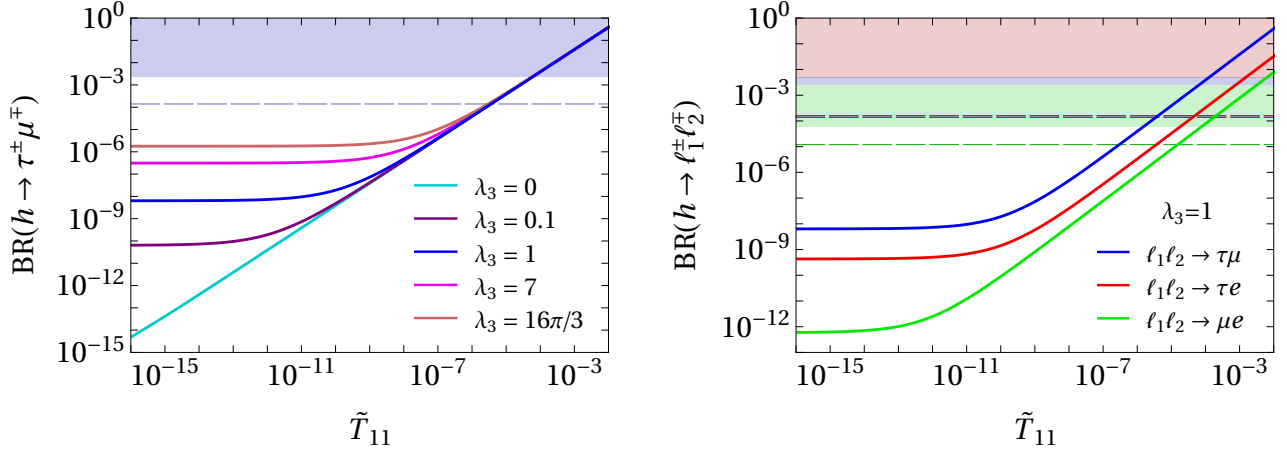


Figure 4: The branching ratios of Higgs decays as functions of the parameter  $\tilde{T}_{11} \equiv 1 - x_2$ . Left panel:  $\text{BR}(h \rightarrow \tau^\pm \mu^\mp)$  versus  $\tilde{T}_{11}$  for various values of the triple-scalar coupling  $\lambda_3$ . Right panel: the three  $\text{BR}(h \rightarrow \ell_1^\pm \ell_2^\mp)$  versus  $\tilde{T}_{11}$  for fixed  $\lambda_3 = 1$ .

### 3.3 Fitting the BRs

In this model there is a large number of parameters. We perform a minimization procedure in order to find adequate values for all of them. For each set of parameters, we compute the branching ratios of the nine LFV decays and we select the sets of parameters for which all six  $\text{BR}(\ell)$  and  $\text{BR}(h)$  are simultaneously between the current experimental upper bounds and the future experimental sensitivities. We are unable to achieve values of the three  $\text{BR}(Z)$  close to the experimental upper bounds, but the minimization procedure seeks to obtain the highest possible values of the  $\text{BR}(Z)$ .

Since in this subsection we are using a fitting procedure, we must enforce bounds on the parameters, lest they acquire either much too small or much too large values. We restrict the parameter space by adopting the following conditions:

- The lightest-neutrino mass lies in between  $10^{-5}$  eV and  $\sim 0.03$  eV for normal ordering or  $\sim 0.015$  eV for inverted ordering. The upper bounds on the lightest neutrino mass are determined by the *Planck* 2018 cosmological upper bound (51).
- The neutrino-oscillation parameters—the mixing angles  $\theta_{12,23,13}$ , the Dirac phase  $\delta$ , and the neutrino squared-mass differences—are varied within their respective  $3\sigma$  ranges taken from Ref. [69] and reproduced in table 2. The Majorana phases  $\alpha_{21}$  and  $\alpha_{31}$  are free, *i.e.* we let them vary from 0 to  $2\pi$ .
- There are some experimental and phenomenological constraints on the mass of the charged scalar  $m_{H^+}$ , as discussed in Appendix F. Our numerical simulations show that, when  $m_{H^+}$  increases, most BRs decrease.<sup>7</sup> Since our goal is to find largish BRs, the fitting procedure tends to produce the lowest  $m_{H^+}$  in the allowed range. Therefore, in this subsection, we fix  $m_{H^+} = 750$  GeV, in agreement with the lower bounds of recent global fits [76, 77].

<sup>7</sup>We can see that in Fig. 11, which is described in subsection 3.4.

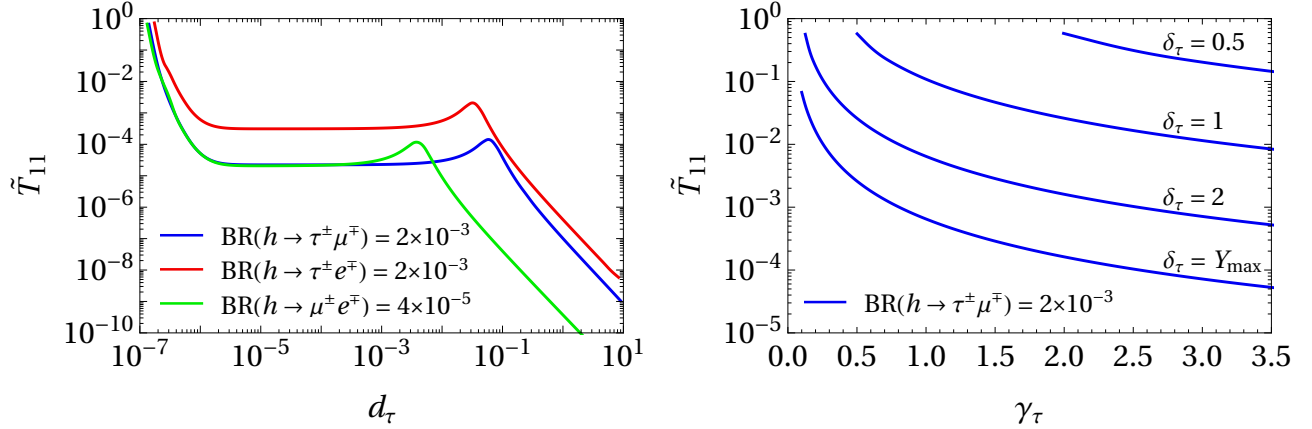


Figure 5: The parameter  $\tilde{T}_{11}$  as a function of the Yukawa couplings. Left panel:  $\tilde{T}_{11}$  versus  $d_\tau$  for fixed values of the  $\text{BR}(h)$  and for  $\delta_\tau = \gamma_\tau = Y_{\text{max}}$ . Right panel:  $\tilde{T}_{11}$  versus  $\gamma_\tau$  for fixed  $\text{BR}(h \rightarrow \tau^\pm \mu^\mp) = 2 \times 10^{-3}$  and for various values of  $\delta_\tau$ , while  $d_\tau = Y_{\text{min}}$  is fixed. The other couplings are fixed through the ratios described in the main text.

- The moduli of the Yukawa coupling constants, *viz.* the  $|d_\ell|$ ,  $|\delta_\ell|$ , and  $|\gamma_\ell|$  are constrained to be larger than  $Y_{\text{min}} = 10^{-6}$  (which is the order of magnitude of the Yukawa coupling of the electron) and smaller than a perturbativity bound  $Y_{\text{max}} = \sqrt{4\pi} \approx 3.5$ .
- We enforce Eqs. (43).
- The triple-scalar couplings are kept fixed:  $\lambda_3 = \lambda_7 = 1$ .
- All the final points are checked to meet the  $3\sigma$  conditions on the  $Z$  invisible decay width in Eq. (E6).

In Fig. 6 and the following figures in this subsection we compare three different fits. In the first case (displayed through blue points and labelled ‘NO’ from now on), we have assumed normal ordering of the light neutrino masses and all the constraints on the other parameters as described in the previous paragraph. The second case (red points and labelled ‘IO’) is similar, but with inverted ordering of the light neutrino masses. In the third case (displayed through green points and labelled ‘ $Y_{\text{min}} = 10^{-7}$ ’) things are as in the first one, except that the lower bound on the Yukawa couplings is set at  $10^{-7}$  instead of  $10^{-6}$ . Furthermore, in all three cases the Yukawa couplings have been assumed real (either positive or negative) throughout. (We have also investigated the case with complex Yukawa couplings and we have found out that its results do not differ much, therefore we do not present a separate case with complex couplings.) Figure 6 shows that points for the NO and IO cases are distributed in similar fashions; in both cases it is possible to find points close to the experimental upper bounds on  $\text{BR}(\ell)$  and/or  $\text{BR}(h)$ . In the numerical analysis we have found that<sup>8</sup> most points have the  $d_\ell$  close to the lower bound  $Y_{\text{min}} = 10^{-6}$ ; therefore, in the third case we have relaxed this bound down to  $10^{-7}$ ;

<sup>8</sup>See the histograms of Fig. 9.

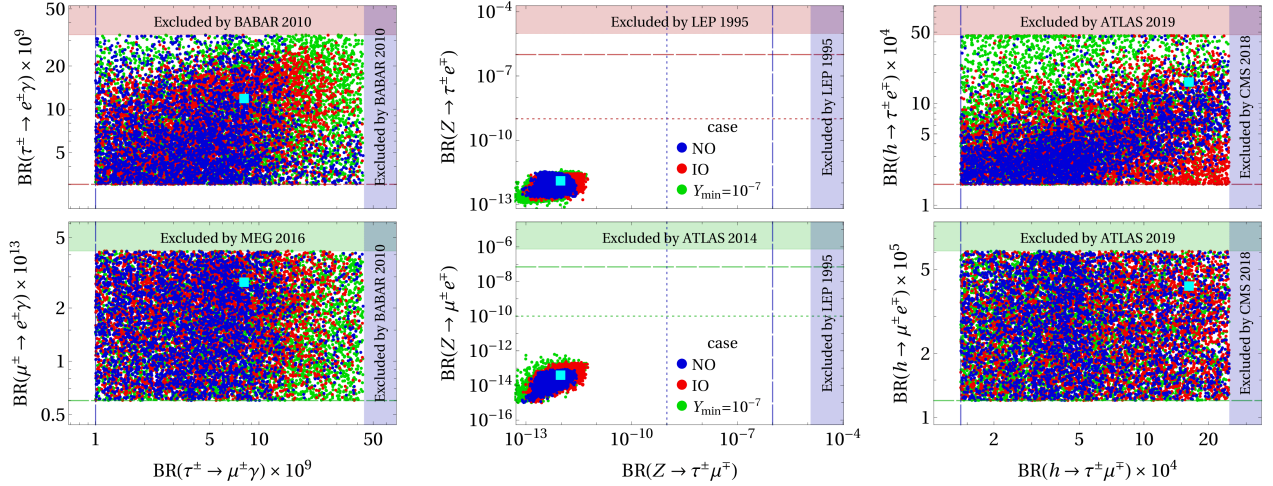


Figure 6: Scatter plots of the branching ratios of LFV decays for three different cases. Blue points have normal ordering (NO) of the light-neutrino masses, red points have inverted ordering, and green points have NO but a lower bound on the Yukawa couplings  $Y_{\min} = 10^{-7}$ . A cyan square marks the benchmark point 1 of table 3. The shadowed bands are the present experimental upper bounds on the BRs; dashed and/or dotted lines show the future experimental sensitivities, as described in table 1.

this larger freedom allows to get larger BRs, as shown by the green points in Fig. 6.<sup>9</sup>

We have also found that free Majorana phases permit larger BRs for the decays with  $\tau^\pm$ ; these branching ratios may be up to six times smaller with fixed  $\alpha_{21} = \alpha_{31} = 0$ . Thus, it is very advantageous to fit the Majorana phases instead of fixing them at any pre-assigned values.

In Fig. 7 we display correlation plots of  $\text{BR}(\ell)$  with  $\text{BR}(Z)$ . One sees that there is a correlation between  $\text{BR}(\tau^\pm \rightarrow \mu^\pm \gamma)$  and  $\text{BR}(Z \rightarrow \tau^\pm \mu^\mp)$ , and a correlation between  $\text{BR}(\tau^\pm \rightarrow e^\pm \gamma)$  and  $\text{BR}(Z \rightarrow \tau^\pm e^\mp)$ ; the origin of these correlations is described in subsection 3.5. We can also see that the present upper bounds (BABAR 2010) on the  $\text{BR}(\tau)$  lead, in our model, to a maximum of  $\text{BR}(Z \rightarrow \tau^\pm \mu^\mp) \sim 6 \times 10^{-12}$  and of  $\text{BR}(Z \rightarrow \tau^\pm e^\mp) \sim 4 \times 10^{-12}$ . Unfortunately, these values  $\text{BR}(Z) \sim 10^{-12}$  are much lower than the future experimental sensitivity. We point out that in other models (see for instance Refs. [24], [38], and [39]) there are also correlations between the  $\text{BR}(Z)$  and the  $\text{BR}(\ell)$ , and also with the branching ratios for three-body LFV decays  $\ell_1^\pm \rightarrow \ell_2^\pm \ell_3^+ \ell_3^-$ .

There are papers claiming that  $\text{BR}(h \rightarrow \tau^\pm \mu^\mp)$  is constrained by either [43,44]  $\text{BR}(\tau^\pm \rightarrow \mu^\pm \gamma)$  or [45]  $\text{BR}(\mu^\pm \rightarrow e^\pm \gamma)$ , in their specific models. In a study of the type-III 2HDM [41] and in a model with  $L_\mu - L_\tau$  symmetry [51] no such constraints have been found, but correlations between  $\text{BR}(h \rightarrow \tau^\pm \mu^\mp)$  and  $\text{BR}(\tau^\pm \rightarrow \mu^\pm \gamma)$  are visible. In our model we did *not* find correlations between the  $\text{BR}(\ell)$  and  $\text{BR}(h)$ .

<sup>9</sup>The numerical analysis also shows that most points have the  $\delta_\ell$  close to the upper bound  $Y_{\max} = \sqrt{4\pi} \approx 3.5$ . Therefore we have also performed a fit where we have relaxed this bound up to  $4\pi \approx 12.5$ . That extra fit, that we do not display in this paper, did *not* seem to produce any improvements in  $\text{BR}(\ell)$  and  $\text{BR}(h)$ , but it did produce larger  $\text{BR}(Z)$ ; however, the latter were still very much below the future experimental sensitivities. Thus, it appears to us that there are no advantages in allowing the Yukawa couplings to be larger than  $\sqrt{4\pi}$ .

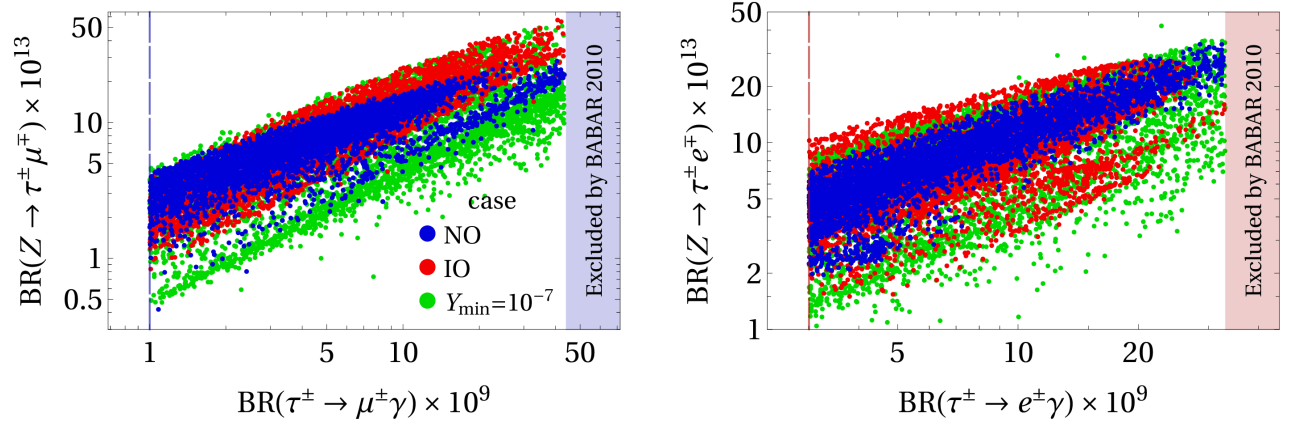


Figure 7: Correlation plots between the BRs of the  $\tau$  decays and the BRs of the  $Z$  decays, for the three different cases of Fig. 6; the points are the same ones as in that figure and with the same colour coding. The shadowed bands are excluded by the present experimental data; dashed lines mark the future experimental sensitivities.

From Fig. 1 we know that large  $\text{BR}(\ell)$  prefer small values of the Yukawa couplings  $d_\ell$ , and that in turn leads to a small heavy-neutrino mass  $m_4$ . This is confirmed by the results of the fits that are shown in Fig. 8. We see that  $m_4$  lies in between  $\sim 0.5$  TeV and  $\sim 2.5$  TeV, except

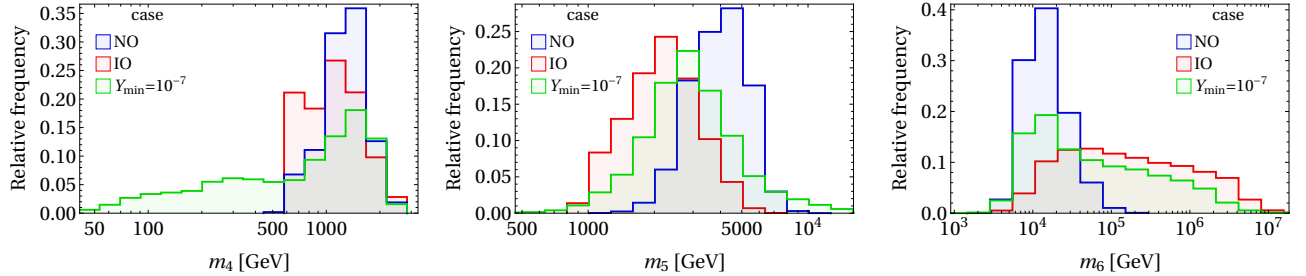


Figure 8: Histograms of the heavy-neutrino masses for the three cases described in the main text and in the caption of Fig. 6.

in the case  $Y_{\min} = 10^{-7}$ , for which  $m_4$  may be as small as 45 GeV. The mass  $m_5$  is in between  $\sim 1$  TeV and  $\sim 10$  TeV for all cases, and the mass  $m_6$  is in between  $\sim 2.5$  TeV and  $\sim 100$  TeV for NO, or  $\sim 10^4$  TeV for IO and  $Y_{\min} = 10^{-7}$ .

In Fig. 9 we display histograms of the moduli of the Yukawa couplings for all three cases. Since we have fitted the  $\text{BR}(\ell)$  to experimentally reachable ranges, the moduli of the  $d_\ell$  always have very small values  $\lesssim 10^{-5}$ ; most points are distributed very close to  $Y_{\min} = 10^{-6}$ , except of course in the case  $Y_{\min} = 10^{-7}$ . If we had set  $Y_{\min}$  much larger than  $10^{-6}$ , then it would not have been possible to obtain  $\text{BR}(\ell)$  visible in the next generation of experiments. For the relaxed bound  $Y_{\min} = 10^{-7}$ , the distribution of the  $|d_\ell|$  is more uniform. The second row in Fig. 9 shows that for all cases the  $|\delta_\ell|$  have values quite close to the unitarity upper bound. In the third row of Fig. 9 one sees that the moduli of the couplings  $\gamma_\ell$  vary in wider ranges, from  $\sim 10^{-4}$  to  $Y_{\max}$ , than the right panel of Fig. 3 might suggest. That happens because the

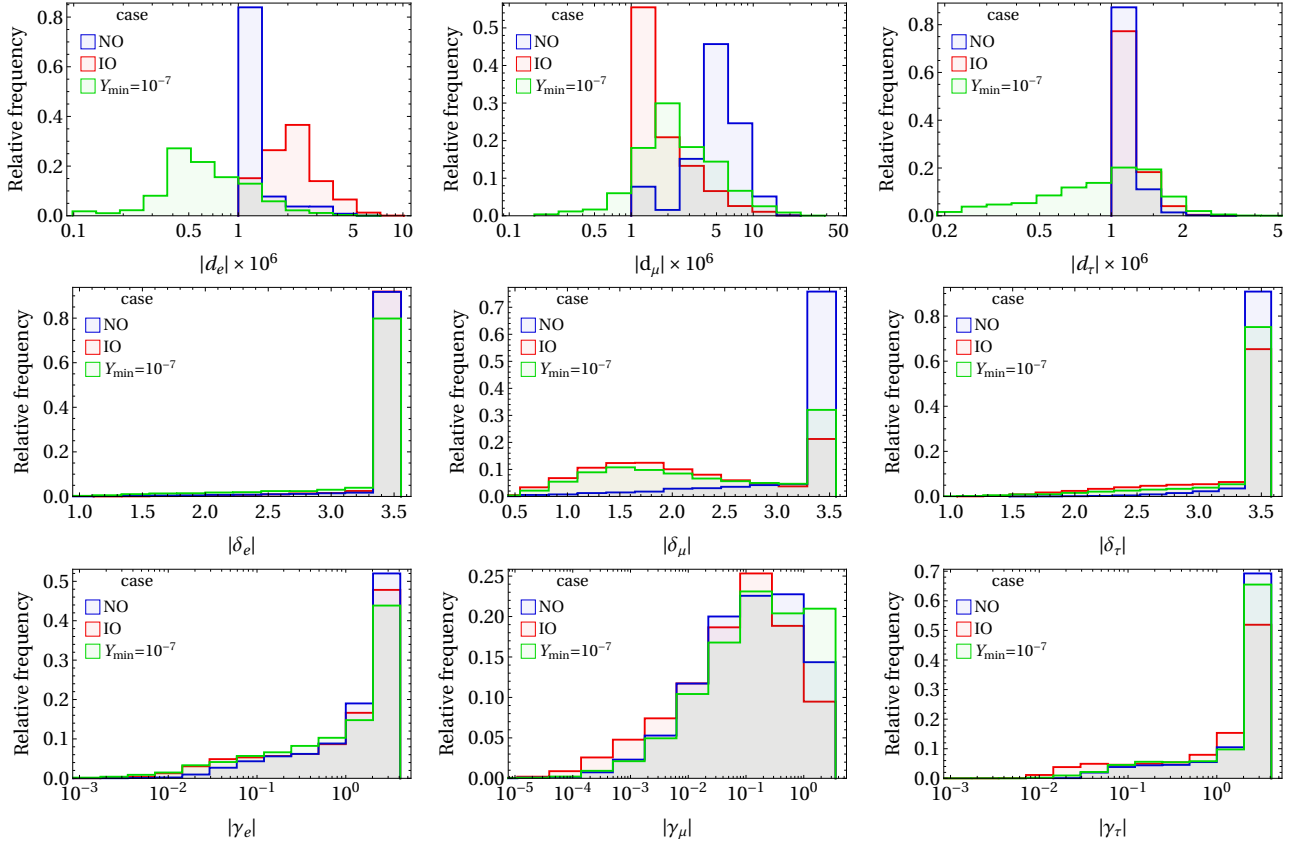


Figure 9: The distributions of the moduli of the Yukawa couplings for the three cases described in the main text and in the caption of Fig. 6.

parameter  $\tilde{T}_{11}$  has a strong impact on  $\text{BR}(h)$  so that, for smaller values of  $\gamma_\ell$ , larger values of  $\tilde{T}_{11}$  still allow  $\text{BR}(h)$  to reach experimentally reachable ranges—as can also be seen in the right panel of Fig. 5.

Still, most points have values of  $|\delta_\ell|$  and  $|\gamma_\ell|$  close to  $Y_{\max}$ , and therefore most points have very small values of  $\tilde{T}_{11} \in [10^{-6}, 10^{-3}]$ , as depicted in Fig. 10. However, if only the  $\text{BR}(h)$  are fitted, then the values of  $\tilde{T}_{11}$  are distributed evenly in the range  $[0, 0.05]$ .

In all three fits, it is found that the mixing angles  $\theta_{12,23,13}$ , the Dirac phase  $\delta$ , and the Majorana phases  $\alpha_{21}$  and  $\alpha_{31}$  may have values anywhere in their ranges.

### 3.4 Benchmark points

We produce in table 3 two benchmark points. The first nine lines of that table contain the fitted values of the Yukawa couplings; in the next four lines one finds the fitted values of the lightest-neutrino mass  $m_1$ , Majorana phases  $\alpha_{21}$  and  $\alpha_{31}$ ,<sup>10</sup> and of  $\tilde{T}_{11} = 1 - T_{11} = 1 - x_2$ ; the next three lines contain the computed masses of the heavy neutrinos, ordered as  $m_4 \leq m_5 \leq m_6$ ; the last nine lines display the computed branching ratios. The phase  $\delta$  has been kept fixed at

<sup>10</sup>In point 2 we have fixed  $\alpha_{21} = \alpha_{31} = 0$  instead of fitting them.



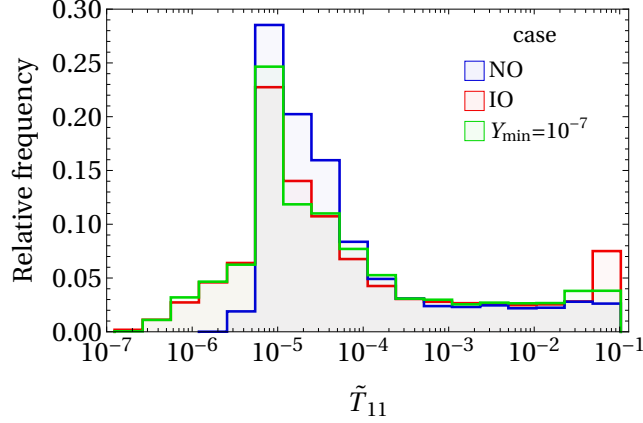


Figure 10: Histograms of  $\tilde{T}_{11}$  for the three cases described in the main text and in the caption of Fig. 6.

its central experimental value during the fit of the BRs.

Point 2 is a fit just of the three Higgs decays, while letting the  $\text{BR}(\ell)$  and  $\text{BR}(Z)$  be as small as they wish. Point 1 indicates that small values of the  $d_\ell$  and large values of the  $\delta_\ell$  are required in order to find  $\text{BR}(\ell)$  in experimentally reachable ranges; point 2 indicates that, for fits just of  $\text{BR}(h)$ , those Yukawa couplings may be relaxed and it is possible to find experimentally reachable  $\text{BR}(h)$  by varying the nine Yukawa couplings in the range  $[0.1, 0.5]$ ; in that case, due to the larger  $d_\ell$ , the masses of the heavy neutrinos become quite large too.

One may study the behaviour of the BRs when varying one parameter of the benchmark point while the other parameters remain fixed. In Fig. 11 we illustrate the evolution of the BRs when the mass of the charged scalar  $m_{H^+}$  is changed, while the other parameters are kept fixed at their values of benchmark point 1. One observes that when  $m_{H^+}$  increases the BRs usually

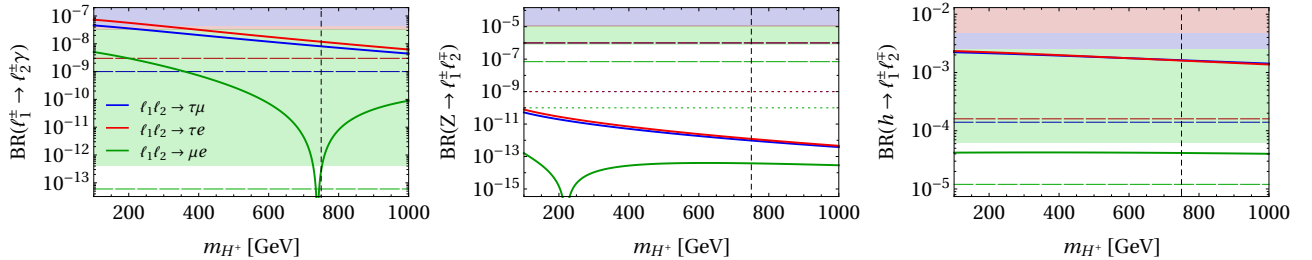


Figure 11: The decay rates *versus* the mass of the charged scalar  $m_{H^+}$ ; all the other parameters are kept at their values of benchmark point 1, *cf.* table 3. The vertical dashed lines mark the value  $m_{H^+} = 750$  GeV.

decrease monotonically, except for  $(\ell_1, \ell_2) = (\mu, e)$ , where one observes a partial cancellation of amplitudes that leads to a sudden drop of  $\text{BR}(\mu^\pm \rightarrow e^\pm \gamma)$  near  $m_{H^+} = 750$  GeV; our fit has indeed used that effect in order to obtain  $\text{BR}(\mu^\pm \rightarrow e^\pm \gamma)$  smaller than its experimental upper bound. It should be noticed that  $m_{H^+}$  has a larger impact on  $\text{BR}(\ell)$  and  $\text{BR}(Z)$  than on  $\text{BR}(h)$ , as seen in Fig. 11.

	Point 1	Point 2
$d_e \times 10^6$	1.0	$10^5$
$d_\mu \times 10^6$	4.0	$10^5$
$d_\tau \times 10^6$	1.0	$3.5 \times 10^5$
$\delta_e$	3.5	0.43
$\delta_\mu$	3.5	0.42
$\delta_\tau$	3.5	0.19
$\gamma_e$	0.1	0.23
$\gamma_\mu$	1.0	0.236
$\gamma_\tau$	3.0	0.19
$m_1$ (meV)	16.5	1.23
$\alpha_{21}$ (rad)	3.515	0
$\alpha_{31}$ (rad)	1.060	0
$\hat{T}_{11}$	$1.0 \times 10^{-4}$	0.047
$m_4$ (TeV)	1.16066	$9.49989 \times 10^9$
$m_5$ (TeV)	3.54866	$6.87952 \times 10^{10}$
$m_6$ (TeV)	6.67826	$9.66979 \times 10^{11}$
$\text{BR}(\tau^\pm \rightarrow \mu^\pm \gamma) \times 10^9$	8.1	—
$\text{BR}(\tau^\pm \rightarrow e^\pm \gamma) \times 10^9$	12	—
$\text{BR}(\mu^\pm \rightarrow e^\pm \gamma) \times 10^{13}$	2.8	—
$\text{BR}(Z \rightarrow \tau^\pm \mu^\mp) \times 10^{13}$	9.6	—
$\text{BR}(Z \rightarrow \tau^\pm e^\mp) \times 10^{13}$	12	—
$\text{BR}(Z \rightarrow \mu^\pm e^\mp) \times 10^{15}$	38	—
$\text{BR}(h \rightarrow \tau^\pm \mu^\mp) \times 10^3$	1.6	1.4
$\text{BR}(h \rightarrow \tau^\pm e^\mp) \times 10^3$	1.6	1.6
$\text{BR}(h \rightarrow \mu^\pm e^\mp) \times 10^5$	4.1	3.6

Table 3: Two benchmark points. The neutrino mass ordering is normal for both points. The phase  $\delta = 3.80$  rad is the same for both points. The mixing angles  $\theta_{12,23,13}$  and the squared-mass differences  $\Delta_{\text{solar}}$  and  $\Delta_{\text{atmospheric}}$  are fixed at their best-fit (NO) values in table 2. The mass of the charged scalar is  $m_{H^+} = 750$  GeV in both points too. The symbol ‘—’ stands for a tiny number  $\lesssim 10^{-20}$ .

In Fig. 12 we display the BRs as functions of the Majorana phase  $\alpha_{31}$ , with the other input variables kept fixed at their values of benchmark point 1. Here too, for  $(\ell_1, \ell_2) = (\mu, e)$ , one observes a sudden drop of the branching ratios when  $\alpha_{31} = 1.06$ , which is precisely the value that we have utilized in benchmark point 1. A similar behaviour of the green lines also occurs with other parameters, besides  $m_{H^+}$  (Fig. 11) and  $\alpha_{31}$  (Fig. 12). This illustrates the fact that the values of the parameters must be chosen very carefully if we want to find all six  $\text{BR}(\ell)$  and  $\text{BR}(h)$  simultaneously close to their experimental upper bounds. The main difficulties arise because of the necessary suppression of the  $\mu$  decays: the upper bound on  $\text{BR}(\mu^\pm \rightarrow e^\pm \gamma)$  differs from the upper bound on  $\text{BR}(\tau^\pm \rightarrow \mu^\pm \gamma)$  by five orders of magnitude. Fortunately, our minimization procedure allows this to be done quite efficiently.



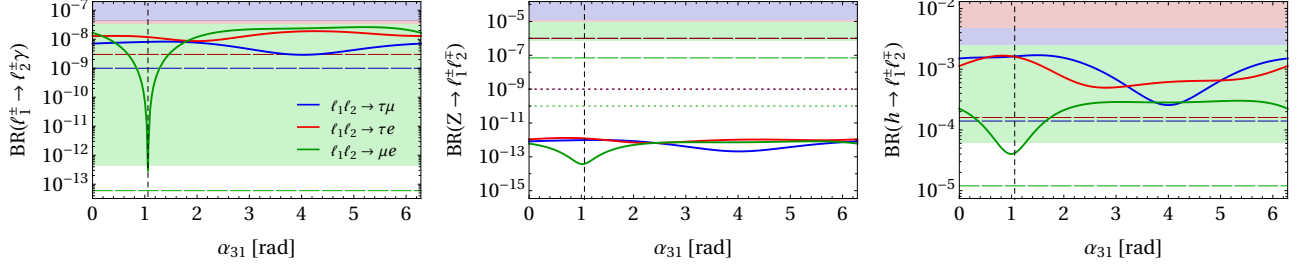


Figure 12: The decay rates *versus* the Majorana phase  $\alpha_{31}$ ; all the other parameters are kept at their values of benchmark point 1, *cf.* table 3. The vertical dashed lines mark the value  $\alpha_{31} = 1.06$  of benchmark point 1.

### 3.5 Amplitudes

Through numerical simulations we have found that actually only few amplitudes have large impact on the  $\text{BR}(\ell)$ , and this allows one to write simpler formulas for the BRs.

For the decays  $\ell_1^\pm \rightarrow \ell_2^\pm \gamma$ , the amplitudes (B14), computed from the diagrams of Fig. 14, are dominant. Specifically, the amplitude  $a_{l,H}$  in Eq. (B14a) gives the main impact on the BRs. Therefore, the approximate decay width is

$$\Gamma(\ell_1^\pm \rightarrow \ell_2^\pm \gamma) \approx \frac{m_{\ell_1}^4 - m_{\ell_2}^4}{16\pi m_{\ell_1}^3} |\mathcal{S}e|^2 |a_{l,H}|^2. \quad (54)$$

This yields the following approximate formulas for the BRs:

$$\text{BR}(\tau^\pm \rightarrow \mu^\pm \gamma) \approx (5.733 \times 10^4) |a_{l,H}|^2, \quad (55a)$$

$$\text{BR}(\tau^\pm \rightarrow e^\pm \gamma) \approx (5.733 \times 10^4) |a_{l,H}|^2, \quad (55b)$$

$$\text{BR}(\mu^\pm \rightarrow e^\pm \gamma) \approx (2.580 \times 10^{10}) |a_{l,H}|^2. \quad (55c)$$

Similarly, the amplitude  $\bar{a}_{l,H}$  in Eq. (C9a) gives the main impact on the  $\text{BR}(Z)$ , and it alone gives the approximate decay width<sup>11</sup>

$$\begin{aligned} \Gamma(Z \rightarrow \ell_1^\pm \ell_2^\mp) &\approx \frac{\sqrt{m_{\ell_1}^4 - 2m_Z^2(m_{\ell_1}^2 + m_{\ell_2}^2) + (m_{\ell_1}^2 - m_{\ell_2}^2)^2}}{48\pi m_Z^5} \\ &\times |\mathcal{S}e|^2 \left[ 2m_Z^4 - m_Z^2(m_{\ell_1}^2 + m_{\ell_2}^2) - (m_{\ell_1}^2 - m_{\ell_2}^2)^2 \right] |\bar{a}_{l,H}|^2, \end{aligned} \quad (56)$$

from which follow the approximate formula for the BRs

$$\text{BR}(Z \rightarrow \ell_1^\pm \ell_2^\mp) \approx (1.781 \times 10^{-6}) |\bar{a}_{l,H}|^2. \quad (57)$$

The amplitudes for the Higgs decays differ from the other decays. In the case of the amplitudes from the self-energy-like diagrams in Fig. 17, with the charged scalar  $H^\pm$ , give the

<sup>11</sup>Due to the similarities between  $a_{l,H}$  in Eq. (B14a) and  $\bar{a}_{l,H}$  in Eq. (C9a), there are correlations between  $\text{BR}(\ell_1^\pm \rightarrow \ell_2^\pm \gamma)$  and  $\text{BR}(Z \rightarrow \ell_1^\pm \ell_2^\mp)$ , as already seen in Fig. 7.

strongest impact on the branching ratios. Specifically, the amplitude  $d_{rb,17(a,b)}$  in Eq. (D4b) is significant for largish values of the Yukawa couplings  $d_\ell$ , while the amplitude  $d_{lb,17(a,b)}$  in Eq. (D4a) is significant for all values of the  $d_\ell$ . Unlike the case of the  $Z$  decays, for the  $h$  decays the amplitudes coming from the diagrams with two internal neutrino lines, depicted in Fig. 20, are important too. Specifically, the amplitudes  $d_{lb,20(a)}$  and  $d_{rb,20(a)}$  in Eqs. (D11) have a strong impact on the decay rates. So, using Eq. (D2) we may write the approximate formulas for the BRs

$$\begin{aligned} \text{BR}(h \rightarrow \tau^\pm \mu^\mp) &\approx (2.451 \times 10^{-2}) \left( |\bar{d}_{lb}|^2 + |\bar{d}_{rb}|^2 \right) \\ &\quad - (1.176 \times 10^{-6}) \text{Re}(\bar{d}_{lb} \bar{d}_{rb}^*), \end{aligned} \quad (58a)$$

$$\begin{aligned} \text{BR}(h \rightarrow \tau^\pm e^\mp) &\approx (2.451 \times 10^{-2}) \left( |\bar{d}_{lb}|^2 + |\bar{d}_{rb}|^2 \right) \\ &\quad - (5.690 \times 10^{-9}) \text{Re}(\bar{d}_{lb} \bar{d}_{rb}^*), \end{aligned} \quad (58b)$$

$$\begin{aligned} \text{BR}(h \rightarrow \mu^\pm e^\mp \gamma) &\approx (2.452 \times 10^{-2}) \left( |\bar{d}_{lb}|^2 + |\bar{d}_{rb}|^2 \right) \\ &\quad - (3.384 \times 10^{-10}) \text{Re}(\bar{d}_{lb} \bar{d}_{rb}^*), \end{aligned} \quad (58c)$$

where

$$\bar{d}_{lb} = d_{lb,17(a,b)} + d_{lb,20(a)}, \quad \bar{d}_{rb} = d_{rb,17(a,b)} + d_{rb,20(a)}. \quad (59)$$

In order to check the correctness of the approximate BRs of Eqs. (55), (57), and (58)–(59) we have calculated the asymmetry between the exact BRs and the approximate ones,

$$\text{BR}_{\text{asymmetry}} \equiv \frac{|\text{BR}_{\text{exact}} - \text{BR}_{\text{approximate}}|}{\text{BR}_{\text{exact}} + \text{BR}_{\text{approximate}}}. \quad (60)$$

Using the points of case ‘NO’, these asymmetries are displayed in Fig. 13. One sees that

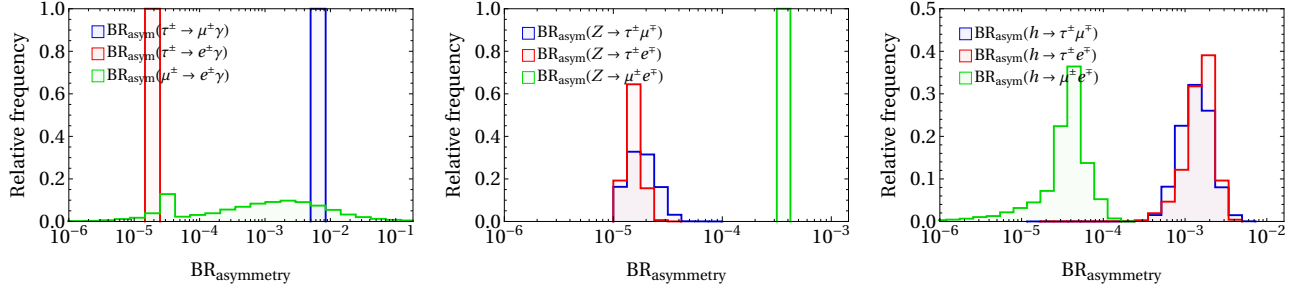


Figure 13: Histograms of the asymmetries between the exact nine branching ratios and their approximate expressions in Eqs. (55), (57), and (58)–(59).

$\text{BR}_{\text{asymmetry}} \lesssim 0.1$ , hence the approximate BRs give quite accurate results. The approximate expressions for the BRs are very useful for intermediate calculations of the fitting procedure, where the calculations need to be repeated many times, before the final result is calculated by using the exact expressions. This computational trick has saved us a lot of calculation time.

## 4 Summary and conclusions

Here we summarize our main findings:

- The amplitudes with the charged scalar are especially important and they allow one to obtain decay rates of  $\ell_1^\pm \rightarrow \ell_2^\pm \gamma$  and  $h \rightarrow \ell_1^\pm \ell_2^\mp$  close to the experimental upper bounds, as shown in Fig. 1.
- Because of the suppression of  $\mu^\pm \rightarrow e^\pm \gamma$ , the values of the parameters must be finetuned in order to find all six decays  $\ell_1^\pm \rightarrow \ell_2^\pm \gamma$  and  $h \rightarrow \ell_1^\pm \ell_2^\mp$  simultaneously close to their respective experimental upper bounds.
- The decays  $\ell_1^\pm \rightarrow \ell_2^\pm \gamma$  necessitate large values of the Yukawa couplings  $\delta_\ell$  and small values of the Yukawa couplings  $d_\ell$  (implying a very low seesaw scale) in order to be visible.
- The decays  $Z \rightarrow \ell_1^\pm \ell_2^\mp$  correlate with the decays  $\ell_1^\pm \rightarrow \ell_2^\pm \gamma$  and behave similarly as functions of the parameters. Unfortunately, though, the decays  $Z \rightarrow \ell_1^\pm \ell_2^\mp$  will remain invisible in all the planned experiments, in the context of our model.
- The decays  $h \rightarrow \ell_1^\pm \ell_2^\mp$  behave quite differently from the  $\ell_1^\pm \rightarrow \ell_2^\pm \gamma$  and  $Z \rightarrow \ell_1^\pm \ell_2^\mp$ . They prefer largish values of the  $d_\ell$  but, thanks to the freedom to adjust parameters  $\gamma_\ell$  and  $T_{11}$ , they might be visible in future experiments, maybe even together with the decays  $\ell_1^\pm \rightarrow \ell_2^\pm \gamma$ .
- The Majorana phases have a significant impact on the branching ratios of all the decays. One should refrain from fixing them at some pre-assigned values if one wants to obtain a good fit.
- Both cases of normal and inverted ordering of the light-neutrino masses yield similar decay rates, when the Majorana phases are included.
- When the mass of the charged scalar increases, the values of BRs decrease. Still, for  $m_{H^\pm} \lesssim 1.5 \text{ TeV}$  the decays  $\ell_1^\pm \rightarrow \ell_2^\pm \gamma$  and  $h \rightarrow \ell_1^\pm \ell_2^\mp$  might be visible in future experiments.
- The approximate expressions of the BRs described in section 3.5 give quite accurate results and are very useful in an initial stage of the fitting procedure.

**Acknowledgements:** D.J. thanks both Jorge C. Romão and Duarte Fontes for useful discussions. He also thanks the Lithuanian Academy of Sciences for financial support through projects DaFi2019 and DaFi2021; he was also supported by a COST STSM grant through action CA16201. L.L. warmly thanks the Institute of Theoretical Physics and Astronomy of the University of Vilnius for the hospitality extended during a visit where part of this work has been done. L.L. also thanks the Portuguese Foundation for Science and Technology for support through projects CERN/FIS-PAR/0004/2019, CERN/FIS-PAR/0008/2019, PTDC/FIS-PAR/29436/2017, UIDB/00777/2020, and UIDP/00777/2020.

## A Passarino–Veltman functions

The relevant Passarino–Veltman (PV) functions are defined in the following way. Let the dimension of space–time be  $d = 4 - \epsilon$  with  $\epsilon \rightarrow 0$ . We define

$$\mathcal{D}k := \mu^\epsilon \frac{d^d k}{(2\pi)^d}, \quad \mathcal{S} := \frac{i}{16\pi^2}, \quad \text{div} := \frac{2}{\epsilon} - \gamma + \ln(4\pi\mu^2), \quad (\text{A1})$$

where  $\gamma$  is Euler’s constant. Then,

$$\int \mathcal{D}k \frac{1}{k^2 - A} \frac{1}{(k+p)^2 - B} = \mathcal{S} B_0(p^2, A, B), \quad (\text{A2a})$$

$$\int \mathcal{D}k k^\theta \frac{1}{k^2 - A} \frac{1}{(k+p)^2 - B} = \mathcal{S} p^\theta B_1(p^2, A, B), \quad (\text{A2b})$$

and

$$\int \mathcal{D}k \frac{1}{k^2 - A} \frac{1}{(k+p)^2 - B} \frac{1}{(k+q)^2 - C} = \mathcal{S} C_0[p^2, (p-q)^2, q^2, A, B, C], \quad (\text{A3a})$$

$$\begin{aligned} \int \mathcal{D}k k^\theta \frac{1}{k^2 - A} \frac{1}{(k+p)^2 - B} \frac{1}{(k+q)^2 - C} &= \mathcal{S} \{ p^\theta C_1[p^2, (p-q)^2, q^2, A, B, C] \\ &\quad + q^\theta C_2[p^2, (p-q)^2, q^2, A, B, C] \}, \end{aligned} \quad (\text{A3b})$$

$$\begin{aligned} \int \mathcal{D}k k^\theta k^\psi \frac{1}{k^2 - A} \frac{1}{(k+p)^2 - B} \frac{1}{(k+q)^2 - C} &= \mathcal{S} \{ p^\theta p^\psi C_{11}[p^2, (p-q)^2, q^2, A, B, C] \\ &\quad + q^\theta q^\psi C_{22}[p^2, (p-q)^2, q^2, A, B, C] \\ &\quad + (p^\theta q^\psi + q^\theta p^\psi) C_{12}[p^2, (p-q)^2, q^2, A, B, C] \\ &\quad + g^{\theta\psi} C_{00}[p^2, (p-q)^2, q^2, A, B, C] \}. \end{aligned} \quad (\text{A3c})$$

By manipulating Eqs. (A2) and (A3) one may derive various identities among the PV functions. For instance, multiplying Eq. (A3c) by  $g_{\theta\psi}$  one finds that

$$\begin{aligned} &(p^2 C_{11} + q^2 C_{22} + 2p \cdot q C_{12} + d C_{00} - A C_0) [p^2, (p-q)^2, q^2, A, B, C] \\ &= B_0[(p-q)^2, B, C], \end{aligned} \quad (\text{A4})$$

which does not depend on  $A$ .

Some PV functions in Eqs. (A2) and (A3) have  $1/\epsilon$  divergences that are independent of the arguments of the PV functions. Thus,

$$B_0(p^2, A, B) = \frac{2}{\epsilon} + \text{finite}, \quad (\text{A5a})$$

$$B_1(p^2, A, B) = -\frac{1}{\epsilon} + \text{finite}, \quad (\text{A5b})$$

$$C_{00} [p^2, (p-q)^2, q^2, A, B, C] = \frac{1}{2\epsilon} + \text{finite}. \quad (\text{A5c})$$

All other PV functions in Eqs. (A2) and (A3) converge when  $\epsilon \rightarrow 0$ .

Defining

$$\Delta_2 := A(1-x) + Bx - p^2 x(1-x), \quad (\text{A6a})$$

$$\begin{aligned} \Delta_3 &:= A(1-x-y) + Bx + Cy \\ &\quad - p^2 x(1-x-y) - (p-q)^2 yx - q^2 (1-x-y)y, \end{aligned} \quad (\text{A6b})$$

one has

$$B_0(p^2, A, B) = \text{div} - \int_0^1 dx \ln \Delta_2, \quad (\text{A7a})$$

$$B_1(p^2, A, B) = -\frac{\text{div}}{2} + \int_0^1 dx x \ln \Delta_2, \quad (\text{A7b})$$

$$C_0[p^2, (p-q)^2, q^2, A, B, C] = \int_0^1 dx \int_0^{1-x} dy \frac{-1}{\Delta_3}, \quad (\text{A8a})$$

$$C_1[p^2, (p-q)^2, q^2, A, B, C] = \int_0^1 dx \int_0^{1-x} dy \frac{x}{\Delta_3}, \quad (\text{A8b})$$

$$C_2[p^2, (p-q)^2, q^2, A, B, C] = \int_0^1 dx \int_0^{1-x} dy \frac{y}{\Delta_3}, \quad (\text{A8c})$$

$$C_{11}[p^2, (p-q)^2, q^2, A, B, C] = \int_0^1 dx \int_0^{1-x} dy \frac{-x^2}{\Delta_3}, \quad (\text{A8d})$$

$$C_{22}[p^2, (p-q)^2, q^2, A, B, C] = \int_0^1 dx \int_0^{1-x} dy \frac{-y^2}{\Delta_3}, \quad (\text{A8e})$$

$$C_{12}[p^2, (p-q)^2, q^2, A, B, C] = \int_0^1 dx \int_0^{1-x} dy \frac{-xy}{\Delta_3}, \quad (\text{A8f})$$

$$C_{00}[p^2, (p-q)^2, q^2, A, B, C] = \frac{\text{div}}{4} - \frac{1}{2} \int_0^1 dx \int_0^{1-x} dy \ln \Delta_3. \quad (\text{A8g})$$

We next introduce specific notations for some PV functions that are used in appendices B, C, and D. Thus,

$$e_0 := C_0(m_{\ell_1}^2, q^2, m_{\ell_2}^2, m_i^2, m_a^2, m_a^2), \quad (\text{A9a})$$

$$e_1 := C_1(m_{\ell_1}^2, q^2, m_{\ell_2}^2, m_i^2, m_a^2, m_a^2), \quad (\text{A9b})$$

$$e_2 := C_2(m_{\ell_1}^2, q^2, m_{\ell_2}^2, m_i^2, m_a^2, m_a^2), \quad (\text{A9c})$$

$$e_{11} := C_{11}(m_{\ell_1}^2, q^2, m_{\ell_2}^2, m_i^2, m_a^2, m_a^2), \quad (\text{A9d})$$

$$e_{22} := C_{22}(m_{\ell_1}^2, q^2, m_{\ell_2}^2, m_i^2, m_a^2, m_a^2), \quad (\text{A9e})$$

$$e_{12} := C_{12}(m_{\ell_1}^2, q^2, m_{\ell_2}^2, m_i^2, m_a^2, m_a^2), \quad (\text{A9f})$$

$$e_{00} := C_{00}(m_{\ell_1}^2, q^2, m_{\ell_2}^2, m_i^2, m_a^2, m_a^2), \quad (\text{A9g})$$

$$f_0 := C_0(m_{\ell_1}^2, q^2, m_{\ell_2}^2, m_i^2, m_W^2, m_W^2), \quad (\text{A10a})$$

$$f_1 := C_1 (m_{\ell_1}^2, q^2, m_{\ell_2}^2, m_i^2, m_W^2, m_W^2), \quad (\text{A10b})$$

$$f_2 := C_2 (m_{\ell_1}^2, q^2, m_{\ell_2}^2, m_i^2, m_W^2, m_W^2), \quad (\text{A10c})$$

$$f_{11} := C_{11} (m_{\ell_1}^2, q^2, m_{\ell_2}^2, m_i^2, m_W^2, m_W^2), \quad (\text{A10d})$$

$$f_{22} := C_{22} (m_{\ell_1}^2, q^2, m_{\ell_2}^2, m_i^2, m_W^2, m_W^2), \quad (\text{A10e})$$

$$f_{12} := C_{12} (m_{\ell_1}^2, q^2, m_{\ell_2}^2, m_i^2, m_W^2, m_W^2), \quad (\text{A10f})$$

$$f_{00} := C_{00} (m_{\ell_1}^2, q^2, m_{\ell_2}^2, m_i^2, m_W^2, m_W^2), \quad (\text{A10g})$$

$$g_0 := C_0 (m_{\ell_1}^2, q^2, m_{\ell_2}^2, m_a^2, m_i^2, m_j^2), \quad (\text{A11a})$$

$$g_1 := C_1 (m_{\ell_1}^2, q^2, m_{\ell_2}^2, m_a^2, m_i^2, m_j^2), \quad (\text{A11b})$$

$$g_2 := C_2 (m_{\ell_1}^2, q^2, m_{\ell_2}^2, m_a^2, m_i^2, m_j^2), \quad (\text{A11c})$$

$$g_{11} := C_{11} (m_{\ell_1}^2, q^2, m_{\ell_2}^2, m_a^2, m_i^2, m_j^2), \quad (\text{A11d})$$

$$g_{22} := C_{122} (m_{\ell_1}^2, q^2, m_{\ell_2}^2, m_a^2, m_i^2, m_j^2), \quad (\text{A11e})$$

$$g_{12} := C_{12} (m_{\ell_1}^2, q^2, m_{\ell_2}^2, m_a^2, m_i^2, m_j^2), \quad (\text{A11f})$$

$$g_{00} := C_{00} (m_{\ell_1}^2, q^2, m_{\ell_2}^2, m_a^2, m_i^2, m_j^2), \quad (\text{A11g})$$

$$h_0 := C_0 (m_{\ell_1}^2, q^2, m_{\ell_2}^2, m_W^2, m_i^2, m_j^2), \quad (\text{A12a})$$

$$h_1 := C_1 (m_{\ell_1}^2, q^2, m_{\ell_2}^2, m_W^2, m_i^2, m_j^2), \quad (\text{A12b})$$

$$h_2 := C_2 (m_{\ell_1}^2, q^2, m_{\ell_2}^2, m_W^2, m_i^2, m_j^2), \quad (\text{A12c})$$

$$h_{11} := C_{11} (m_{\ell_1}^2, q^2, m_{\ell_2}^2, m_W^2, m_i^2, m_j^2), \quad (\text{A12d})$$

$$h_{22} := C_{22} (m_{\ell_1}^2, q^2, m_{\ell_2}^2, m_W^2, m_i^2, m_j^2), \quad (\text{A12e})$$

$$h_{12} := C_{12} (m_{\ell_1}^2, q^2, m_{\ell_2}^2, m_W^2, m_i^2, m_j^2), \quad (\text{A12f})$$

$$h_{00} := C_{00} (m_{\ell_1}^2, q^2, m_{\ell_2}^2, m_W^2, m_i^2, m_j^2), \quad (\text{A12g})$$

$$j_0 := C_0 (m_{\ell_1}^2, q^2, m_{\ell_2}^2, m_i^2, m_a^2, m_{a'}^2), \quad (\text{A13a})$$

$$j_1 := C_1 (m_{\ell_1}^2, q^2, m_{\ell_2}^2, m_i^2, m_a^2, m_{a'}^2), \quad (\text{A13b})$$

$$j_2 := C_2 (m_{\ell_1}^2, q^2, m_{\ell_2}^2, m_i^2, m_a^2, m_{a'}^2), \quad (\text{A13c})$$

$$k_0 := C_0 (m_{\ell_1}^2, q^2, m_{\ell_2}^2, m_i^2, m_W^2, m_a^2), \quad (\text{A14a})$$

$$k_1 := C_1 (m_{\ell_1}^2, q^2, m_{\ell_2}^2, m_i^2, m_W^2, m_a^2), \quad (\text{A14b})$$

$$k_2 := C_2 (m_{\ell_1}^2, q^2, m_{\ell_2}^2, m_i^2, m_W^2, m_a^2), \quad (\text{A14c})$$

$$k_{00} := C_{00} (m_{\ell_1}^2, q^2, m_{\ell_2}^2, m_i^2, m_W^2, m_a^2), \quad (\text{A14d})$$

$$k_{11} := C_{11} (m_{\ell_1}^2, q^2, m_{\ell_2}^2, m_i^2, m_W^2, m_a^2), \quad (\text{A14e})$$

$$k_{22} := C_{22} (m_{\ell_1}^2, q^2, m_{\ell_2}^2, m_i^2, m_W^2, m_a^2), \quad (\text{A14f})$$

$$k_{12} := C_{12} (m_{\ell_1}^2, q^2, m_{\ell_2}^2, m_i^2, m_W^2, m_a^2), \quad (\text{A14g})$$

$$l_0 := C_0 (m_{\ell_1}^2, q^2, m_{\ell_2}^2, m_i^2, m_a^2, m_W^2), \quad (\text{A15a})$$

$$l_1 := C_1 (m_{\ell_1}^2, q^2, m_{\ell_2}^2, m_i^2, m_a^2, m_W^2), \quad (\text{A15b})$$

$$l_2 := C_2 (m_{\ell_1}^2, q^2, m_{\ell_2}^2, m_i^2, m_a^2, m_W^2), \quad (\text{A15c})$$

$$l_{00} := C_{00} (m_{\ell_1}^2, q^2, m_{\ell_2}^2, m_i^2, m_a^2, m_W^2), \quad (\text{A15d})$$

$$l_{11} := C_{11} (m_{\ell_1}^2, q^2, m_{\ell_2}^2, m_i^2, m_a^2, m_W^2), \quad (\text{A15e})$$

$$l_{22} := C_{22} (m_{\ell_1}^2, q^2, m_{\ell_2}^2, m_i^2, m_a^2, m_W^2), \quad (\text{A15f})$$

$$l_{12} := C_{12} (m_{\ell_1}^2, q^2, m_{\ell_2}^2, m_i^2, m_a^2, m_W^2), \quad (\text{A15g})$$

where  $m_{\ell_1}$  and  $m_{\ell_2}$  are the masses of the charged leptons  $\ell_1^\pm$  and  $\ell_2^\pm$ , respectively,  $m_i$  and  $m_j$  are the masses of the neutrinos  $\nu_i$  and  $\nu_j$ , respectively,  $m_a$  and  $m_{a'}$  are the masses of the charged scalars  $H_a^\pm$  and  $H_{a'}^\pm$ , respectively, and  $m_W$  is the mass of the gauge bosons  $W^\pm$ .

## B $\ell_1^\pm \rightarrow \ell_2^\pm \gamma$

We compute the process  $\ell_1^-(p_1) \rightarrow \ell_2^-(p_2) \gamma(q)$ , where  $q = p_1 - p_2$ . Obviously,

$$p_1^2 = m_{\ell_1}^2, \quad p_2^2 = m_{\ell_2}^2, \quad 2p_1 \cdot p_2 = m_{\ell_1}^2 + m_{\ell_2}^2 - q^2. \quad (\text{B1})$$

If the outgoing photon is physical, then  $q^2 = 0$ ; but we keep  $q^2 \neq 0$  for generality. The amplitude for a photon with polarization  $\sigma$  is

$$T^\sigma = \mathcal{S} e \bar{u}_{\ell_2}(p_2) [\gamma^\sigma (a_l P_L + a_r P_R) + p_1^\sigma (b_l P_L + b_r P_R) + p_2^\sigma (c_l P_L + c_r P_R)] u_{\ell_1}(p_1), \quad (\text{B2})$$

where  $\mathcal{S}$  has been defined in Eq. (A1) and  $e$  is the electric charge of the proton. Clearly,

$$\not{p}_1 u_{\ell_1}(p_1) = m_{\ell_1} u_{\ell_1}(p_1), \quad \bar{u}_{\ell_2}(p_2) \not{p}_2 = m_{\ell_2} \bar{u}_{\ell_2}(p_2). \quad (\text{B3})$$

If  $T^\sigma$  in Eq. (B2) is multiplied by  $q_\sigma$  and then Eqs. (B1) and (B3) are utilized, one must obtain zero because of gauge invariance. Thus,

$$2m_{\ell_1} a_r - 2m_{\ell_2} a_l + (m_{\ell_1}^2 - m_{\ell_2}^2) (b_l + c_l) + q^2 (b_l - c_l) = 0, \quad (\text{B4a})$$

$$2m_{\ell_1} a_l - 2m_{\ell_2} a_r + (m_{\ell_1}^2 - m_{\ell_2}^2) (b_r + c_r) + q^2 (b_r - c_r) = 0. \quad (\text{B4b})$$

We have used Eqs. (B4)—that hold even when  $q^2 \neq 0$ —as a check on our calculations.

The decay width is, in the rest frame of the decaying  $\ell_1^-$ ,<sup>12</sup>

$$\Gamma = \frac{m_{\ell_1}^2 - m_{\ell_2}^2}{16\pi m_{\ell_1}^3} |\mathcal{S} e|^2 [(m_{\ell_1}^2 + m_{\ell_2}^2) (|a_l|^2 + |a_r|^2) - 4m_{\ell_1} m_{\ell_2} \text{Re}(a_l^* a_r)]. \quad (\text{B6})$$

In our model each of the coefficients  $a_l, \dots, c_r$  is the sum of two contributions, *viz.*

$$a_l = a_{l,H} + a_{l,W}, \quad \dots, \quad c_r = c_{r,H} + c_{r,W}. \quad (\text{B7})$$

The contributions with sub-index  $H$  arise from the diagrams in Fig. 14 and are given in Eqs. (B14) below, and the contributions with sub-index  $W$  come from the diagrams in Fig. 15 and are given in Eqs. (B22) below. Notice that Fig. 14 includes diagrams with the charged Goldstone bosons  $G^\pm \equiv H_1^\pm$ .

In all our calculations we utilize Feynman's gauge. Let  $m_a$  denote the mass of  $H_a^\pm$ ; for  $a = 1$  one must use  $m_{a=1} = m_W$  because we are in Feynman's gauge.

### B.1 $H_a^\pm$

The charged scalars  $H_a^\pm$  couple to the charged leptons and the neutrinos according to Eq. (28). The charged scalars include as a particular case the charged Goldstone bosons. For  $G^\pm = H_1^\pm$ , one has [18]

$$R_{1\ell i} = \frac{e}{\sqrt{2}s_w m_W} U_{\ell i} m_i, \quad L_{1\ell i} = \frac{e}{\sqrt{2}s_w m_W} U_{\ell i} m_\ell, \quad (\text{B8})$$

where  $U$  is the lepton mixing matrix and  $s_w$  is the sine of the weak mixing angle.



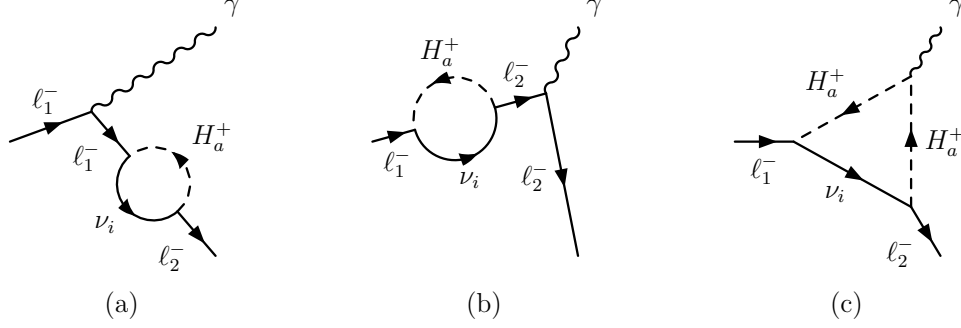


Figure 14: The three diagrams for  $\ell_1^- \rightarrow \ell_2^- \gamma$  with a loop containing  $H_a^\pm$ .

The diagrams in Figs. 14(a) and 14(b) produce

$$\begin{aligned}
T_{1(a)}^\sigma + T_{1(b)}^\sigma &= \mathcal{S} e \sum_{i=1}^6 \sum_{a=1}^n [\bar{u}_{\ell_2}(p_2) \gamma^\sigma (x_{ia} P_R + y_{ia} P_L) u_{\ell_1}(p_1) m_{\ell_2} \mathbf{b}_0 \\
&\quad + \bar{u}_{\ell_2}(p_2) \gamma^\sigma (x_{ia} P_L + y_{ia} P_R) u_{\ell_1}(p_1) m_{\ell_1} \mathbf{b}_0 \\
&\quad + \bar{u}_{\ell_2}(p_2) \gamma^\sigma (z_{ia} P_L + w_{ia} P_R) u_{\ell_1}(p_1) \mathbf{b}_1 \\
&\quad + \bar{u}_{\ell_2}(p_2) \gamma^\sigma (z_{ia} P_R + w_{ia} P_L) u_{\ell_1}(p_1) m_{\ell_2} m_{\ell_1} \mathbf{b}_2], \tag{B9}
\end{aligned}$$

where

$$x_{ia} := R_{al_2 i} L_{al_1 i}^* m_i, \tag{B10a}$$

$$y_{ia} := L_{al_2 i} R_{al_1 i}^* m_i, \tag{B10b}$$

$$z_{ia} := R_{al_2 i} R_{al_1 i}^*, \tag{B10c}$$

$$w_{ia} := L_{al_2 i} L_{al_1 i}^*, \tag{B10d}$$

and

$$\mathbf{b}_0 := \frac{B_0(m_{\ell_1}^2, m_i^2, m_a^2) - B_0(m_{\ell_2}^2, m_i^2, m_a^2)}{m_{\ell_1}^2 - m_{\ell_2}^2}, \tag{B11a}$$

$$\mathbf{b}_1 := \frac{m_{\ell_1}^2 B_1(m_{\ell_1}^2, m_i^2, m_a^2) - m_{\ell_2}^2 B_1(m_{\ell_2}^2, m_i^2, m_a^2)}{m_{\ell_1}^2 - m_{\ell_2}^2}, \tag{B11b}$$

$$\mathbf{b}_2 := \frac{B_1(m_{\ell_1}^2, m_i^2, m_a^2) - B_1(m_{\ell_2}^2, m_i^2, m_a^2)}{m_{\ell_1}^2 - m_{\ell_2}^2}. \tag{B11c}$$

Notice that in our model

$$\sum_{i=1}^6 z_{ia} = \sum_{i=1}^6 R_{al_2 i} R_{al_1 i}^* = \sum_{k, k'=1}^{n_d} \mathcal{U}_{ka}^* \mathcal{U}_{k'a} \left( \Delta_k^\dagger \Delta_{k'} \right)_{\ell_2 \ell_1}, \tag{B12a}$$

<sup>12</sup>Instead of Eq. (B6) there is another way to express the decay width, *viz.*

$$\Gamma = \frac{(m_{\ell_1}^2 - m_{\ell_2}^2)^3}{64\pi m_{\ell_1}^3} |\mathcal{S} e|^2 \left( |b_l + c_l|^2 + |b_r + c_r|^2 \right). \tag{B5}$$

This agrees with Eq. (7) of Ref. [78], that has a factor  $e^2$  missing, though.

$$\sum_{i=1}^6 w_{ia} = \sum_{i=1}^6 L_{a\ell_2 i} L_{a\ell_1 i}^* = \sum_{k,k'=1}^{n_d} \mathcal{U}_{ka}^* \mathcal{U}_{k'a} \left( \Gamma_k \Gamma_{k'}^\dagger \right)_{\ell_2 \ell_1}, \quad (\text{B12b})$$

$$\sum_{i=1}^6 x_{ia} = \sum_{i=1}^6 R_{a\ell_2 i} L_{a\ell_1 i}^* m_i = \sum_{k,k'=1}^{n_d} \mathcal{U}_{ka}^* \mathcal{U}_{k'a} \left( \Delta_k^\dagger M_D \Gamma_{k'}^\dagger \right)_{\ell_2 \ell_1}, \quad (\text{B12c})$$

$$\sum_{i=1}^6 y_{ia} = \sum_{i=1}^6 L_{a\ell_2 i} R_{a\ell_1 i}^* m_i = \sum_{k,k'=1}^{n_d} \mathcal{U}_{ka}^* \mathcal{U}_{k'a} \left( \Gamma_k M_D^\dagger \Delta_{k'} \right)_{\ell_2 \ell_1} \quad (\text{B12d})$$

vanish when  $\ell_2 \neq \ell_1$  by virtue of the matrices  $\Gamma_k$ ,  $\Delta_k$ , and  $M_D$  being diagonal.

The diagram 14(c) produces

$$\begin{aligned} T_{1(c)}^\sigma &= \mathcal{S} e \sum_{i=1}^6 \sum_{a=1}^n \bar{u}_{\ell_2}(p_2) \{ [(e_0 + 2e_1) p_1^\sigma + (e_0 + 2e_2) p_2^\sigma] (x_{ia} P_R + y_{ia} P_L) \\ &\quad + [(e_2 + 2e_{22}) p_2^\sigma + (e_2 + 2e_{12}) p_1^\sigma] m_{\ell_2} (z_{ia} P_L + w_{ia} P_R) \\ &\quad + [(e_1 + 2e_{11}) p_1^\sigma + (e_1 + 2e_{12}) p_2^\sigma] m_{\ell_1} (z_{ia} P_R + w_{ia} P_L) \\ &\quad + 2e_{00} \gamma^\sigma (z_{ia} P_L + w_{ia} P_R) \} u_{\ell_1}(p_1), \end{aligned} \quad (\text{B13})$$

where the  $e$  functions have been defined in Eqs. (A9).

Thus, adding Eqs. (B9) and (B13), one obtains

$$a_{l,H} = \sum_{i=1}^6 \sum_{a=1}^n [\mathbf{b}_0 m_{\ell_1} x_{ia} + \mathbf{b}_0 m_{\ell_2} y_{ia} + (2e_{00} + \mathbf{b}_1) z_{ia} + \mathbf{b}_2 m_{\ell_2} m_{\ell_1} w_{ia}], \quad (\text{B14a})$$

$$a_{r,H} = \sum_{i=1}^6 \sum_{a=1}^n [\mathbf{b}_0 m_{\ell_2} x_{ia} + \mathbf{b}_0 m_{\ell_1} y_{ia} + \mathbf{b}_2 m_{\ell_2} m_{\ell_1} z_{ia} + (2e_{00} + \mathbf{b}_1) w_{ia}], \quad (\text{B14b})$$

$$b_{l,H} = \sum_{i=1}^6 \sum_{a=1}^n [(e_0 + 2e_1) y_{ia} + (e_2 + 2e_{12}) m_{\ell_2} z_{ia} + (e_1 + 2e_{11}) m_{\ell_1} w_{ia}], \quad (\text{B14c})$$

$$b_{r,H} = \sum_{i=1}^6 \sum_{a=1}^n [(e_0 + 2e_1) x_{ia} + (e_1 + 2e_{11}) m_{\ell_1} z_{ia} + (e_2 + 2e_{12}) m_{\ell_2} w_{ia}], \quad (\text{B14d})$$

$$c_{l,H} = \sum_{i=1}^6 \sum_{a=1}^n [(e_0 + 2e_2) y_{ia} + (e_2 + 2e_{22}) m_{\ell_2} z_{ia} + (e_1 + 2e_{12}) m_{\ell_1} w_{ia}], \quad (\text{B14e})$$

$$c_{r,H} = \sum_{i=1}^6 \sum_{a=1}^n [(e_0 + 2e_2) x_{ia} + (e_1 + 2e_{12}) m_{\ell_1} z_{ia} + (e_2 + 2e_{22}) m_{\ell_2} w_{ia}]. \quad (\text{B14f})$$

One may use

$$\begin{aligned} B_0(m_{\ell_1}^2, m_i^2, m_a^2) &= d e_{00} - m_a^2 e_0 + m_{\ell_1}^2 (e_1 + e_{11} + e_{12}) \\ &\quad + m_{\ell_2}^2 (e_0 + e_1 + 2e_2 + e_{22} + e_{12}) - q^2 (e_1 + e_{12}), \end{aligned} \quad (\text{B15a})$$

$$\begin{aligned} B_0(m_{\ell_2}^2, m_i^2, m_a^2) &= d e_{00} - m_a^2 e_0 + m_{\ell_1}^2 (e_0 + 2e_1 + e_2 + e_{11} + e_{12}) \\ &\quad + m_{\ell_2}^2 (e_2 + e_{22} + e_{12}) - q^2 (e_2 + e_{12}), \end{aligned} \quad (\text{B15b})$$

$$B_1(m_{\ell_1}^2, m_i^2, m_a^2) = (m_{\ell_2}^2 - m_{\ell_1}^2)(e_1 + e_{11} + e_{12}) - 2e_{00} + q^2(e_{12} - e_{11}), \quad (\text{B15c})$$

$$B_1(m_{\ell_2}^2, m_i^2, m_a^2) = (m_{\ell_1}^2 - m_{\ell_2}^2)(e_2 + e_{22} + e_{12}) - 2e_{00} + q^2(e_{12} - e_{22}), \quad (\text{B15d})$$

where  $d$  is the dimension of space-time, to derive

$$\mathbf{b}_0 = -e_0 - e_1 - e_2 + \frac{q^2}{m_{\ell_1}^2 - m_{\ell_2}^2}(e_2 - e_1), \quad (\text{B16a})$$

$$\begin{aligned} 2e_{00} + \mathbf{b}_1 &= -m_{\ell_1}^2(e_1 + e_{11}) - m_{\ell_2}^2(e_2 + e_{22}) + (q^2 - m_{\ell_1}^2 - m_{\ell_2}^2)e_{12} \\ &\quad + \frac{q^2}{m_{\ell_1}^2 - m_{\ell_2}^2}(m_{\ell_2}^2 e_{22} - m_{\ell_1}^2 e_{11}), \end{aligned} \quad (\text{B16b})$$

$$\mathbf{b}_2 = -e_1 - e_2 - e_{11} - e_{22} - 2e_{12} + \frac{q^2}{m_{\ell_1}^2 - m_{\ell_2}^2}(e_{22} - e_{11}). \quad (\text{B16c})$$

As a consequence of Eqs. (B16), the constraints (B4) hold for the contributions with sub-index  $H$ .

## B.2 $W^\pm$

Besides the diagrams exclusively with  $G^\pm$ , there are five diagrams with  $W^\pm$ , *cf.* Fig. 15. Fig-

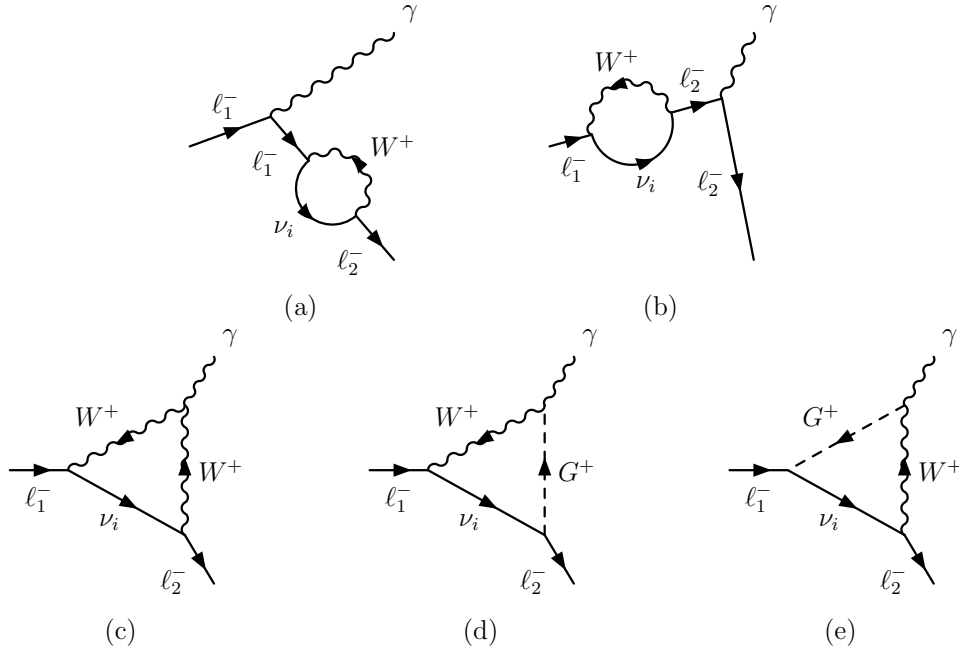


Figure 15: The five diagrams for  $\ell_1^- \rightarrow \ell_2^- \gamma$  with a loop containing  $W^\pm$ .

ures 15(d) and 15(e) have the outgoing photon attaching to  $W^\pm G^\mp$ . Those diagrams produce

$$a_{l,de} = -\frac{e^2}{2s_w^2} \sum_{i=1}^6 U_{\ell_2 i} U_{\ell_1 i}^* (2m_i^2 f_0 + m_{\ell_1}^2 f_1 + m_{\ell_2}^2 f_2), \quad (\text{B17a})$$

$$a_{r,de} = \frac{e^2 m_{\ell_2} m_{\ell_1}}{2s_w^2} \sum_{i=1}^6 U_{\ell_2 i} U_{\ell_1 i}^* (f_1 + f_2), \quad (\text{B17b})$$

$$b_{l,de} = -\frac{e^2 m_{\ell_2}}{s_w^2} \sum_{i=1}^6 U_{\ell_2 i} U_{\ell_1 i}^* f_1, \quad (\text{B17c})$$

$$b_{r,de} = 0, \quad (\text{B17d})$$

$$c_{l,de} = 0, \quad (\text{B17e})$$

$$c_{r,de} = -\frac{e^2 m_{\ell_1}}{s_w^2} \sum_{i=1}^6 U_{\ell_2 i} U_{\ell_1 i}^* f_2, \quad (\text{B17f})$$

where the  $f$  functions have been defined in Eqs. (A10). The diagram of Fig. 15(c) produces

$$a_{l,c} = \frac{e^2}{2s_w^2} \sum_{i=1}^6 U_{\ell_2 i} U_{\ell_1 i}^* [(3m_{\ell_1}^2 + 2m_{\ell_2}^2 - 2q^2) f_1 + (2m_{\ell_1}^2 + 3m_{\ell_2}^2 - 2q^2) f_2 + 2m_{\ell_1}^2 f_{11} + 2m_{\ell_2}^2 f_{22} + 2(m_{\ell_1}^2 + m_{\ell_2}^2 - q^2) f_{12} + 12f_{00}], \quad (\text{B18a})$$

$$a_{r,c} = \frac{3e^2 m_{\ell_2} m_{\ell_1}}{2s_w^2} \sum_{i=1}^6 U_{\ell_2 i} U_{\ell_1 i}^* (f_1 + f_2), \quad (\text{B18b})$$

$$b_{l,c} = -\frac{e^2 m_{\ell_2}}{s_w^2} \sum_{i=1}^6 U_{\ell_2 i} U_{\ell_1 i}^* (f_1 + f_2 - 2f_{12}), \quad (\text{B18c})$$

$$b_{r,c} = \frac{e^2 m_{\ell_1}}{s_w^2} \sum_{i=1}^6 U_{\ell_2 i} U_{\ell_1 i}^* (f_1 + 2f_{11}), \quad (\text{B18d})$$

$$c_{l,c} = \frac{e^2 m_{\ell_2}}{s_w^2} \sum_{i=1}^6 U_{\ell_2 i} U_{\ell_1 i}^* (f_2 + 2f_{22}), \quad (\text{B18e})$$

$$c_{r,c} = -\frac{e^2 m_{\ell_1}}{s_w^2} \sum_{i=1}^6 U_{\ell_2 i} U_{\ell_1 i}^* (f_1 + f_2 - 2f_{12}). \quad (\text{B18f})$$

A crucial property of the lepton mixing matrix  $U$  in our model is

$$(UU^\dagger)_{\ell_2 \ell_1} = \sum_{i=1}^6 U_{\ell_2 i} U_{\ell_1 i}^* = 0, \quad (\text{B19})$$

*cf.* Eq. (20). In spite of  $f_{00}$  containing a divergence  $1/(2\epsilon)$ ,  $a_{l,c}$  in Eq. (B18a) is finite because of Eq. (B19).

Finally, there are the diagrams of Figs. 15(a) and 15(b), producing

$$a_{l,ab} = \frac{e^2}{s_w^2} \sum_{i=1}^6 U_{\ell_2 i} U_{\ell_1 i}^* \mathbf{b}_4, \quad (\text{B20a})$$

$$a_{r,ab} = \frac{e^2 m_{\ell_2} m_{\ell_1}}{s_w^2} \sum_{i=1}^6 U_{\ell_2 i} U_{\ell_1 i}^* \mathbf{b}_5, \quad (\text{B20b})$$

$$b_{l,ab} = b_{r,ab} = c_{l,ab} = c_{r,ab} = 0, \quad (\text{B20c})$$

where

$$\mathbf{b}_4 := \frac{m_{\ell_1}^2 B_1(m_{\ell_1}^2, m_i^2, m_W^2) - m_{\ell_2}^2 B_1(m_{\ell_2}^2, m_i^2, m_W^2)}{m_{\ell_1}^2 - m_{\ell_2}^2} \quad (\text{B21a})$$

$$= -2f_{00} - m_{\ell_1}^2 (f_1 + f_{11} + f_{12}) - m_{\ell_2}^2 (f_2 + f_{22} + f_{12}) \\ + q^2 f_{12} + \frac{q^2}{m_{\ell_1}^2 - m_{\ell_2}^2} (m_{\ell_2}^2 f_{22} - m_{\ell_1}^2 f_{11}), \quad (\text{B21b})$$

$$\mathbf{b}_5 := \frac{B_1(m_{\ell_1}^2, m_i^2, m_W^2) - B_1(m_{\ell_2}^2, m_i^2, m_W^2)}{m_{\ell_1}^2 - m_{\ell_2}^2} \quad (\text{B21c})$$

$$= -f_1 - f_2 - f_{11} - f_{22} - 2f_{12} + \frac{q^2}{m_{\ell_1}^2 - m_{\ell_2}^2} (f_{22} - f_{11}). \quad (\text{B21d})$$

Thus, the sum total of the diagrams of Fig. 15 is

$$a_{l,W} = \frac{e^2}{s_w^2} \sum_{i=1}^6 U_{\ell_2 i} U_{\ell_1 i}^* \left[ -m_i^2 f_0 + m_{\ell_2}^2 f_1 + m_{\ell_1}^2 f_2 + 4f_{00} \right. \\ \left. - q^2 (f_1 + f_2) + \frac{q^2}{m_{\ell_1}^2 - m_{\ell_2}^2} (m_{\ell_2}^2 f_{22} - m_{\ell_1}^2 f_{11}) \right], \quad (\text{B22a})$$

$$a_{r,W} = \frac{e^2 m_{\ell_2} m_{\ell_1}}{s_w^2} \sum_{i=1}^6 U_{\ell_2 i} U_{\ell_1 i}^* [f_1 + f_2 - f_{11} - f_{22} - 2f_{12} \\ + \frac{q^2}{m_{\ell_1}^2 - m_{\ell_2}^2} (f_{22} - f_{11})], \quad (\text{B22b})$$

$$b_{l,W} = \frac{e^2 m_{\ell_2}}{s_w^2} \sum_{i=1}^6 U_{\ell_2 i} U_{\ell_1 i}^* (2f_{12} - 2f_1 - f_2), \quad (\text{B22c})$$

$$b_{r,W} = \frac{e^2 m_{\ell_1}}{s_w^2} \sum_{i=1}^6 U_{\ell_2 i} U_{\ell_1 i}^* (f_1 + 2f_{11}), \quad (\text{B22d})$$

$$c_{l,W} = \frac{e^2 m_{\ell_2}}{s_w^2} \sum_{i=1}^6 U_{\ell_2 i} U_{\ell_1 i}^* (f_2 + 2f_{22}), \quad (\text{B22e})$$

$$c_{r,W} = \frac{e^2 m_{\ell_1}}{s_w^2} \sum_{i=1}^6 U_{\ell_2 i} U_{\ell_1 i}^* (2f_{12} - f_1 - 2f_2). \quad (\text{B22f})$$

## C $Z \rightarrow \ell_1^+ \ell_2^-$

We compute the process  $Z(q) \rightarrow \ell_1^+(p_1) \ell_2^-(-p_2)$ , where  $q^2 = m_Z^2$  and Eqs. (B1) hold. The amplitude for a  $Z$  with polarization  $\sigma$  is written

$$T^\sigma = \mathcal{S} e \bar{u}_{\ell_2}(-p_2) [\gamma^\sigma (\bar{a}_l P_L + \bar{a}_r P_R) + p_1^\sigma (\bar{b}_l P_L + \bar{b}_r P_R) + p_2^\sigma (\bar{c}_l P_L + \bar{c}_r P_R)] v_{\ell_1}(p_1). \quad (\text{C1})$$

The decay width in the rest frame of the decaying  $Z$  is

$$\Gamma = \frac{\sqrt{\lambda}}{16\pi m_Z^3} |\mathcal{S} e|^2 \left( \frac{\lambda \aleph_0}{12m_Z^2} + \aleph_1 + \frac{\aleph_2}{3m_Z^2} \right), \quad (\text{C2})$$

where

$$\lambda := m_Z^4 + m_{\ell_1}^4 + m_{\ell_2}^4 - 2(m_Z^2 m_{\ell_1}^2 + m_Z^2 m_{\ell_2}^2 + m_{\ell_1}^2 m_{\ell_2}^2) \quad (\text{C3})$$

and

$$\begin{aligned} \aleph_0 &= (m_Z^2 - m_{\ell_1}^2 - m_{\ell_2}^2) \left( |\bar{b}_l + \bar{c}_l|^2 + |\bar{b}_r + \bar{c}_r|^2 \right) - 4m_{\ell_1} m_{\ell_2} \text{Re} [(\bar{b}_l + \bar{c}_l)(\bar{b}_r^* + \bar{c}_r^*)] \\ &\quad - 4m_{\ell_1} \text{Re} [\bar{a}_r^* (\bar{b}_l + \bar{c}_l) + \bar{a}_l^* (\bar{b}_r + \bar{c}_r)] \\ &\quad - 4m_{\ell_2} \text{Re} [\bar{a}_l^* (\bar{b}_l + \bar{c}_l) + \bar{a}_r^* (\bar{b}_r + \bar{c}_r)], \end{aligned} \quad (\text{C4a})$$

$$\aleph_1 = 4m_{\ell_1} m_{\ell_2} \text{Re} (\bar{a}_l \bar{a}_r^*), \quad (\text{C4b})$$

$$\aleph_2 = \left[ 2m_Z^4 - m_Z^2 (m_{\ell_1}^2 + m_{\ell_2}^2) - (m_{\ell_1}^2 - m_{\ell_2}^2)^2 \right] (|\bar{a}_l|^2 + |\bar{a}_r|^2). \quad (\text{C4c})$$

We define

$$t_l := \frac{s_w^2 - c_w^2}{2c_w s_w}, \quad t_r := \frac{s_w}{c_w}, \quad (\text{C5})$$

so that the coupling of the  $Z$  to the charged leptons is given by

$$\mathcal{L}_{\text{nc}} = \dots + e Z_\sigma \sum_{\ell=e,\mu,\tau} \bar{\ell} \gamma^\sigma (t_l P_L + t_r P_R) \ell, \quad (\text{C6})$$

*cf.* Eq. (26a). Notice that

$$-\frac{1}{t_r} = 2t_l - t_r. \quad (\text{C7})$$

We shall write the coefficients  $\bar{a}_l, \dots, \bar{c}_r$  as the sum of three pieces, *viz.*

$$\begin{aligned} \bar{a}_l &= \bar{a}_{l,H} + \bar{a}_{l,W} + \bar{a}_{l,2\nu}, \\ &\vdots \\ \bar{c}_r &= \bar{c}_{r,H} + \bar{c}_{r,W} + \bar{c}_{r,2\nu}. \end{aligned} \quad (\text{C8})$$

### C.1 $H_a^\pm$

We recover the diagrams of Fig. 14, with the photon substituted by a  $Z$ . Diagrams 14(a) and 14(b) produce the result in Eq. (B9) with the transformations  $P_L \rightarrow t_l P_L$  and  $P_R \rightarrow t_r P_R$ .

Diagram 14(c) produces the result in Eq. (B13) multiplied by  $t_l$ . Thus, the full result of Fig. 14 with  $Z$  instead of  $\gamma$  is

$$\bar{a}_{l,H} = t_l \sum_{i=1}^6 \sum_{a=1}^n [(m_{\ell_1} x_{ia} + m_{\ell_2} y_{ia}) \mathbf{b}_0 + z_{ia} (2e_{00} + \mathbf{b}_1) + m_{\ell_2} m_{\ell_1} w_{ia} \mathbf{b}_2], \quad (\text{C9a})$$

$$\bar{a}_{r,H} = \sum_{i=1}^6 \sum_{a=1}^n \{t_r [(m_{\ell_2} x_{ia} + m_{\ell_1} y_{ia}) \mathbf{b}_0 + m_{\ell_2} m_{\ell_1} z_{ia} \mathbf{b}_2 + w_{ia} \mathbf{b}_1] + 2t_l w_{ia} e_{00}\}, \quad (\text{C9b})$$

$$\bar{b}_{l,H} = t_l \sum_{i=1}^6 \sum_{a=1}^n [y_{ia} (e_0 + 2e_1) + m_{\ell_2} z_{ia} (e_2 + 2e_{12}) + m_{\ell_1} w_{ia} (e_1 + 2e_{11})], \quad (\text{C9c})$$

$$\bar{b}_{r,H} = t_l \sum_{i=1}^6 \sum_{a=1}^n [x_{ia} (e_0 + 2e_1) + m_{\ell_1} z_{ia} (e_1 + 2e_{11}) + m_{\ell_2} w_{ia} (e_2 + 2e_{12})], \quad (\text{C9d})$$

$$\bar{c}_{l,H} = t_l \sum_{i=1}^6 \sum_{a=1}^n [y_{ia} (e_0 + 2e_2) + m_{\ell_2} z_{ia} (e_2 + 2e_{22}) + m_{\ell_1} w_{ia} (e_1 + 2e_{12})], \quad (\text{C9e})$$

$$\bar{c}_{r,H} = t_l \sum_{i=1}^6 \sum_{a=1}^n [x_{ia} (e_0 + 2e_2) + m_{\ell_1} z_{ia} (e_1 + 2e_{12}) + m_{\ell_2} w_{ia} (e_2 + 2e_{22})]. \quad (\text{C9f})$$

## C.2 $W^\pm$

We consider the diagrams of Fig. 15 with a  $Z$  instead of the  $\gamma$ . They produce

$$\begin{aligned} \bar{a}_{l,W} &= \bar{a}_{l,de} + \bar{a}_{l,c} + \bar{a}_{l,ab}, \\ &\vdots \\ \bar{c}_{r,W} &= \bar{c}_{r,de} + \bar{c}_{r,c} + \bar{c}_{r,ab}. \end{aligned} \quad (\text{C10})$$

Figures 15(d) and 15(e) yield

$$\bar{a}_{l,de} = t_r a_{l,de}, \quad (\text{C11a})$$

$$\bar{a}_{r,de} = t_r a_{r,de}, \quad (\text{C11b})$$

$$\bar{b}_{l,de} = t_r b_{l,de}, \quad (\text{C11c})$$

$$\bar{b}_{r,de} = 0, \quad (\text{C11d})$$

$$\bar{c}_{l,de} = 0, \quad (\text{C11e})$$

$$\bar{c}_{r,de} = t_r c_{r,de}. \quad (\text{C11f})$$

Figure 15(c) produces

$$\bar{a}_{l,c} = -\frac{1}{t_r} a_{l,c}, \quad (\text{C12a})$$

$$\bar{a}_{r,c} = -\frac{1}{t_r} a_{r,c}, \quad (\text{C12b})$$

$$\bar{b}_{l,c} = -\frac{1}{t_r} c_{l,c}, \quad (\text{C12c})$$

$$\bar{b}_{r,c} = -\frac{1}{t_r} b_{r,c}, \quad (\text{C12d})$$

$$\bar{c}_{l,c} = -\frac{1}{t_r} c_{l,c}, \quad (\text{C12e})$$

$$\bar{c}_{r,c} = -\frac{1}{t_r} c_{r,c}. \quad (\text{C12f})$$

Notice that in Eqs. (C12) one may use Eq. (C7). Figures 15(a) and 15(b) give

$$\bar{a}_{l,ab} = t_l a_{l,ab}, \quad (\text{C13a})$$

$$\bar{a}_{r,ab} = t_r a_{r,ab}, \quad (\text{C13b})$$

$$\bar{b}_{l,ab} = \bar{b}_{r,ab} = \bar{c}_{l,ab} = \bar{c}_{r,ab} = 0. \quad (\text{C13c})$$

### C.3 Diagrams with two neutrino internal lines

There are also diagrams where the  $Z$  boson attaches to the neutrino line as depicted in Fig. 16. The relevant vertex is given in Eq. (26b). We have

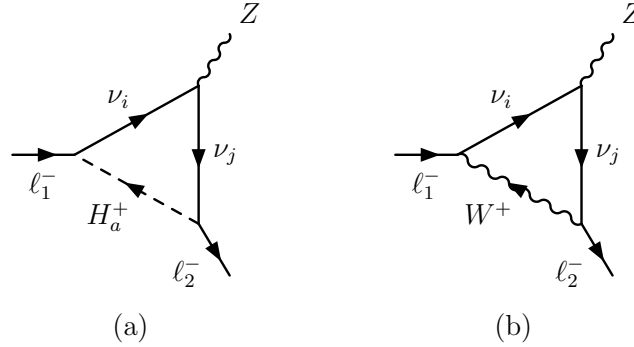


Figure 16: Two diagrams for  $Z \rightarrow \ell_1^+ \ell_2^-$  where the  $Z$  attaches to two neutrino lines.

$$\begin{aligned} \bar{a}_{l,2\nu} &= \bar{a}_{l,16(a)} + \bar{a}_{l,16(b)}, \\ &\vdots \\ \bar{c}_{r,2\nu} &= \bar{c}_{r,16(a)} + \bar{c}_{r,16(b)}. \end{aligned} \quad (\text{C14})$$

From the diagram 16(a) one obtains

$$\begin{aligned} \bar{a}_{l,16(a)} &= \frac{1}{2c_w s_w} \sum_{a=1}^n \sum_{i,j=1}^6 \{ m_{\ell_1} x_{ija} [m_i q_{ij} g_1 + m_j q_{ji} (g_0 + g_1)] \\ &\quad + m_{\ell_2} y_{ija} [m_j q_{ij} g_2 + m_i q_{ji} (g_0 + g_2)] \\ &\quad + z_{ija} q_{ij} [-2g_{00} + q^2 g_{12} - m_{\ell_2}^2 (g_2 + g_{12} + g_{22}) - m_{\ell_1}^2 (g_1 + g_{12} + g_{11})] \\ &\quad - z_{ija} q_{ji} m_i m_j g_0 - w_{ija} q_{ji} m_{\ell_2} m_{\ell_1} (g_0 + g_1 + g_2) \}, \\ \bar{a}_{r,16(a)} &= \frac{1}{2c_w s_w} \sum_{a=1}^n \sum_{i,j=1}^6 \{ -m_{\ell_2} x_{ija} [m_i q_{ij} (g_0 + g_2) + m_j q_{ji} g_2] + m_i m_j w_{ija} q_{ij} g_0 \} \end{aligned} \quad (\text{C15a})$$



$$-m_{\ell_1} y_{ija} [m_j q_{ij} (g_0 + g_1) + m_i q_{ji} g_1] + m_{\ell_2} m_{\ell_1} z_{ija} q_{ij} (g_0 + g_1 + g_2) + w_{ija} q_{ji} [2g_{00} - q^2 g_{12} + m_{\ell_2}^2 (g_2 + g_{12} + g_{22}) + m_{\ell_1}^2 (g_1 + g_{12} + g_{11})] \}, \quad (\text{C15b})$$

$$\bar{b}_{l,16(a)} = \frac{1}{c_w s_w} \sum_{a=1}^n \sum_{i,j=1}^6 [m_i y_{ija} q_{ji} g_1 + m_{\ell_2} z_{ija} q_{ij} g_{12} - m_{\ell_1} w_{ija} q_{ji} (g_1 + g_{11})], \quad (\text{C15c})$$

$$\bar{b}_{r,16(a)} = \frac{1}{c_w s_w} \sum_{a=1}^n \sum_{i,j=1}^6 [-m_i x_{ija} q_{ij} g_1 + m_{\ell_1} z_{ija} q_{ij} (g_1 + g_{11}) - m_{\ell_2} w_{ija} q_{ji} g_{12}], \quad (\text{C15d})$$

$$\bar{c}_{l,16(a)} = \frac{1}{c_w s_w} \sum_{a=1}^n \sum_{i,j=1}^6 [-m_j y_{ija} q_{ij} g_2 + m_{\ell_2} z_{ija} q_{ij} (g_2 + g_{22}) - m_{\ell_1} w_{ija} q_{ji} g_{12}], \quad (\text{C15e})$$

$$\bar{c}_{r,16(a)} = \frac{1}{c_w s_w} \sum_{a=1}^n \sum_{i,j=1}^6 [m_j x_{ija} q_{ji} g_2 + m_{\ell_1} z_{ija} q_{ij} g_{12} - m_{\ell_2} w_{ija} q_{ji} (g_2 + g_{22})]. \quad (\text{C15f})$$

In Eqs. (C15),

$$x_{ija} := R_{a\ell_2 j} L_{a\ell_1 i}^*, \quad (\text{C16a})$$

$$y_{ija} := L_{a\ell_2 j} R_{a\ell_1 i}^*, \quad (\text{C16b})$$

$$z_{ija} := R_{a\ell_2 j} R_{a\ell_1 i}^*, \quad (\text{C16c})$$

$$w_{ija} := L_{a\ell_2 j} L_{a\ell_1 i}^*, \quad (\text{C16d})$$

and the  $g$  functions are defined in Eqs. (A11). Note that the divergences cancel out in  $\bar{a}_{l,16(a)}$  and  $\bar{a}_{r,16(a)}$ . Indeed,

$$\begin{aligned} \sum_{i,j=1}^6 z_{ija} q_{ij} &= \sum_{i,j=1}^6 R_{a\ell_2 j} R_{a\ell_1 i}^* q_{ij} = \sum_{k,k'=1}^{n_d} \sum_{i,j=1}^6 \mathcal{U}_{ka}^* \left( \Delta_k^\dagger X \right)_{\ell_2 j} \mathcal{U}_{k'a} \left( X^\dagger \Delta_{k'} \right)_{i\ell_1} (U^\dagger U)_{ij} \\ &= \sum_{k,k'=1}^{n_d} \mathcal{U}_{ka}^* \mathcal{U}_{k'a} \left( \Delta_k^\dagger X U^T U^* X^\dagger \Delta_{k'} \right)_{\ell_2 \ell_1} \\ &= 0, \end{aligned} \quad (\text{C17})$$

because the unitarity of the matrix  $U_6$  of Eq. (19) implies  $U X^T = 0_{3 \times 3}$ ; and

$$\begin{aligned} \sum_{i,j=1}^6 w_{ija} q_{ji} &= \sum_{i,j=1}^6 L_{a\ell_2 j} L_{a\ell_1 i}^* q_{ji} = \sum_{k,k'=1}^{n_d} \sum_{i,j=1}^6 \mathcal{U}_{ka}^* (\Gamma_k U)_{\ell_2 j} \mathcal{U}_{k'a} \left( U^\dagger \Gamma_{k'}^\dagger \right)_{i\ell_1} (U^\dagger U)_{ji} \\ &= \sum_{k,k'=1}^{n_d} \mathcal{U}_{ka}^* \mathcal{U}_{k'a} \left( \Gamma_k U U^\dagger U U^\dagger \Gamma_{k'}^\dagger \right)_{\ell_2 \ell_1} \\ &= \sum_{k,k'=1}^{n_d} \mathcal{U}_{ka}^* \mathcal{U}_{k'a} \left( \Gamma_k \Gamma_{k'}^\dagger \right)_{\ell_2 \ell_1} \end{aligned} \quad (\text{C18})$$

vanishes if  $\ell_2 \neq \ell_1$  because the matrices  $\Gamma_k$  are diagonal.

The diagram 16(b) yields

$$\bar{a}_{l,16(b)} = \frac{e^2}{2c_w s_w^3} \sum_{i,j=1}^6 U_{\ell_2 j} U_{\ell_1 i}^* [q_{ij} m_i m_j h_0 + 2q_{ji} h_{00}]$$

$$+q_{ji} (m_{\ell_1}^2 + m_{\ell_2}^2 - q^2) (h_0 + h_1 + h_2 + h_{12}) \\ +q_{ji} m_{\ell_1}^2 (h_1 + h_{11}) + q_{ji} m_{\ell_2}^2 (h_2 + h_{22}) \Big], \quad (\text{C19a})$$

$$\bar{a}_{r,16(\text{b})} = \frac{e^2 m_{\ell_2} m_{\ell_1}}{2c_w s_w^3} \sum_{i,j=1}^6 U_{\ell_2 j} U_{\ell_1 i}^* q_{ji} (h_0 + h_1 + h_2), \quad (\text{C19b})$$

$$\bar{b}_{l,16(\text{b})} = -\frac{e^2 m_{\ell_2}}{c_w s_w^3} \sum_{i,j=1}^6 U_{\ell_2 j} U_{\ell_1 i}^* q_{ji} (h_0 + h_1 + h_2 + h_{12}), \quad (\text{C19c})$$

$$\bar{b}_{r,16(\text{b})} = -\frac{e^2 m_{\ell_1}}{c_w s_w^3} \sum_{i,j=1}^6 U_{\ell_2 j} U_{\ell_1 i}^* q_{ji} (h_1 + h_{11}), \quad (\text{C19d})$$

$$\bar{c}_{l,16(\text{b})} = -\frac{e^2 m_{\ell_2}}{c_w s_w^3} \sum_{i,j=1}^6 U_{\ell_2 j} U_{\ell_1 i}^* q_{ji} (h_2 + h_{22}), \quad (\text{C19e})$$

$$\bar{c}_{r,16(\text{b})} = -\frac{e^2 m_{\ell_1}}{c_w s_w^3} \sum_{i,j=1}^6 U_{\ell_2 j} U_{\ell_1 i}^* q_{ji} (h_0 + h_1 + h_2 + h_{12}), \quad (\text{C19f})$$

where the  $h$  functions are defined in Eqs. (A12). When writing Eq. (C19a) we have used the fact that

$$\sum_{i,j=1}^6 U_{\ell_2 j} U_{\ell_1 i}^* q_{ji} = \sum_{i,j=1}^6 U_{\ell_2 j} U_{i\ell_1}^\dagger (U^\dagger U)_{ji} = \delta_{\ell_2 \ell_1}, \quad (\text{C20})$$

because  $UU^\dagger$  is the  $3 \times 3$  unit matrix, *cf.* Eq. (20).

## D $S_b^0 \rightarrow \ell_1^+ \ell_2^-$

We compute the process  $S_b^0(q) \rightarrow \ell_1^+(p_1) \ell_2^-(-p_2)$ , where  $S_b^0$  is a physical neutral scalar, *i.e.*  $b \neq 1$ . Equations (B1) hold and  $q^2 = m_b^2$ . The amplitude is written

$$T_b = \mathcal{S} \bar{u}_{\ell_2}(-p_2) (d_{lb} P_L + d_{rb} P_R) v_{\ell_1}(p_1), \quad (\text{D1})$$

where  $\mathcal{S}$  was defined in Eq. (A1). The decay width in the rest frame of  $S_b^0$  is

$$\Gamma = \frac{\sqrt{\lambda}}{16\pi m_b^3} |\mathcal{S}|^2 [(m_b^2 - m_{\ell_1}^2 - m_{\ell_2}^2) (|d_{lb}|^2 + |d_{rb}|^2) - 4 m_{\ell_1} m_{\ell_2} \text{Re}(d_{lb} d_{rb}^*)], \quad (\text{D2})$$

where

$$\lambda := m_b^4 + m_{\ell_1}^4 + m_{\ell_2}^4 - 2(m_b^2 m_{\ell_1}^2 + m_b^2 m_{\ell_2}^2 + m_{\ell_1}^2 m_{\ell_2}^2). \quad (\text{D3})$$

### D.1 Diagrams in which $S_b^0$ attaches to charged leptons

There are self-energy-like diagrams with a loop of either  $H_a^\pm$ —diagrams (a) and (b) in Fig. 17— or  $W^\pm$ —diagrams (c) and (d) in Fig. 17. The vertex of  $S_b^0$  with the charged leptons is given

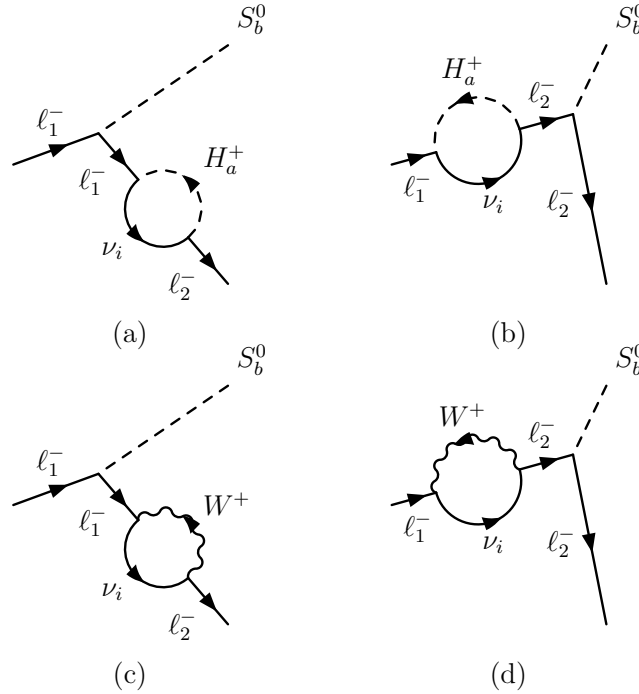


Figure 17: The four self-energy-like diagrams for  $S_b^0 \rightarrow \ell_1^+ \ell_2^-$ .

by Eq. (30a). One obtains

$$d_{lb,17(a,b)} = \frac{1}{\sqrt{2} (m_{\ell_1}^2 - m_{\ell_2}^2)} \sum_{a=1}^n \sum_{i=1}^6 \{ \gamma_{b\ell_1} (m_{\ell_2} x_{ia} + m_{\ell_1} y_{ia}) B_0(m_{\ell_2}^2, m_i^2, m_a^2) \}$$

$$\begin{aligned}
& +\gamma_{b\ell_1} m_{\ell_2} (m_{\ell_1} z_{ia} + m_{\ell_2} w_{ia}) B_1 (m_{\ell_2}^2, m_i^2, m_a^2) \\
& -\gamma_{b\ell_2} (m_{\ell_1} x_{ia} + m_{\ell_2} y_{ia}) B_0 (m_{\ell_1}^2, m_i^2, m_a^2) \\
& -\gamma_{b\ell_2} m_{\ell_1} (m_{\ell_1} z_{ia} + m_{\ell_2} w_{ia}) B_1 (m_{\ell_1}^2, m_i^2, m_a^2) \}, \tag{D4a}
\end{aligned}$$

$$\begin{aligned}
d_{rb,17(a,b)} &= \frac{1}{\sqrt{2} (m_{\ell_1}^2 - m_{\ell_2}^2)} \sum_{a=1}^n \sum_{i=1}^6 \{ \gamma_{b\ell_1}^* (m_{\ell_1} x_{ia} + m_{\ell_2} y_{ia}) B_0 (m_{\ell_2}^2, m_i^2, m_a^2) \\
& +\gamma_{b\ell_1}^* m_{\ell_2} (m_{\ell_2} z_{ia} + m_{\ell_1} w_{ia}) B_1 (m_{\ell_2}^2, m_i^2, m_a^2) \\
& -\gamma_{b\ell_2}^* (m_{\ell_2} x_{ia} + m_{\ell_1} y_{ia}) B_0 (m_{\ell_1}^2, m_i^2, m_a^2) \\
& -\gamma_{b\ell_2}^* m_{\ell_1} (m_{\ell_2} z_{ia} + m_{\ell_1} w_{ia}) B_1 (m_{\ell_1}^2, m_i^2, m_a^2) \}, \tag{D4b}
\end{aligned}$$

$$\begin{aligned}
d_{lb,17(c,d)} &= \frac{e^2 m_{\ell_1}}{\sqrt{2} s_w^2 (m_{\ell_1}^2 - m_{\ell_2}^2)} \sum_{i=1}^6 U_{\ell_2 i} U_{\ell_1 i}^* [\gamma_{b\ell_1} m_{\ell_2} B_1 (m_{\ell_2}^2, m_i^2, m_W^2) \\
& -\gamma_{b\ell_2} m_{\ell_1} B_1 (m_{\ell_1}^2, m_i^2, m_W^2)] , \tag{D4c}
\end{aligned}$$

$$\begin{aligned}
d_{rb,17(c,d)} &= \frac{e^2 m_{\ell_2}}{\sqrt{2} s_w^2 (m_{\ell_1}^2 - m_{\ell_2}^2)} \sum_{i=1}^6 U_{\ell_2 i} U_{\ell_1 i}^* [\gamma_{b\ell_1}^* m_{\ell_2} B_1 (m_{\ell_2}^2, m_i^2, m_W^2) \\
& -\gamma_{b\ell_2}^* m_{\ell_1} B_1 (m_{\ell_1}^2, m_i^2, m_W^2)] . \tag{D4d}
\end{aligned}$$

## D.2 Diagrams in which $S_b^0$ attaches to charged scalars

There is a diagram, depicted in Fig. 18, wherein the  $S_b^0$  attaches to two charged scalars that may

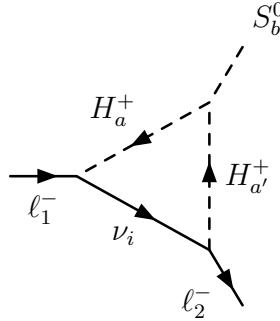


Figure 18: Diagram for  $S_b^0 \rightarrow \ell_1^+ \ell_2^-$  with the neutral scalar attaching to two charged scalars.

in principle be different. We parameterize the vertex of the three scalars through Eq. (12), where the coefficients  $\lambda_{aa'b}$  are in general complex but obey  $\lambda_{aa'b} = \lambda_{a'ab}^*$  because of the Hermiticity of the Lagrangian. The values of the  $\lambda_{aa'b}$  depend on the scalar potential and are unconstrained by gauge invariance, unless either  $a = 1$  or  $a' = 1$ . The diagram of Fig. 18 yields

$$d_{lb,18} = \sum_{a,a'=1}^n \sum_{i=1}^6 \lambda_{aa'b} (R_{a'\ell_2 i} R_{a\ell_1 i}^* m_{\ell_2} j_2 + L_{a'\ell_2 i} L_{a\ell_1 i}^* m_{\ell_1} j_1 + L_{a'\ell_2 i} R_{a\ell_1 i}^* m_i j_0) , \tag{D5a}$$

$$d_{rb,18} = \sum_{a,a'=1}^n \sum_{i=1}^6 \lambda_{aa'b} (R_{a'\ell_2 i} R_{a\ell_1 i}^* m_{\ell_1} j_1 + L_{a'\ell_2 i} L_{a\ell_1 i}^* m_{\ell_2} j_2 + R_{a'\ell_2 i} L_{a\ell_1 i}^* m_i j_0) , \tag{D5b}$$

where  $j_{0,1,2}$  are defined by Eqs. (A13).

Note that the diagram of Fig. 18 implicitly contains the cases where either  $H_a^\pm$  or  $H_{a'}^\pm$  (or both) coincide with the charged Goldstone bosons  $G^\pm := H_1^\pm$ . In those cases one must use  $m_{a=1} = m_W$  together with Eqs. (13).

### D.3 Diagrams in which $S_b^0$ attaches to $W$ bosons

We next compute the diagrams in Fig. 19. The relevant terms of the Lagrangian are the ones

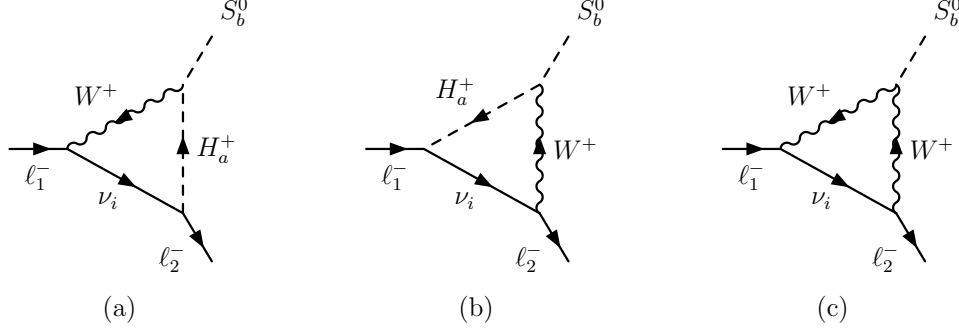


Figure 19: Three diagrams for  $S_b^0 \rightarrow \ell_1^+ \ell_2^-$  with the neutral scalar attaching to a gauge boson.

of Eq. (11) [18, 57]. Diagram 19(a) produces

$$d_{lb,19(a)} = \frac{e^2}{2\sqrt{2}s_w^2} \sum_{a=1}^n \sum_{i=1}^6 U_{\ell_1 i}^* (\mathcal{V}^\dagger \mathcal{U})_{ba} \left\{ -R_{a\ell_2 i} m_i m_{\ell_2} (2k_0 + k_2) \right. \\ \left. - L_{a\ell_2 i} [4k_{00} + m_{\ell_1}^2 (k_{11} + k_{12} + k_1) + m_{\ell_2}^2 (k_{22} + k_{12} + 2k_1 + 2k_2) \right. \\ \left. - q^2 (k_{12} + 2k_1) \right\}, \quad (D6a)$$

$$d_{rb,19(a)} = \frac{e^2}{2\sqrt{2}s_w^2} \sum_{a=1}^n \sum_{i=1}^6 U_{\ell_1 i}^* (\mathcal{V}^\dagger \mathcal{U})_{ba} m_{\ell_1} [R_{a\ell_2 i} m_i (k_0 - k_1) + L_{a\ell_2 i} m_{\ell_2} (2k_1 + k_2)], \quad (D6b)$$

with the  $k$  functions defined in Eqs. (A14). Diagram 19(b) produces

$$d_{lb,19(b)} = \frac{e^2}{2\sqrt{2}s_w^2} \sum_{a=1}^n \sum_{i=1}^6 U_{\ell_2 i} (\mathcal{U}^\dagger \mathcal{V})_{ab} m_{\ell_2} [R_{a\ell_1 i}^* m_i (l_0 - l_2) + L_{a\ell_1 i}^* m_{\ell_1} (l_1 + 2l_2)], \quad (D7a)$$

$$d_{rb,19(b)} = \frac{e^2}{2\sqrt{2}s_w^2} \sum_{a=1}^n \sum_{i=1}^6 U_{\ell_2 i} (\mathcal{U}^\dagger \mathcal{V})_{ab} \left\{ -R_{a\ell_1 i}^* m_i m_{\ell_1} (2l_0 + l_1) \right. \\ \left. - L_{a\ell_1 i}^* [4l_{00} + m_{\ell_1}^2 (l_{11} + l_{12} + 2l_1 + 2l_2) + m_{\ell_2}^2 (l_{22} + l_{12} + l_2) \right. \\ \left. - q^2 (l_{12} + 2l_2) \right\}, \quad (D7b)$$

with the  $l$  functions defined in Eqs. (A15). Equations (D6) and (D7) contain no divergences because

$$\sum_{i=1}^6 L_{ali} U_{\ell'i}^* = \sum_{k=1}^{n_d} \mathcal{U}_{ka}^* (\Gamma_k U U^\dagger)_{\ell\ell'} = \sum_{k=1}^{n_d} \mathcal{U}_{ka}^* (\Gamma_k)_{\ell\ell'} \quad (\text{D8})$$

vanishes if  $\ell \neq \ell'$  since the matrices  $\Gamma_k$  are diagonal.

Equations (D6) and (D7) include the particular case when  $a = 1$ ; then,  $H_a^\pm$  coincides with the Goldstone bosons  $G^\pm$ . In that particular case one must use  $m_{a=1} = m_W$  together with Eqs. (B8) and

$$(\mathcal{U}^\dagger \mathcal{V})_{1b} = (\mathcal{V}^\dagger \mathcal{U})_{b1} = x_b, \quad (\text{D9})$$

where  $x_b$  is the real number defined in Eq. (9).

In order to compute diagram 19(c) one must know the vertex of a neutral scalar with two  $W^\pm$  gauge bosons, which is given by Eq. (10) [57]. One then obtains

$$d_{lb,19(c)} = -\frac{e^3 m_W m_{\ell_2} x_b}{s_w^3} \sum_{i=1}^6 U_{\ell_2 i} U_{\ell_1 i}^* f_2, \quad (\text{D10a})$$

$$d_{rb,19(c)} = -\frac{e^3 m_W m_{\ell_1} x_b}{s_w^3} \sum_{i=1}^6 U_{\ell_2 i} U_{\ell_1 i}^* f_1, \quad (\text{D10b})$$

where  $f_1$  and  $f_2$  are defined in Eqs. (A10). Notice that Eqs. (D10) only hold for  $b \neq 1$ ; indeed,  $d_{l1,19(c)} = d_{r1,19(c)} = 0$  because the vertex  $W^+ W^- G^0$  does not exist.

#### D.4 Diagrams where $S_b^0$ attaches to neutrino lines

The neutral scalar  $S_b^0$  may also attach to two internal neutrino lines. The relevant diagrams are displayed in Fig. 20. The vertex of the neutral scalars with the neutrinos is given by Eq. (30b).

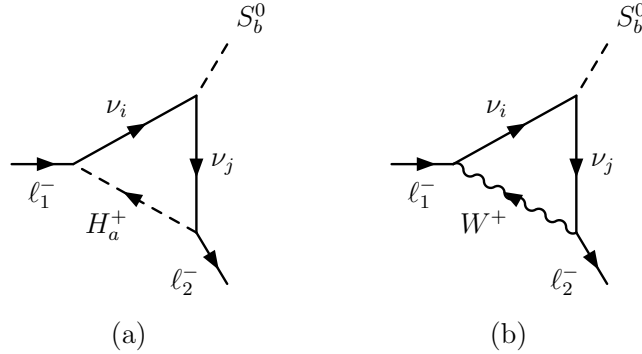


Figure 20: Two diagrams for  $S_b^0 \rightarrow \ell_1^+ \ell_2^-$  where  $S_b^0$  attaches to neutrinos.

From Fig. 20(a) one obtains

$$d_{lb,20(a)} = \frac{1}{\sqrt{2}} \sum_{i,j=1}^6 \sum_{a=1}^n \{ -x_{ija} f_{bji} m_{\ell_2} m_{\ell_1} (g_0 + g_1 + g_2) - y_{ija} f_{bji} m_i m_j g_0$$

$$\begin{aligned}
& -y_{ija}f_{bji}^* [4g_{00} + m_{\ell_1}^2 (g_1 + g_{11} + g_{12}) + m_{\ell_2}^2 (g_2 + g_{22} + g_{12}) - q^2 g_{12}] \\
& + z_{ija}f_{bji}m_i m_{\ell_2} (g_0 + g_2) + z_{ija}f_{bji}^* m_j m_{\ell_2} g_2 \\
& + w_{ija}f_{bji}^* m_i m_{\ell_1} g_1 + w_{ija}f_{bji}m_j m_{\ell_1} (g_0 + g_1) \}, \tag{D11a}
\end{aligned}$$

$$\begin{aligned}
d_{rb,20(a)} &= \frac{1}{\sqrt{2}} \sum_{i,j=1}^6 \sum_{a=1}^n \{ -y_{ija}f_{bji}^* m_{\ell_2} m_{\ell_1} (g_0 + g_1 + g_2) - x_{ija}f_{bji}^* m_i m_j g_0 \\
& - x_{ija}f_{bji} [4g_{00} + m_{\ell_1}^2 (g_1 + g_{11} + g_{12}) + m_{\ell_2}^2 (g_2 + g_{22} + g_{12}) - q^2 g_{12}] \\
& + z_{ija}f_{bji}^* m_j m_{\ell_1} (g_0 + g_1) + z_{ija}f_{bji}m_i m_{\ell_1} g_1 \\
& + w_{ija}f_{bji}m_j m_{\ell_2} g_2 + w_{ija}f_{bji}^* m_i m_{\ell_2} (g_0 + g_2) \}, \tag{D11b}
\end{aligned}$$

where the relevant symbols are defined in Eqs. (C16) and (A11). The divergences originating in the function  $g_{00}$  vanish in Eqs. (D11) because

$$\begin{aligned}
\sum_{i,j=1}^6 \sum_{a=1}^n y_{ija}f_{bji}^* &= \sum_{i,j=1}^6 \sum_{a=1}^n L_{a\ell_2 j} R_{a\ell_1 i}^* f_{bji}^* \\
&= \sum_{i,j=1}^6 \sum_{a=1}^n \sum_{k,k',k''=1}^{n_d} \mathcal{U}_{ka}^* (\Gamma_k U)_{\ell_2 j} \mathcal{U}_{k'a} (X^\dagger \Delta_{k'})_{i\ell_1} \\
&\quad \times \mathcal{V}_{k''b}^* (U^\dagger \Delta_{k''}^* X + X^T \Delta_{k''}^* U^*)_{ij} \\
&= \sum_{i,j=1}^6 \sum_{a=1}^n \sum_{k,k',k''=1}^{n_d} (\mathcal{U}\mathcal{U}^\dagger)_{k'k} \mathcal{V}_{k''b}^* \\
&\quad \times (\Gamma_k U U^\dagger \Delta_{k''}^* X X^\dagger \Delta_{k'} + \Gamma_k U X^T \Delta_{k''}^* U^* X^\dagger \Delta_{k'})_{\ell_2 \ell_1} \\
&= \sum_{i,j=1}^6 \sum_{a=1}^n \sum_{k,k',k''=1}^{n_d} \delta_{k'k} \mathcal{V}_{k''b}^* (\Gamma_k \Delta_{k''}^* \Delta_{k'})_{\ell_2 \ell_1} \\
&= 0, \tag{D12a}
\end{aligned}$$

since the Yukawa-coupling matrices  $\Gamma_k$  and  $\Delta_k$  are all diagonal. In a similar fashion one easily demonstrates that

$$\sum_{i,j=1}^6 \sum_{a=1}^n x_{ija}f_{bji} = 0. \tag{D13}$$

From Fig. 20(b) one obtains

$$d_{lb,20(b)} = \frac{e^2 m_{\ell_2}}{\sqrt{2} s_w^2} \sum_{i,j=1}^6 U_{\ell_2 j} U_{\ell_1 i}^* [f_{bji} m_j h_2 + f_{bji}^* m_i (h_0 + h_2)], \tag{D14a}$$

$$d_{rb,20(b)} = \frac{e^2 m_{\ell_1}}{\sqrt{2} s_w^2} \sum_{i,j=1}^6 U_{\ell_2 j} U_{\ell_1 i}^* [f_{bji}^* m_i h_1 + f_{bji} m_j (h_0 + h_1)], \tag{D14b}$$

*cf.* Eqs (A12).

## E The $Z$ invisible decay width

The determination by LEP of the number of light active neutrinos provides a constraint to heavy-neutrino mixing. The  $Z$  invisible decay width was measured by LEP [68, 79] to be

$$\Gamma(Z \rightarrow \text{invisible})_{\text{experimental}} = (0.499 \pm 0.0015) \text{ GeV}. \quad (\text{E1})$$

This is almost  $2\sigma$  below the SM theoretical expectation

$$\Gamma(Z \rightarrow \text{invisible})_{\text{SM}} = \sum_{\nu} \Gamma(Z \rightarrow \nu\bar{\nu})_{\text{SM}} = (0.50169 \pm 0.00006) \text{ GeV}. \quad (\text{E2})$$

The tree-level  $Z$  invisible decay width in the presence of six Majorana neutrinos with masses  $m_i$  reads [80]

$$\Gamma(Z \rightarrow \text{invisible})_{\text{tree}} = \sum_{i=1}^6 \sum_{j=i}^6 \Delta_{ij} \Theta(m_Z - m_i - m_j) \frac{\sqrt{\lambda(m_Z, m_i, m_j)}}{24\pi m_Z v^2} \left\{ \left[ 2m_Z^2 - m_i^2 - m_j^2 - \frac{(m_i^2 - m_j^2)^2}{m_Z^2} \right] |x^{ij}|^2 - 6 m_i m_j \text{Re}(x^{ij})^2 \right\}, \quad (\text{E3})$$

where  $\Theta$  is the Heaviside step function, *i.e.* the sum in Eq. (E3) extends over pairs of neutrinos  $\nu_i$  and  $\nu_j$  that have masses  $m_i$  and  $m_j$ , respectively, such that  $m_i + m_j$  is smaller than the mass  $m_Z$  of the  $Z$ ; the kinematical function  $\lambda$  is defined as

$$\lambda(a, b, c) = a^4 + b^4 + c^4 - 2(a^2 b^2 + a^2 c^2 + b^2 c^2). \quad (\text{E4})$$

The factor  $\Delta_{ij} = 1 - \delta_{ij}/2$  in Eq. (E3) accounts for the Majorana character of the neutrinos. The coupling  $x^{ij}$  is

$$x^{ij} = \sum_{\ell=e,\mu,\tau} U_{\ell i}^* U_{\ell j} = (U^\dagger U)_{ij}, \quad (\text{E5})$$

and the vacuum expectation value is defined through  $v \equiv (\sqrt{2} G_F)^{-1/2} \approx 246.22 \text{ GeV}$ , where  $G_F$  is the Fermi coupling constant.

In a correct computation of the full invisible width of the  $Z$  one must include a parameter  $\rho$  that accounts for that part of the radiative corrections coming from the SM loops. Thus,

$$\Gamma(Z \rightarrow \text{invisible}) = \rho \Gamma(Z \rightarrow \text{invisible})_{\text{tree}}, \quad (\text{E6})$$

where  $\rho$  is evaluated as [24, 81]

$$\rho = \frac{\Gamma(Z \rightarrow \text{invisible})_{\text{SM}}}{\sum_{\nu} \Gamma(Z \rightarrow \nu\bar{\nu})_{\text{tree, SM}}} = \frac{8\pi v^2 \Gamma(Z \rightarrow \text{invisible})_{\text{SM}}}{m_Z^3}. \quad (\text{E7})$$

After accounting for the uncertainties of  $\Gamma(Z \rightarrow \text{invisible})_{\text{SM}}$ , one obtains  $\rho = 1.00812 \pm 0.00012$ .

In our numerical results, the tree-level  $Z$  invisible decay width in Eq. (E3) is always within the  $1\sigma$  experimental bands of Eq. (E1), while the decay width of Eq. (E6), including the corrections, is within the  $2\sigma$  experimental bands. Therefore, the  $Z$  invisible decay width does not



effectively constrain the branching ratios of LFV processes in our model. This is distinct from LFV studies in the inverse seesaw model [24] or in the effective field theory of the seesaw [37]. That happens because in our case the masses  $m_{4,5,6}$  of the heavy neutrinos are sufficiently high that the  $Z$  may never decay into a heavy neutrino plus a light neutrino, except for very small values  $|d_\ell| \lesssim 10^{-7}$  of the Yukawa couplings; and because the non-unitarity of the matrix  $U$  has a very weak impact on the couplings of the active neutrinos to the  $Z$  boson in our model.

## F Constraints on the mass of the charged scalar

Direct constraints on  $m_{H^\pm}$  may be obtained from collider experiments on the production and decay of on-shell charged Higgs bosons. The search sensitivity is limited by the kinematic reach of experiments, but collider constraints have the advantage of being robust and model-independent. The bound obtained from direct searches at LEP for any value of  $\tan\beta$  is  $m_{H^\pm} > 78.6 \text{ GeV}$  at 95% CL [82]. Combining data of the four LEP experiments, a limit of  $m_{H^\pm} \gtrsim 80 \text{ GeV}$  is obtained [68,83], while  $m_{H^\pm} \gtrsim 150 \text{ GeV}$  may be derived from the searches at LHC [84, 85]. Stronger mass limits on  $m_{H^\pm}$  may be obtained for specific regions of  $\tan\beta$ .

Some constraints on  $m_{H^\pm}$  from flavour physics depend strongly on the 2HDM Yukawa type, while others are type-independent. Among the flavour processes, the constraints from  $b \rightarrow s\gamma$  are most stringent due to the necessarily constructive interference of the  $H^\pm$  contribution with the SM contribution. For a type-II 2HDM, the lower limit  $m_{H^\pm} > 480 \text{ GeV}$  at 95% CL [86] includes NNLO QCD corrections and is rather independent of  $\tan\beta$ . In a recent study [87], the branching ratio of  $b \rightarrow s\gamma$  enforces  $m_{H^\pm} \gtrsim 580 \text{ GeV}$  at 95% CL both for the type-II and for the flipped 2HDM.

The recent global fits in Refs. [76, 77, 85, 88] give bounds on the charged-Higgs mass for various 2HDM Yukawa types. In those studies only 2HDMs with a  $\mathbb{Z}_2$ -symmetric potential are considered, but one may suppose that the bounds would be similar for the general 2HDM. In Ref. [85] it is found that for the type-II 2HDM flavour-physics observables impose a combined lower bound  $m_{H^\pm} \gtrsim 600 \text{ GeV}$  that is independent of  $\tan\beta$  when  $\tan\beta > 1$  but increases to  $m_{H^\pm} \gtrsim 650 \text{ GeV}$  when  $\tan\beta < 1$ . In Ref. [76],  $m_{H^\pm} > 740 \text{ GeV}$  in both the type-II and flipped 2HDMs, but  $m_{H^\pm} \gtrsim 460 \text{ GeV}$  for the lepton-specific 2HDM. In Ref. [77] on the aligned 2HDM, one finds  $m_{H^\pm} \gtrsim 500 \text{ GeV}$  or  $m_{H^\pm} \gtrsim 750 \text{ GeV}$ , depending on the fitted mass range. However, for the type-I and lepton-specific 2HDMs the restrictions on  $m_{H^\pm}$  from flavour constraints are weaker [85, 88, 89].

## References

- [1] **Super-Kamiokande** Collaboration, Y. Fukuda et al., *Evidence for oscillation of atmospheric neutrinos*, *Phys. Rev. Lett.* **81** (1998) 1562–1567, [[hep-ex/9807003](#)].
- [2] **Super-Kamiokande** Collaboration, S. Fukuda et al., *Tau neutrinos favored over sterile neutrinos in atmospheric muon-neutrino oscillations*, *Phys. Rev. Lett.* **85** (2000) 3999–4003, [[hep-ex/0009001](#)].
- [3] S. Glashow, J. Iliopoulos, and L. Maiani, *Weak Interactions with Lepton-Hadron Symmetry*, *Phys. Rev. D* **2** (1970) 1285–1292.
- [4] **BaBar** Collaboration, B. Aubert et al., *Searches for Lepton Flavor Violation in the Decays  $\tau^\pm \rightarrow e^\pm \gamma$  and  $\tau^\pm \rightarrow \mu^\pm \gamma$* , *Phys. Rev. Lett.* **104** (2010) 021802, [[arXiv:0908.2381](#)].
- [5] **Belle-II** Collaboration, W. Altmannshofer et al., *The Belle II Physics Book*, *PTEP* **2019** (2019), no. 12 123C01, [[arXiv:1808.10567](#)]. [Erratum: *PTEP* 2020, 029201 (2020)].
- [6] M. Dam, *Tau-lepton Physics at the FCC-ee circular  $e^+e^-$  Collider*, *SciPost Phys. Proc.* **1** (2019) 041, [[arXiv:1811.09408](#)].
- [7] **FCC** Collaboration, A. Abada et al., *FCC Physics Opportunities: Future Circular Collider Conceptual Design Report Volume 1*, Tech. Rep. 6, 2019.
- [8] T. Aushev et al., *Physics at Super B Factory*, [arXiv:1002.5012](#).
- [9] **MEG** Collaboration, A. Baldini et al., *Search for the lepton flavour violating decay  $\mu^+ \rightarrow e^+ \gamma$  with the full dataset of the MEG experiment*, *Eur. Phys. J. C* **76** (2016), no. 8 434, [[arXiv:1605.05081](#)].
- [10] A. Baldini et al., *MEG Upgrade Proposal*, [arXiv:1301.7225](#).
- [11] **DELPHI** Collaboration, P. Abreu et al., *Search for lepton flavor number violating  $Z0$  decays*, *Z. Phys. C* **73** (1997) 243–251.
- [12] **OPAL** Collaboration, R. Akers et al., *A Search for lepton flavor violating  $Z0$  decays*, *Z. Phys. C* **67** (1995) 555–564.
- [13] **ATLAS** Collaboration, G. Aad et al., *Search for the lepton flavor violating decay  $Z \rightarrow e\mu$  in  $pp$  collisions at  $\sqrt{s}$  TeV with the ATLAS detector*, *Phys. Rev. D* **90** (2014), no. 7 072010, [[arXiv:1408.5774](#)].
- [14] **CMS** Collaboration, A. M. Sirunyan et al., *Search for lepton flavour violating decays of the Higgs boson to  $\mu\tau$  and  $e\tau$  in proton-proton collisions at  $\sqrt{s} = 13$  TeV*, *JHEP* **06** (2018) 001, [[arXiv:1712.07173](#)].
- [15] Q. Qin, Q. Li, C.-D. Lü, F.-S. Yu, and S.-H. Zhou, *Charged lepton flavor violating Higgs decays at future  $e^+e^-$  colliders*, *Eur. Phys. J. C* **78** (2018), no. 10 835, [[arXiv:1711.07243](#)].

- [16] **ATLAS** Collaboration, G. Aad et al., *Searches for lepton-flavour-violating decays of the Higgs boson in  $\sqrt{s} = 13$  TeV  $pp$  collisions with the ATLAS detector*, *Phys. Lett. B* **800** (2020) 135069, [[arXiv:1907.06131](#)].
- [17] **ATLAS** Collaboration, The ATLAS collaboration, *Search for the decays of the Higgs boson  $H \rightarrow ee$  and  $H \rightarrow e\mu$  in  $pp$  collisions at  $\sqrt{s} = 13$  TeV with the ATLAS detector*, *ATLAS-CONF-2019-037* (2019).
- [18] W. Grimus and L. Lavoura, *Soft lepton flavor violation in a multi Higgs doublet seesaw model*, *Phys. Rev. D* **66** (2002) 014016, [[hep-ph/0204070](#)].
- [19] A. Ilakovac and A. Pilaftsis, *Flavor violating charged lepton decays in seesaw-type models*, *Nucl. Phys. B* **437** (1995) 491, [[hep-ph/9403398](#)].
- [20] E. Arganda, A. M. Curiel, M. J. Herrero, and D. Temes, *Lepton flavor violating Higgs boson decays from massive seesaw neutrinos*, *Phys. Rev. D* **71** (2005) 035011, [[hep-ph/0407302](#)].
- [21] X. Marcano and R. A. Morales, *Flavor techniques for LFV processes: Higgs decays in a general seesaw model*, *Front. in Phys.* **7** (2020) 228, [[arXiv:1909.05888](#)].
- [22] E. Arganda, M. Herrero, X. Marcano, and C. Weiland, *Imprints of massive inverse seesaw model neutrinos in lepton flavor violating Higgs boson decays*, *Phys. Rev. D* **91** (2015), no. 1 015001, [[arXiv:1405.4300](#)].
- [23] E. Arganda, M. Herrero, X. Marcano, R. Morales, and A. Szynekman, *Effective lepton flavor violating  $H\ell_i\ell_j$  vertex from right-handed neutrinos within the mass insertion approximation*, *Phys. Rev. D* **95** (2017), no. 9 095029, [[arXiv:1612.09290](#)].
- [24] V. De Romeri, M. Herrero, X. Marcano, and F. Scarcella, *Lepton flavor violating  $Z$  decays: A promising window to low scale seesaw neutrinos*, *Phys. Rev. D* **95** (2017), no. 7 075028, [[arXiv:1607.05257](#)].
- [25] M. Herrero, X. Marcano, R. Morales, and A. Szynekman, *One-loop effective LFV  $Zl_kl_m$  vertex from heavy neutrinos within the mass insertion approximation*, *Eur. Phys. J. C* **78** (2018), no. 10 815, [[arXiv:1807.01698](#)].
- [26] G. M. Pruna and A. Signer, *The  $\mu \rightarrow e\gamma$  decay in a systematic effective field theory approach with dimension 6 operators*, *JHEP* **10** (2014) 014, [[arXiv:1408.3565](#)].
- [27] S. Davidson,  *$\mu \rightarrow e\gamma$  in the 2HDM: an exercise in EFT*, *Eur. Phys. J. C* **76** (2016), no. 5 258, [[arXiv:1601.01949](#)].
- [28] W. Dekens, E. E. Jenkins, A. V. Manohar, and P. Stoffer, *Non-perturbative effects in  $\mu \rightarrow e\gamma$* , *JHEP* **01** (2019) 088, [[arXiv:1810.05675](#)].
- [29] P. Paradisi, *Higgs-mediated  $\tau \rightarrow \mu\mu$  and  $\tau \rightarrow e$  transitions in II Higgs doublet model and supersymmetry*, *JHEP* **02** (2006) 050, [[hep-ph/0508054](#)].
- [30] S. Davidson and G. J. Grenier, *Lepton flavour violating Higgs and tau to mu gamma*, *Phys. Rev. D* **81** (2010) 095016, [[arXiv:1001.0434](#)].

- [31] T. Hong, H. Hung, H. Phuong, L. Phuong, and L. Hue, *Lepton flavor violating decays of the SM-like Higgs boson  $h \rightarrow e_i e_j$ , and  $e_i \rightarrow e_j \gamma$  in a flipped 3-3-1 model*, [arXiv:2002.06826](#).
- [32] L. Calibbi and G. Signorelli, *Charged Lepton Flavour Violation: An Experimental and Theoretical Introduction*, *Riv. Nuovo Cim.* **41** (2018), no. 2 71–174, [[arXiv:1709.00294](#)].
- [33] J. Korner, A. Pilaftsis, and K. Schilcher, *Leptonic flavor changing  $Z^0$  decays in  $SU(2) \times U(1)$  theories with right-handed neutrinos*, *Phys. Lett. B* **300** (1993) 381–386, [[hep-ph/9301290](#)].
- [34] J. I. Illana and T. Riemann, *Charged lepton flavor violation from massive neutrinos in  $Z$  decays*, *Phys. Rev. D* **63** (2001) 053004, [[hep-ph/0010193](#)].
- [35] A. Flores-Tlalpa, J. Hernandez, G. Tavares-Velasco, and J. Toscano, *Effective Lagrangian description of the lepton flavor violating decays  $Z \rightarrow \ell_i^\mp \ell_j^\pm$* , *Phys. Rev. D* **65** (2002) 073010, [[hep-ph/0112065](#)].
- [36] S. Davidson, S. Lacroix, and P. Verdier, *LHC sensitivity to lepton flavour violating  $Z$  boson decays*, *JHEP* **09** (2012) 092, [[arXiv:1207.4894](#)].
- [37] R. Coy and M. Frigerio, *Effective approach to lepton observables: the seesaw case*, *Phys. Rev. D* **99** (2019), no. 9 095040, [[arXiv:1812.03165](#)].
- [38] E. Iltan and I. Turan, *Lepton flavor violating  $Z \rightarrow l_1^+ l_2^-$  decay in the general Higgs doublet model*, *Phys. Rev. D* **65** (2002) 013001, [[hep-ph/0106068](#)].
- [39] I. Cortes Maldonado, A. Moyotl, and G. Tavares-Velasco, *Lepton flavor violating decay  $Z \rightarrow \ell_i^\pm \ell_j^\mp$  in the 331 model*, *Int. J. Mod. Phys. A* **26** (2011) 4171–4185, [[arXiv:1109.0661](#)].
- [40] N. Thao, L. Hue, H. Hung, and N. Xuan, *Lepton flavor violating Higgs boson decays in seesaw models: new discussions*, *Nucl. Phys. B* **921** (2017) 159–180, [[arXiv:1703.00896](#)].
- [41] D. Aristizabal Sierra and A. Vicente, *Explaining the CMS Higgs flavor violating decay excess*, *Phys. Rev. D* **90** (2014), no. 11 115004, [[arXiv:1409.7690](#)].
- [42] N. Bizot, S. Davidson, M. Frigerio, and J. L. Kneur, *Two Higgs doublets to explain the excesses  $pp \rightarrow \gamma\gamma(750 \text{ GeV})$  and  $h \rightarrow \tau^\pm \mu^\mp$* , *JHEP* **03** (2016) 073, [[arXiv:1512.08508](#)].
- [43] A. Crivellin, J. Heeck, and P. Stoffer, *A perturbed lepton-specific two-Higgs-doublet model facing experimental hints for physics beyond the Standard Model*, *Phys. Rev. Lett.* **116** (2016), no. 8 081801, [[arXiv:1507.07567](#)].
- [44] X. Liu, L. Bian, X.-Q. Li, and J. Shu, *Type-III two Higgs doublet model plus a pseudoscalar confronted with  $h \rightarrow \mu\tau$ , muon  $g - 2$  and dark matter*, *Nucl. Phys. B* **909** (2016) 507–524, [[arXiv:1508.05716](#)].
- [45] F. Botella, G. Branco, M. Nebot, and M. Rebelo, *Flavour Changing Higgs Couplings in a Class of Two Higgs Doublet Models*, *Eur. Phys. J. C* **76** (2016), no. 3 161, [[arXiv:1508.05101](#)].

- [46] Y. Omura, E. Senaha, and K. Tobe, *Lepton-flavor-violating Higgs decay  $h \rightarrow \mu\tau$  and muon anomalous magnetic moment in a general two Higgs doublet model*, *JHEP* **05** (2015) 028, [[arXiv:1502.07824](#)].
- [47] K. Tobe, *Michel parameters for  $\tau$  decays  $\tau \rightarrow l\nu\bar{\nu}$  ( $l = e, \mu$ ) in a general two Higgs doublet model with  $\mu - \tau$  flavor violation*, *JHEP* **10** (2016) 114, [[arXiv:1607.04447](#)].
- [48] W.-S. Hou and G. Kumar, *The Coming Decade of  $h \rightarrow \tau\mu$  and  $\tau \rightarrow \mu\gamma$  Interplay in  $\tau$  Flavor Violation Search*, [arXiv:2003.03827](#).
- [49] L. de Lima, C. Machado, R. Matheus, and L. do Prado, *Higgs Flavor Violation as a Signal to Discriminate Models*, *JHEP* **11** (2015) 074, [[arXiv:1501.06923](#)].
- [50] T. Nguyen, T. T. Le, T. Hong, and L. Hue, *Decay of standard model-like Higgs boson  $h \rightarrow \mu\tau$  in a 3-3-1 model with inverse seesaw neutrino masses*, *Phys. Rev. D* **97** (2018), no. 7 073003, [[arXiv:1802.00429](#)].
- [51] W. Altmannshofer, M. Carena, and A. Crivellin,  *$L_\mu - L_\tau$  theory of Higgs flavor violation and  $(g - 2)_\mu$* , *Phys. Rev. D* **94** (2016), no. 9 095026, [[arXiv:1604.08221](#)].
- [52] C.-H. Chen and T. Nomura,  *$L_\mu - L_\tau$  gauge-boson production from lepton flavor violating  $\tau$  decays at Belle II*, *Phys. Rev. D* **96** (2017), no. 9 095023, [[arXiv:1704.04407](#)].
- [53] A. Vicente, *Higgs lepton flavor violating decays in Two Higgs Doublet Models*, *Front. in Phys.* **7** (2019) 174, [[arXiv:1908.07759](#)].
- [54] A. Crivellin, A. Kokulu, and C. Greub, *Flavor-phenomenology of two-Higgs-doublet models with generic Yukawa structure*, *Phys. Rev. D* **87** (2013), no. 9 094031, [[arXiv:1303.5877](#)].
- [55] R. Benbrik, C.-H. Chen, and T. Nomura,  *$h, Z \rightarrow \ell_i \bar{\ell}_j$ ,  $\Delta a_\mu$ ,  $\tau \rightarrow (3\mu, \mu\gamma)$  in generic two-Higgs-doublet models*, *Phys. Rev. D* **93** (2016), no. 9 095004, [[arXiv:1511.08544](#)].
- [56] W. Grimus and H. Neufeld, *Radiative Neutrino Masses in an  $SU(2) \times U(1)$  Model*, *Nucl.Phys.* **B325** (1989) 18.
- [57] W. Grimus, L. Lavoura, O. Og Reid, and P. Osland, *A Precision constraint on multi-Higgs-doublet models*, *J. Phys. G* **35** (2008) 075001, [[arXiv:0711.4022](#)].
- [58] L. Lavoura and J. P. Silva, *Fundamental CP violating quantities in a  $SU(2) \times U(1)$  model with many Higgs doublets*, *Phys. Rev. D* **50** (1994) 4619–4624, [[hep-ph/9404276](#)].
- [59] E. H. Aeikens, P. M. Ferreira, W. Grimus, D. Jurčiukonis, and L. Lavoura, *Radiative seesaw corrections and charged-lepton decays in a model with soft flavour violation*, *JHEP* **12** (2020) 122, [[arXiv:2009.13479](#)].
- [60] G. Branco, P. Ferreira, L. Lavoura, M. Rebelo, M. Sher, and J. P. Silva, *Theory and phenomenology of two-Higgs-doublet models*, *Phys. Rept.* **516** (2012) 1–102, [[arXiv:1106.0034](#)].
- [61] D. Jurčiukonis and L. Lavoura, *The three- and four-Higgs couplings in the general two-Higgs-doublet model*, *JHEP* **12** (2018) 004, [[arXiv:1807.04244](#)].

- [62] P. Minkowski,  $\mu \rightarrow e\gamma$  at a Rate of One Out of  $10^9$  Muon Decays?, *Phys. Lett. B* **67** (1977) 421–428.
- [63] T. Yanagida, *Horizontal gauge symmetry and masses of neutrinos in: Workshop on the Baryon Number of the Universe and Unified Theories, Conf. Proc. C* **7902131** (1979) 95–99.
- [64] S. Glashow, *The Future of Elementary Particle Physics in: Cargese Summer Institute: Quarks and Leptons, NATO Sci. Ser. B* **61** (1980) 687.
- [65] M. Gell-Mann, P. Ramond, and R. Slansky, *Complex Spinors and Unified Theories, in Supergravity, Proceedings of the Workshop, Stony Brook, New York, Conf.Proc.* **C790927** (1979) 315–321, [[arXiv:1306.4669](#)].
- [66] R. N. Mohapatra and G. Senjanovic, *Neutrino Mass and Spontaneous Parity Nonconservation, Phys. Rev. Lett.* **44** (1980) 912.
- [67] **Planck** Collaboration, Y. Akrami et al., *Planck 2018 results. I. Overview and the cosmological legacy of Planck*, [arXiv:1807.06205](#).
- [68] **Particle Data Group** Collaboration, P. Zyla et al., *Review of Particle Physics, PTEP* **2020** (2020), no. 8 083C01.
- [69] P. F. de Salas, D. V. Forero, C. A. Ternes, M. Tortola, and J. W. F. Valle, *Status of neutrino oscillations 2018:  $3\sigma$  hint for normal mass ordering and improved CP sensitivity, Phys. Lett.* **B782** (2018) 633–640, [[arXiv:1708.01186](#)].
- [70] F. Capozzi, E. Lisi, A. Marrone, and A. Palazzo, *Current unknowns in the three neutrino framework, Prog. Part. Nucl. Phys.* **102** (2018) 48–72, [[arXiv:1804.09678](#)].
- [71] I. Esteban, M. Gonzalez-Garcia, A. Hernandez-Cabezudo, M. Maltoni, and T. Schwetz, *Global analysis of three-flavour neutrino oscillations: synergies and tensions in the determination of  $\theta_{23}$ ,  $\delta_{CP}$ , and the mass ordering, JHEP* **01** (2019) 106, [[arXiv:1811.05487](#)].
- [72] D. Fontes and J. C. Romão, *FeynMaster: a plethora of Feynman tools, Comput. Phys. Commun.* **256** (2020) 107311, [[arXiv:1909.05876](#)].
- [73] A. Denner, S. Dittmaier, and L. Hofer, *Collier: a fortran-based Complex One-Loop Library in Extended Regularizations, Comput. Phys. Commun.* **212** (2017) 220–238, [[arXiv:1604.06792](#)].
- [74] T. Hahn and M. Perez-Victoria, *Automatized one loop calculations in four-dimensions and D-dimensions, Comput. Phys. Commun.* **118** (1999) 153–165, [[hep-ph/9807565](#)].
- [75] H. H. Patel, *Package-X: A Mathematica package for the analytic calculation of one-loop integrals, Comput. Phys. Commun.* **197** (2015) 276–290, [[arXiv:1503.01469](#)].
- [76] D. Chowdhury and O. Eberhardt, *Update of Global Two-Higgs-Doublet Model Fits, JHEP* **05** (2018) 161, [[arXiv:1711.02095](#)].

- [77] O. Eberhardt, A. P. n. Martínez, and A. Pich, *Global fits in the Aligned Two-Higgs-Doublet model*, *JHEP* **05** (2021) 005, [[arXiv:2012.09200](#)].
- [78] L. Lavoura, *General formulae for  $f_1 \rightarrow f_2 \gamma$* , *Eur. Phys. J. C* **29** (2003) 191–195, [[hep-ph/0302221](#)].
- [79] **ALEPH, DELPHI, L3, OPAL, SLD, LEP Electroweak Working Group, SLD Electroweak Group, SLD Heavy Flavour Group** Collaboration, S. Schael et al., *Precision electroweak measurements on the Z resonance*, *Phys. Rept.* **427** (2006) 257–454, [[hep-ex/0509008](#)].
- [80] A. Abada, A. Teixeira, A. Vicente, and C. Weiland, *Sterile neutrinos in leptonic and semileptonic decays*, *JHEP* **02** (2014) 091, [[arXiv:1311.2830](#)].
- [81] V. Brdar, M. Lindner, S. Vogl, and X.-J. Xu, *Revisiting neutrino self-interaction constraints from Z and  $\tau$  decays*, *Phys. Rev. D* **101** (2020), no. 11 115001, [[arXiv:2003.05339](#)].
- [82] **LEP Higgs Working Group for Higgs boson searches, ALEPH, DELPHI, L3, OPAL** Collaboration, *Search for charged Higgs bosons: Preliminary combined results using LEP data collected at energies up to 209-GeV*, in *Proceedings, 2001 Europhysics Conference on High Energy Physics (EPS-HEP 2001): Budapest, Hungary, July 12-18, 2001*, 7, 2001. [hep-ex/0107031](#).
- [83] **ALEPH, DELPHI, L3, OPAL, LEP** Collaboration, G. Abbiendi et al., *Search for Charged Higgs bosons: Combined Results Using LEP Data*, *Eur. Phys. J. C* **73** (2013) 2463, [[arXiv:1301.6065](#)].
- [84] **CMS** Collaboration, V. Khachatryan et al., *Search for a charged Higgs boson in pp collisions at  $\sqrt{s} = 8$  TeV*, *JHEP* **11** (2015) 018, [[arXiv:1508.07774](#)].
- [85] A. Arbey, F. Mahmoudi, O. Stal, and T. Stefaniak, *Status of the Charged Higgs Boson in Two Higgs Doublet Models*, *Eur. Phys. J. C* **78** (2018), no. 3 182, [[arXiv:1706.07414](#)].
- [86] M. Misiak et al., *Updated NNLO QCD predictions for the weak radiative B-meson decays*, *Phys. Rev. Lett.* **114** (2015), no. 22 221801, [[arXiv:1503.01789](#)].
- [87] M. Misiak and M. Steinhauser, *Weak radiative decays of the B meson and bounds on  $M_{H^\pm}$  in the Two-Higgs-Doublet Model*, *Eur. Phys. J. C* **77** (2017), no. 3 201, [[arXiv:1702.04571](#)].
- [88] J. Haller, A. Hoecker, R. Kogler, K. Mönig, T. Peiffer, and J. Stelzer, *Update of the global electroweak fit and constraints on two-Higgs-doublet models*, *Eur. Phys. J. C* **78** (2018), no. 8 675, [[arXiv:1803.01853](#)].
- [89] P. Sanyal, *Limits on the Charged Higgs Parameters in the Two Higgs Doublet Model using CMS  $\sqrt{s} = 13$  TeV Results*, *Eur. Phys. J. C* **79** (2019), no. 11 913, [[arXiv:1906.02520](#)].